Copyright Warning & Restrictions

The copyright law of the United States (Title 17, United States Code) governs the making of photocopies or other reproductions of copyrighted material.

Under certain conditions specified in the law, libraries and archives are authorized to furnish a photocopy or other reproduction. One of these specified conditions is that the photocopy or reproduction is not to be "used for any purpose other than private study, scholarship, or research." If a, user makes a request for, or later uses, a photocopy or reproduction for purposes in excess of "fair use" that user may be liable for copyright infringement,

This institution reserves the right to refuse to accept a copying order if, in its judgment, fulfillment of the order would involve violation of copyright law.

Please Note: The author retains the copyright while the New Jersey Institute of Technology reserves the right to distribute this thesis or dissertation

Printing note: If you do not wish to print this page, then select "Pages from: first page # to: last page #" on the print dialog screen

ABSTRACT

DEVELOPMENT OF NOVEL MEMBRANES FOR NANOCARBON ENHANCED SEPARATION WITH APPLICATION IN BIOFUELS AND SOLVENT RECOVERY

by
Oindrila Gupta

Pharmaceutical industries historically have had one of the highest amounts of solvent waste generated per unit of drug manufactured. Energy requirements and carbon footprint of current solvent recycling processes tend to be quite high, and the incineration of the solvents for waste disposal produces toxic air emissions. Also, rapidly increasing demand for energy and strict regulation on engine pollutant emissions have necessitated the use of alcohol as carbon-neutral fuels. Thermal distillation is one of the most common methods for the separation of alcohol-water mixtures. However, its application is limited due to energy requirements and high operating costs, and heating to boiling point can lead to undesirable side reactions. In this dissertation, three major challenges related to organic solvent separation are addressed. Approaches to enhance the performance of membrane distillation by modifying the commercial membranes with different carbon-based nanomaterials and alternative heating technologies to reduce energy consumption are explored. These form the basis of this dissertation.

In the first application, carbon nanotube immobilized membrane (CNIM) for enhanced separation of organic solvents from their aqueous mixtures via sweep gas membrane distillation is explored. The presence of carbon nanotubes (CNTs) on the hydrophobic membrane surface significantly alters the liquid–membrane interactions to promote isopropanol (IPA) transport in IPA-water mixture by inhibiting water penetration

into the membrane pores. The isopropanol flux, selectivity and mass transfer coefficient obtained with CNIM are significantly higher than the corresponding unmodified Polytetraflouroethylene (PTFE) membrane at different isopropanol concentrations and temperatures. Performance enhancement in CNIM can be mainly attributed to the preferential sorption on the CNTs followed by rapid desorption from its surface.

The second application demonstrates enhanced organic separation via microwave-induced sweep gas membrane distillation from its aqueous mixture. Microwave heated ethanol–water mixtures are separated on PTFE and CNIM. The membrane performances in terms of ethanol vapor flux and separation factors are evaluated and compared between microwave-induced membrane distillation (MIMD) and membrane distillation (MD) using conventional heating. The combination of CNIM and microwave heating is most effective. Performance improvements in MIMD are due to nonthermal effects such as localized superheating and break down of hydrogen-bonded ethanol–water clusters. Moreover, MIMD requires less energy to operate than conventional MD under similar conditions. The lower energy consumption along with higher flux and separation factor in MIMD represents a major advancement in the state of the art in solvent separation by MD. Furthermore, a novel approach for Acetone-Butanol-Ethanol (ABE) recovery using MIMD is investigated. CNTs and octadecyl amide (ODA) functionalized CNTs are used. The ABE flux, separation factor and mass transfer coefficient obtained with CNT and CNT-ODA immobilized membranes are remarkably higher than those of the commercial pristine membrane under various experimental conditions.

In the third major application, nanocarbon-immobilized membranes are applied for the separation and recovery of tetrahydrofuran (THF) from water via MD. Several

nanocarbons, namely CNTs, graphene oxide (GO), reduced graphene oxide (rGO), and an rGO–CNT hybrid is immobilized on PTFE membranes. Among the nanocarbons, rGO–CNT performs the best in terms of flux and separation factor over the plain PTFE membrane. The improved membrane performances of the rGO–CNT membrane is due to the preferential sorption of THF on rGO–CNT, nanocapillary effect through graphene sheets, along with the activated diffusion of THF via a frictionless CNT surface.

This dissertation shows that the modification of the membranes with carbon-based materials namely CNTs, GO and their derivatives along with microwave heating as an alternative heating source are effective strategies to enhance the performance of MD. These fabricated membranes along with modification of the system configuration have great potentials for solvent removal from aqueous solution for use as biofuels and by cosmetic, paint and pharmaceutical industries using MD.

DEVELOPMENT OF NOVEL MEMBRANES FOR NANOCARBON ENHANCED SEPARATION WITH APPLICATION IN BIOFUELS AND SOLVENT RECOVERY

by
Oindrila Gupta

A Dissertation
Submitted to the Faculty of
New Jersey Institute of Technology
in Partial Fulfillment of the Requirements for the Degree of
Doctor of Philosophy in Environmental Science

Department of Chemistry and Environmental Science

December 2020

APPROVAL PAGE

DEVELOPMENT OF NOVEL MEMBRANES FOR NANOCARBON ENHANCED SEPARATION WITH APPLICATION IN BIOFUELS AND SOLVENT RECOVERY

Oindrila Gupta

Dr. Somenath Mitra, Dissertation Advisor — Date
Distinguished Professor of Chemistry and Environmental Science, NJIT

Dr. Tamara Gund, Committee Member — Date
Professor of Chemistry and Environmental Science, NJIT

Dr. Nuggehalli M Ravindra, Committee Member — Date
Professor of Physics, NJIT

Dr. Mengyan Li, Committee Member — Date
Associate Professor of Chemistry and Environmental Science, NJIT

Dr. Pradyot Patnaik, Committee Member — Date
Consultant, Radiance

BIOGRAPHICAL SKETCH

Author: Oindrila Gupta

Degree: Doctor of Philosophy

Date: December 2020

Undergraduate and Graduate Education:

- Doctor of Philosophy in Environmental Science,
  New Jersey Institute of Technology, Newark, NJ, USA, 2020

- Bachelor of Technology in Chemical Engineering,
  West Bengal University of Technology, Kolkata, India, 2013

Major: Environmental Science

Publications:

Gupta, O., Roy, S., and Mitra, S., Nanocarbon-immobilized membranes for separation of tetrahydrofuran from Water via membrane distillation. *ACS Applied Nanomaterials*, 2020, 3(7), 6344.

Gupta, O., Roy, S., and Mitra, S., Low temperature recovery of acetone–butanol–ethanol (ABE) fermentation products via microwave induced membrane distillation on carbon nanotube immobilized membranes. *Sustainable Energy & Fuels*, 2020.

Gupta, O., Roy, S., and Mitra, S., Microwave induced membrane distillation for enhanced ethanol –water separation on carbon nanotube immobilized membrane. *Industrial & Engineering Chemistry*, 2019, 58, 313.

Gupta, O., Roy, S., and Mitra, S., Enhanced membrane distillation of organic solvents from their aqueous mixtures using a carbon nanotube immobilized membrane. *Journal of Membrane Science*, 2018, 568, 134.

Presentations:

Gupta, O., Roy, S., and Mitra, S., Novel separation technique for alcohol separation from water using carbon nanotube-based membranes. *Air & Waste Management Association Student Poster Competition*, Rutgers, New Brunswick, NJ, Feb. 27th, 2019.

Gupta, O., Roy, S., and Mitra, S., Enhanced membrane distillation using nanomaterial-based membranes for organic solvent separation from their aqueous mixtures. *ACS* National Meeting in Orlando, FL, Mar. 31st – Apr. 4th, 2019.

Gupta, O., Roy, S., and Mitra, S., Process modification for organic solvent separation via carbon nanotube immobilized membrane using membrane distillation. *ACS* National Meeting in San Diego, CA, Aug. 25th – Aug. 29th, 2019.

Gupta, O., Roy, S., and Mitra, S., Recovery of organic solvents via membrane distillation on carbon nanotube immobilized membranes for use as biofuels. *ACS* National Meeting (virtual), Mar. 22nd – Mar. 26th, 2020.

Gupta, O., Roy, S., and Mitra, S., Microwave induced membrane distillation of acetone-butanol-ethanol (ABE) fermentation products on carbon nanotube immobilized membranes for use as biofuels. *ACS* National Meeting (virtual), Aug. 17th – Aug. 20th, 2020.

Gupta, O., Roy, S., and Mitra, S., Hybrid nanocarbon immobilized membranes for selective membrane distillation of tetrahydrofuran (THF) from water. *ACS* National Meeting (virtual), Aug. 17th – Aug. 20th, 2020.

To my beloved parents and sister, I would like to extend my deepest gratitude for your unconditional love and support throughout my journey as an international student in a foreign land. To a very special person; many thanks to you for your affection, encouragement, understanding and patience. This success is dedicated to all of you.

ACKNOWLEDGMENTS

Being an international student in a foreign land is never an easy task but I was fortunate enough to have come across so many people during the entire duration of my stay at NJIT who made me feel at home. Without them, I would not have been able to accomplish my childhood dream of coming to United States of America and getting my doctorate degree here. I would like to acknowledge some very important people here who are very close to my heart and would take this opportunity to express my sincere gratitude to them and remind them that you will be remained etched in my memory for a lifetime.

First, I wish to express my deepest gratitude to my advisor, Professor Somenath Mitra for his immense support from my Ph. D application days to my graduation. He has been a father figure to me all these years and has provided me with some valuable guidance and financial support, without which I would not have been able to come this far. His supervision always helped me when I stumbled with research challenges in the last four years. It has been an absolute honor to work under his valued supervision.

Next, I would like to sincerely thank my committee members, Dr. Tamara Gund, Dr. Nuggehalli Ravindra, Dr. Mengyan Li, and Dr. Pradyot Patnaik for serving as my dissertation committee members and providing encouragement and insightful comments which motivated me to strive harder.

Of special importance, I would like to acknowledge the Chemistry & Environmental Science Department for supporting me as a Teaching Assistant and giving me the opportunity to interact with students and making me realize the importance of knowledge transfer. The Chemical, Bioengineering, Environmental, and Transport

Systems Division, National Science Foundation, USA (Grant no. CBET-1603314) is also gratefully acknowledged for the research funding.

In addition, I wish to thank Dr. Jeong Seop Shim, Dr. Larisa Krishtopa, and Dr. Xueyan Zhang for their technical support, I would also like to recognize Genti Price and Leslie Williams for always catering to my need for lab resources. I am deeply indebted to Mr. Yogesh Gandhi for his immense support and kind assistance.

I would like to thank Dr. Kun Chen and Dr. Xiangyan Meng for their suggestions and assistance. I would like to greatly appreciate the efforts that Dr. Madihah Humoud and Dr. Worawit Intrchom took to teach me some major experimental techniques when I first came to the lab and for being my first few friends in New Jersey. For my current research group members—Dr. Zhiqian Wang, Indrani Gupta, Mitun Chandra Bhoumick, Sumona Paul, Samar Azizighannad, and Mohammad Saiful Islam—thank you for being my friends and not just colleagues. My special thanks also go to Dr. Sagar Roy, who constantly motivated me during times of stress and provided excellent technical guidance while also giving me a homely feeling and never let me miss home-cooked meals when I was an amateur in the kitchen.

Last and foremost, I am profoundly grateful to my dad, Goutam Gupta, mom, Ruma Gupta and my sister, Indrani Gupta, who is also a team member in Dr. Mitra's research group for their unconditional love, encouragement, and continuous support and believing in me that I can be Dr. Oindrila despite repeated challenges. I would also like to thank a very special friend, someone I knew since my first day as an undergraduate student for his patience, understanding and standing beside me in the toughest of times. With all their support, I have successfully earned the doctorate title before my name.

TABLE OF CONTENTS

Chapter	Page
1 INTRODUCTION……..……..……..…….	1
1.1 Background…….....……..…….....	1
2 LITERATURE REVIEW …….……..	6
2.1 Background of Membrane Distillation …….….....	6
2.2 MD Configurations …….....	9
2.2.1 Direct Contact Membrane Distillation (DCMD) …….....	10
2.2.2 Air Gap Membrane Distillation (AGMD) …….……..……	11
2.2.3 Sweep Gas Membrane Distillation (SGMD) ……..……	11
2.2.4 Vacuum Membrane Distillation (VMD) …….……...……	12
2.3 Membranes …….....	13
2.3.1 MD Membrane Characteristics …….……..	13
2.3.2 Membrane Modules …….....	20
2.3.3 Types of MD Membranes …….....	22
2.4 MD Applications …….……..	39
3 ENHANCED MEMBRANE DISTILLATION OF ORGANIC SOLVENTS FROM THEIR SQUEOUS MIXTURES USING A CARBON NANOTUBE IMMOBILIZED MEMBRANE…….….....	41
3.1 Introduction..……..……	41
3.2 Experimental……..……	43
3.2.1 Chemicals and Materials …….……...	43

TABLE OF CONTENTS
(Continued)

Chapter **Page**

3.2.2 CNIM Fabrication…….. 44

3.2.3 Experimental Set Up…….. 45

3.2.4 Gas Permeation Test…….. 47

3.3 Results and discussion……. 48

3.3.1 SGMD Performance Using CNIM and Unmodified Membrane …….. 51

3.4 Mass Transfer Coefficient ……... 56

3.5 Membrane Stability ……. 58

3.6 Proposed Mechanism …….. 59

3.7 Concluding Remarks ……... 60

4 MICROWAVE INDUCED MEMBRANE DISTILLATION FOR ETHANOL-WATER SEPARATION ON CARBON NANOTUBE IMMOBILIZED MEMBRANES…… 61

4.1 Introduction…….. 61

4.2 Materials and Methods……. 63

4.2.1 Chemicals and Materials…… 63

4.2.2 CNIM Fabrication ……. 64

4.2.3 Experimental Setup…… 64

4.3 Results and Discussion……. 65

4.3.1 Mass Transfer Coefficient……..... 71

TABLE OF CONTENTS
(Continued)

Chapter **Page**

4.3.2 Power Consumption in MIMD……..... 72

4.4 Proposed Mechanism……..……. 73

4.5 Conclusions…….. 77

5 LOW TEMPERATURE RECOVERY OF ACETONE-BUTANOL-ETHANOL (ABE) FERMENTATION PRODUCTS VIA MICROWAVE INDUCED MEMBRANE DISTILLATION ON CARBON NANOTUBE IMMOBILIZED MEMBRANES……... 79

5.1 Introduction…….. 79

5.2 Materials and Methods……. 81

5.2.1 Chemicals and Materials…… 81

5.2.2 CNIM Fabrication and Characterization …….. 82

5.2.3 Experimental Setup…… 82

5.2.4 Experimental Procedure…… 83

5.3 Results and Discussion……. 85

5.3.1 Membrane Characterization……... 85

5.3.2 MD separation performance ……. 91

5.3.3 Mass Transfer Coefficient …… 103

5.3.4 Membrane Stability……... 104

5.4 Proposed Mechanism……... 105

5.5 Concluding Remarks ……... 107

TABLE OF CONTENTS
(Continued)

Chapter	Page
6 NANOCARBON-IMMOBILIZED MEMBRANES FOR SEPARATION OF TETRAHYDROFURAN FROM WATER VIA MEMBRANE DISTILLATION…….	108
6.1 Introduction……..	108
6.2 Materials and Methods ……	111
6.2.1 Chemicals and Materials……	111
6.2.2 CNIM Fabrication and Characterization ……..	111
6.2.3 Experimental Setup……...	112
6.2.4 Experimental Procedure ……	113
6.3 Results and Discussion ……	114
6.3.1 Membrane Characterization ……..	114
6.3.2 MD separation performance …….	119
6.3.3 Mass Transfer Coefficient ……	127
6.3.4 Membrane Stability ……..	128
6.4 Proposed Mechanism ……..	129
6.5 Concluding Remarks ……...	130
7 CONCLUSIONS AND FUTURE PERSPECTIVES ……	132

TABLE OF CONTENTS
(Continued)

Chapter **Page**

7.1 Conclusions ……. 127

7.2 Future Perspectives ……. 129

REFERENCES ……... 136

LIST OF TABLES

Table		Page
2.1	Configurations and Their Advantages and Disadvantages…….……	14
3.1	Mass Transfer Coefficient of IPA and Enhancement % at Various Feed Temperature at 15 Volume % Feed and 112 mL/min……...……	59
3.2	Mass Transfer Coefficient of IPA and Enhancement% at Various Feed Flow Rate and 10 Volume % IPA at 50 °C……...……...	59
4.1	Mass Transfer Coefficients with Conventional and Microwave Heating for PTFE and CNIM ……...……	72
4.2	Contact Angles in Degrees with PTFE Membrane and CNIM (^{0}) …...……...	76
5.1	Contact Angles of Pure Water & ABE Mixture…….……	90
5.2	Apparent Activation Energy (E_{app}) Values for Acetone (1.5 Vol%), Butanol (3 Vol%), Ethanol (0.5 Vol%) and Water (95 Vol %) in Feed….……	101
5.3	Mass Transfer Coefficient of ABE at Different Temperature and 1.5, 3 & 0.5 Vol % ABE Feed at 112 mL/min……	105
6.1	Activation Energy of Unmodified PTFE and Fabricated Membranes…….……..	128
6.2	Mass Transfer Coefficient of THF at Different Temperature and 5 (w/w %) THF in Feed at 112 mL/min……...…….	129

LIST OF FIGURES

Figure		Page
2.1	Schematic of MD configurations……....	14
3.1	Experimental setup for sweep gas membrane distillation……...	47
3.2	UV absorbance calibration curve of IPA at different concentrations…….	48
3.3	Scanning electron micrograph of **(a)** CNIM and **(b)** unmodified PTFE **(c)** thermogravimetric analysis of PTFE and CNIM…….....	51
3.4	**(a)** Photograph of isopropanol- water mixture (10 volume %) drop on unmodified PTFE and **(b)** CNIM; **(c)** contact angle measurements on unmodified PTFE and CNIM membrane……	52
3.5	**(a)** Effect of feed concentration on IPA flux and separation factor; **(b)** effect of feed temperature on IPA flux and separation factor; **(c)** effect of feed flowrate on IPA flux and separation factor……...	57
3.6	Schematic of proposed mechanism for CNIM…….……...	60
4.1	Experimental setup…….…….....	66
4.2	The influence of feed concentration on ethanol flux and separation factor with **(a)** CNIM, and **(b)** PTFE membrane…….....	69
4.3	**(a)** The influence of feed temperature on ethanol flux and separation factor with CNIM, and **(b)** with PTFE membrane……	71
4.4	Power consumption with conventional and microwave heating…….……	74
4.5	Contact angle of **(a)** PTFE with conventional heating, **(b)** PTFE with microwave heating, **(c)** CNIM with conventional heating, and **(d)** CNIM with microwave heating. (10% ethanol in feed) ……...…….	76
4.6	FTIR spectra of ethanol-water solution (50% v/v) ……...…….	77
4.7	Schematic of the proposed mechanism of microwave heating……...	78
5.1	Schematic diagram of the experimental setup for the SGMD……	86
5.2	SEM images of **a)** unmodified PTFE membrane, **b)** CNIM, **c)** CNIM-ODA……	87

LIST OF FIGURES
(Continued)

Figure		Page
5.3	**a)** Thermogravimetric analysis of unmodified PTFE. CNIM and CNIM-ODA, **b)** differential TGA curves of the corresponding membranes…….……...	88
5.4	Picture of ABE- water solution (0.6, 1.2 and 0.2 vol % respectively) droplet on **a)** CNIM-ODA, **b)** PTFE, **c)** CNIM……...	90
5.5	AFM images featuring the topography of the **a)** unmodified membrane surface (PTFE), **b)** CNIM and **c)** CNIM-ODA……...	91
5.6	Effect of feed concentration on flux for **a)** acetone, **b)** butanol and **c)** ethanol, and on separation factor for **d)** acetone, **e)** butanol and **f)** ethanol…….	96
5.7	Effect of feed temperature on flux for **a)** acetone, **b)** butanol, **c)** ethanol, and on separation factor for **d)** acetone, **e)** butanol, **f)** ethanol, **g)** effect of feed temperature on water flux……...	101
5.8	Effect of feed concentration on flux and separation factor for **a)** acetone, **b)** butanol, **c)** ethanol……...……...	104
5.9	**a)** H-Bonded ABE-Water clusters, **b)** proposed mechanism schematic….……...	107
6.1	Schematic diagram of the experimental setup for the DCMD……	115
6.2	SEM images of **a)** unmodified PTFE membrane, **b)** GOIM, **c)** rGOIM, **d)** CNIM and **e)** rGO CNIM…….....	117
6.3	**a)** Thermogravimetric analysis of unmodified PTFE and rGO-CNIM, **b)** differential TGA curves of the corresponding membranes……...…..……	118
6.4	Contact angle measurements of pure water and 5 (w/w %) THF membrane surfaces……...	119
6.5	Effect of feed concentration on **a)** THF flux, and **b)** THF separation factor…..….	123
6.6	Effect of feed temperature on **a)** THF flux, and **b)** THF separation factor….……	125
6.7	Effect of feed flowrate on **a)** THF flux, and **b)** separation factor…….…….	127

LIST OF FIGURES
(Continued)

Figure **Page**

6.8 **a)** Schematic of the proposed mechanism for rGO-CNIM, **b)** nanocapillary action through rGO layers……... 132

CHAPTER 1

INTRODUCTION

1.1 Background

The usage of fossil fuels has increased global warming to a significant extent that results in frequent droughts, heavier rainfall, and other changes in the natural systems, leading to melting glaciers, rising sea levels, disruption of coral reefs and alpine meadows and lack of fresh water sources. This global problem represents one of the biggest challenges for the international community. Mitigating this problem will require considerable efforts and innovations, both technical and intellectual. Specifically, we will have to think about energy differently. Reducing energy consumption through conservation and improved technology will surely play a part. However, since it is difficult to think of a world where humanity consumes no energy, we also must find replacements for fossil fuels. While progress has been made in recent years to improve our use of renewable energy, road transportation still functions mainly with fossil fuels. Transport represents 28.2% of global greenhouse gas (hereafter GHG) emissions. Over 90 percent of the fuel used for transportation is petroleum based, which includes primarily gasoline and diesel [1]. Substantial reductions in CO_2 emissions from the transport sector can be achieved by increasing vehicle and modal efficiency, reducing travel demand, and changing travel patterns toward more efficient modes. However, achieving deep CO_2 reductions will also require a shift to very low-carbon energy carriers, of which the three most likely to play a prominent role are electricity, biofuels, and hydrogen.

Biofuel, a sustainable energy offers a strategic solution in addressing current energy and environmental crises that emerge from a heavy dependence on fossil fuels. The U.S. Energy Information Administration's (EIA) Annual Energy Outlook 2020 (AEO2020) projects that U.S. biofuel production will slowly grow through 2050, primarily driven by economic and policy factors resulting in 55% growth in biofuels production in 2050. Biofuels like ethanol are currently produced from renewable processes such as the fermentation of glucose. The fermentation of biomass (e.g., grains, starches, sugars, cellulose) to alcohols is a well-established technology. It is the primary step in the production of various beverages and alcohol fuels. Although alternatives have been developed, batch operation is typical of most processes [2, 3]. As fermentation proceeds, the increase in product concentration hampers the microbial activity by product inhibition [2]. This is incentive to continually remove products as by-products. For batch operation, the target ethanol concentration in the fermentation broth is generally 5–8 wt. % relative to water. The removal of ethanol during fermentation also serves as a pre-concentration step. Currently, conventional distillation techniques are employed to concentrate the ethanol extracted from the fermentation broth (3–8 w/w% ethanol) to an azeotropic limit of 95 w/w% [4, 5]. However, a higher purity of ethanol (>99.5 w/w %) is required for combustible fuel application. Despite the advancements presented in the development of biofuel technology, many challenges in biofuel production and purification must be overcome before it can be widely accepted as a worthy substitute for fossil fuels. The global focus on greener technologies also requires the development of separation techniques that are both energy efficient and environmentally friendly.

Membrane technology has been growing over the past 30 years. Today, membrane processes have progressively matured and are industrially available for the large-scale separation of various mixtures within the chemical and biochemical industries. They are recognized as being economical and a feasible substitute for conventional energy-intensive separations. Membrane separation process is a process where a membrane, acting as a filter separates individual elements in an aqueous solution by eliminating unwanted substances and selectively other components to pass through the membrane. Membranes can change the composition of a solution depending on the rate of relative permeation. It has a wide range of applications such as reverse osmosis, gas separations, controlled release of pharmaceutical formulations, and the artificial kidney. The scientific and engineering disciplines involved include physical and polymer chemistry, electrochemistry, and chemical engineering. However, the common link that connects all these different applications and disciplines together is the transport across membranes.

Several approaches have been proposed for the removal of ethanol from fermentation broths. In vacuum fermentation, the fermenter pressure is reduced to vaporize ethanol without increasing the critical broth temperature. In extractive fermentation, ethanol is selectively removed by other solvents. In the last few years, attention has been directed toward membrane processes for this application. Numerous studies have been performed to test the application of pervaporation [6-8]. Pervaporation involves the preferential passage of ethanol through a dense membrane matrix. Although pervaporation is a promising solution, additional efforts will be required to develop a highly ethanol-selective membrane and to increase the flux [9].

Membrane distillation (MD) is an emerging membrane-based technology which can fulfil the demands of pure water. The driving force for the separation is the vapor pressure gradient that enables separation of the liquid and the vapor phase within the membrane pores using a microporous hydrophobic membrane. Water vapor is driven by the high partial pressure at the hot feed side passing through the porous membrane, and the water is condensed at the permeate side that has lower water vapor pressure [10]. MD has been successfully tested for desalination [11], purification applications [12], and other wastewater treatments [13]. For these purposes, MD can be used as a stand-alone system and a hybrid process [14, 15]. MD consists of a hot feed side, a membrane, and a membrane module, and a permeate condensing side. With simple units, this makes MD easy to operate. Compared to pressure driven membrane processes, MD has much lower membrane fouling and has high solute or salt rejection [16]. In addition, MD can be performed at low temperatures (30-70 ºC), so low grade energies such as heat waste, solar power, and geothermal energy have been used for MD operation [17, 18].Vapors formed are able to pass through the membrane, whereas the liquid feed including dissolved components, is retained by the membrane. Thus, this technique can be used for the separation of non-volatile solutes from water, removal of volatile organic compounds from water, where the volatile organic compounds pass through the membrane pores faster compared to the less volatile water molecules.

Techniques such as membrane distillation, reverse osmosis, and CO_2 removal from natural gas for water and gas purification are membrane-based processes. Therefore, the development and expansion of advanced membrane-based separation technologies with controlled pore size is of utmost importance for achieving a more effective and cost-

efficient purification. Current polymeric membranes suffer from limitations between selectivity and permeability, and prone to membrane fouling and demonstrate low chemical resistance. The unique and tunable properties of carbon-based nanomaterials can be used for identifying and addressing environmental challenges. Therefore, in this dissertation, the approaches to separate Volatile Organic Compounds (VOCs) from their aqueous medium and production of biofuels using carbon-based nanomaterials via membrane distillation and later a hybrid system are presented.

CHAPTER 2

LITERATURE REVIEW

2.1 Background of Membrane Distillation

Increasing industrial growth in various sectors such as in oil and gas, petrochemical, pharmaceutical, metallurgical and food industries resulted in the production of a huge quantity of wastewater. Alongside, rapid population growth worldwide have resulted in increased demand for clean water particularly in arid regions [19]. Hence, the present surface resources will be no longer adequate to meet the needs of future generations.

Reusing water is a potential option to overcome the above-mentioned challenges which requires the development of advanced technologies, such as membrane technologies. The membrane separation market is rapidly growing due to continuous research efforts and development in both academia and industries. Furthermore, the membrane separation technology is a relatively new technology for use in desalination to generate pure water and other applications such as the separation of oil/water mixture to efficiently eliminate the oil droplets which current commercial technologies cannot [20-22]. Adsorption using activated carbon, zeolites and resins, oxidation, electrochemical process, photocatalytic treatment, Fenton process, ozone treatment, ionic liquids at room temperature has major drawbacks such as high cost, usage of toxic compounds, large footprint and production of secondary pollutants. Membrane based separation techniques serve as an emerging development in the 21st century. However, a major challenge in separation-based processes, membrane fouling, persists in the separation industries.

Loeb and Sourirajan [23] developed the industrial scale defect-free, high-flux, and anisotropic RO thin film composite membranes. The RO membrane resulted in significantly higher flux than that of other commercial membranes in desalination. The first successful artificial kidney in the Netherlands was developed by Kolf in 1944 and took several years to get commercialized [24]. The membrane techniques by Alza are widely used in the pharmaceutical industry to improve the efficiency and safety of drug delivery.

The applications of membrane technology are widespread and performs without addition of chemicals, with lower energy consumption and is easy to handle. Membranes show more efficiency in creation of process water from ground water, surface water or wastewater and becoming increasingly competitive for conventional techniques in water purification.

The mechanism of membrane separation relies on three basic principles: adsorption, sieving and electrostatic phenomenon. The adsorption mechanism has been correlated with solute and membrane hydrophobic interactions. This interaction results in a decrease in the pore size of the membranes leading to more rejection of unwanted solutes. The pressure-driven membrane processes mainly consist of microfiltration (MF), ultrafiltration (UF), nanofiltration (NF) and reverse osmosis (RO). They are conceptually similar but the key difference is surface pore size of the membranes which defines their applications [25].

UF is one of the most effective treatments for wastewater among the other pressure driven membrane processes and requires no external chemical additives and has low energy costs [26]. The UF membranes showed around 96% rejection of total hydrocarbon concentration, 54% rejection of benzene, toluene, and xylene (BTX), and 95% rejection of

some heavy metals like Cu, and Zn. This efficiency was not observed in MF membranes as reported in another study [27]. Microfiltration membranes can achieve high flux, however, if salt content in the wastewater is too high, it can be treated by reverse osmosis and nanofiltration membranes [28].

Besides the aforementioned membrane processes, forward osmosis (FO), an osmotically driven membrane process, is an emerging treatment which requires a minimal hydraulic pressure and offers several advantages such as, lower fouling tendency, simpler fouling removal and high recovery of pure water [29, 30]. Although some applications have at present developed significantly, some challenges are still required to be addressed to overcome the issues with respect to separation performance, antifouling property, and long-time stability.

Most of membrane transport processes are isothermal and their driving forces are transmembrane hydrostatic pressures, concentrations, electrical or chemical potentials. Membrane distillation (MD) is a non-isothermal process known for more than forty years but still needs improvement for its industrial implementation. The first patent was filed by Bodell in 1968 [31]. However, the process did not garner interest until the early of 1980s when membranes such as Gore-Tex Membrane (expanded polytetrafluoroethylene, PTFE, porous membrane supplied by Gore & Associated Co.) and modules with better characteristics became available [32, 33].

The term MD is like conventional distillation (i.e., simple, and multi-effect distillation) in terms of theory (vapor/liquid equilibrium) for separation and heat requirement to obtain the essential latent heat of vaporization. It is a non-isothermal membrane process in which the driving force is the partial pressure gradient across a

membrane that is porous, not wetted by the process liquids, does not alter the vapor/liquid equilibrium of the involved species, does not permit condensation to occur inside its pores, and is maintained in direct contact with the hot feed liquid solution to be treated.

The potential applications of MD are production of high-purity water, concentration of ionic, colloid, or other non-volatile aqueous solutions and removal of trace volatile organic compounds (VOCs) from wastewater. Various applications (desalination, environmental/waste cleanup, water-reuse, food, medical, etc.) have been studied using MD. All these characteristics make MD attractive within the academic community as a didactic application. Furthermore, the lower operating temperatures than the conventional distillation, the lower operating hydrostatic pressures than the pressure-driven processes (i.e., reverse osmosis, nanofiltration, ultrafiltration and microfiltration), the less demanding membrane mechanical properties and the high rejection factor achieved when solutions containing no-volatile solutes (salts, colloids, etc.) make MD more attractive than other popular separation processes. Additionally, the possibility of using waste heat and renewable energy sources enable MD technique to cooperate in conjunction with other processes in an industrial scale.

2.2 MD Configurations

A variety of methods is used to apply a low vapor pressure on permeate side, distinguishing the four basic configurations (Figure 2.1). In direct contact membrane distillation (DCMD), a cold liquid is in direct contact with the membrane on permeate side, while an additional compartment with an air gap separates a cold condensing plate from the membrane in air gap membrane distillation (AGMD). A cold sweep gas provides the driving force in sweep

gas membrane distillation (SGMD) and a vacuum pressure is applied on the permeate side in vacuum membrane distillation (VMD). Recently, also permeate gap membrane distillation (PGMD) is introduced as a hybrid configuration combining AGMD and DCMD, where the gap between membrane and cold condensing foil is filled with permeate. All these configurations have their own advantages and disadvantages, which are thoroughly described in literature and summarized in Table 1. In this section, different MD configurations that have been utilized to separate aqueous feed solution using a microporous hydrophobic membrane will be addressed.

2.2.1 Direct Contact Membrane Distillation (DCMD)

In this configuration, the hot solution (feed) is in direct contact with the hot membrane side surface. Therefore, evaporation takes place at the feed-membrane surface. The vapor is moved by the pressure difference across the membrane to the permeate side and condenses inside the membrane module. Because of the hydrophobic characteristic, the feed cannot penetrate the membrane (only the gas phase exists inside the membrane pores). DCMD is the simplest MD configuration and is widely employed in desalination processes and concentration of aqueous solutions in food industries, or acids manufacturing [16]. The main drawback of this design is the heat lost by conduction.

2.2.2 Air Gap Membrane Distillation (AGMD)

The feed solution is in direct contact with the hot side of the membrane surface only. Stagnant air is introduced between the membrane and the condensation surface. The vapor crosses the air gap to condense over the cold surface inside the membrane cell. The benefit of this design is the reduced heat lost by conduction. However, additional resistance to mass transfer is created, which is considered a disadvantage. This configuration is suitable for desalination and removing volatile compounds from aqueous solutions.

2.2.3 Sweep Gas Membrane Distillation (SGMD)

SGMD is a membrane distillation (MD) configuration in which a stripping gas is used as a carrier for the vapor transferred from a warm aqueous feed through a porous hydrophobic membrane. The nature of the membrane prevents from penetration of liquid into the pores; therefore, the liquid/vapor interface is formed at each pore entrance. The volatile molecules evaporate through the membrane pores, and a cold inert gas flowing along the other side of the membrane sweeps the permeate carrying it away from the module. The condensation of the vapor occurs in an external condenser. The driving force for the mass transfer in SGMD is the difference in the partial pressure of volatile substances on both sides of the membrane. Since in MD heat is transferred from the feed side through the membrane, thus the sweep gas temperature increases considerably along a module. However, SGMD combines a relatively low conductive heat loss through the membrane with a reduced mass transfer resistance.

2.2.4 Vacuum Membrane Distillation (VMD)

Vacuum membrane distillation (VMD) is believed to be attractive and cost-competitive membrane separation technology [34]. The vacuum pressure is applied to the permeate side

of the membrane [35] and it is maintained at just less than the saturation pressure of the volatile solvent to be separated from the hot feed solution [34]. Vacuum membrane distillation is characterized by a lower operating temperature, lower operating hydrostatic pressure, and less demanding membrane mechanical properties, and higher salt rejection can be achieved for non-volatile solutes. Compared with the other MD configurations, VMD permits higher partial pressure gradients, and hence higher permeate flux can be achieved. Besides, it overshoots reverse osmosis (RO) in reducing the energy consumption [36]. Also, higher permeation flux and lesser negative environmental impact can be produced when VMD is coupled with RO as a complementary process, wherein a high concentrated RO brine can be converted to fresh water [37].

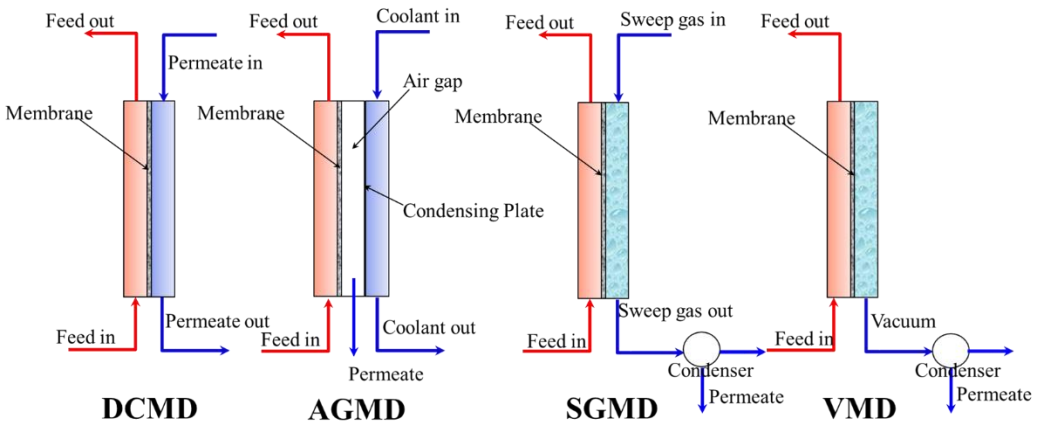

Figure 2.1 Schematic of MD configurations.

Table 2.1 Configurations and their Advantages and Disadvantages

Configuration	Advantages	Disadvantages
DCMD	High flux and simplicity in design Internal heat recovery is feasible.	High temperature and concentration polarization. High heat loss by conduction. Low thermal efficiency.
AGMD	Highest energy efficiency. High permeate flux. Low conductive heat loss. Low fouling tendency. Internal heat recovery is feasible.	Creation of additional mass transfer resistance. Lowest obtained output ratio. Difficulty in module designing and modeling.
SGMD	Low conductive heat loss. Low mass transfer resistance.	Low flux. Difficulty of heat recovery. Required large external condenser.
VMD	Highest permeate flux. Negligible conductive heat loss. Very low thermal polarization.	Higher possibility of membrane pore wetting. High membrane fouling. Low selectivity. Required vacuum pump and external condenser. Difficulty in heat recovery.

2.3 MD Membranes

2.3.1 MD Membrane Characteristics

Some of the key MD membrane characteristics include the following:

a) The membrane may be that of a single-layer or multi-layers with the requirement of at least one layer being made of a hydrophobic material and porous.

b) The pore size range may be from several nanometers to few micrometers. The pore size distribution should be as narrow as possible, and the feed liquid should not penetrate the pores. The liquid entry pressure (LEP), defined as the minimum transmembrane pressure that is required for distilled water or other feed solutions to enter the pore, by overcoming the hydrophobic forces, should be as high as possible. Otherwise pore wetting will occur leading to the deterioration of the quality and rate of the production. The LEP is a characteristic of each membrane and a high LEP can be achieved by using materials of low surface energy or high

hydrophobicity (i.e., large contact angles to water and feed solutions) and small maximum pore size. However, a small maximum pore size indicates small mean pore size and, consequently, low membrane permeability. Therefore, a compromise between the high LEP and the high productivity should be made by choosing an appropriate pore size and pore size distribution.

c) The tortuosity factor (i.e., the measure of the deviation of the pore structure from straight cylindrical pores normal to the surface) should be small. This is inversely proportional to the MD membrane permeability. In MD studies, to predict the transmembrane flux, a value of 2 is frequently assumed for membrane tortuosity factor or used as an adjusting parameter in theoretical models.

d) The porosity (void volume fraction open to MD vapor flux) of the single-layer membrane or that of the hydrophobic layer in the case of multi-layered membranes should be as high as possible. This is proportional to the MD membrane permeability. In fact, membranes with higher porosity can provide large spaces for evaporation. Therefore, it is generally agreed upon that the higher membrane porosity results in the higher permeate flux regardless of the MD configuration.

e) The thickness of the single-layer membrane should have an optimized value as the thickness is inversely proportional to the rate of mass and heat transport through the membrane. In case of multi-layered membranes, the hydrophobic layer thickness should be as thin as possible. While a high mass transport is favored for the MD process, a high heat transport is a heat loss. Therefore, a compromise should be made, again, between the mass and heat transfer, by properly adjusting the membrane thickness. One advantage of the multi-layered membrane is that a high mass transport is enabled by making the hydrophobic layer as thin as possible, while a low heat transfer is enabled by making the overall membrane thickness (hydrophobic layer + hydrophilic layer) as thick as possible.

f) The thermal conductivity of the membrane material should be as low as possible. It must be mentioned that most of the hydrophobic polymers have quite similar thermal conductivity coefficients, within the same order of magnitude. The thermal conductivity of commercial membranes lies between 0.04 W/m K and 0.06 W/m K. However, it is possible to diminish the membrane heat transfer by conduction using membranes of high porosities, since the conductive heat transfer coefficients of the gases entrapped in the pores are an order of magnitude smaller than most of the used membrane materials. Another possibility is to use bi-layered or multi-layered composite porous membranes with hydrophobic and hydrophilic layers. As previously mentioned, the hydrophobic layer must be as thin as possible. Furthermore, supported membranes can be used as a MD membrane. The purpose of using the hydrophilic layer is to enhance the resistance for the conductive heat transfer resistance and to make the membrane strong enough to prevent its deflection and rupture. However, the hydrophilic layer should not increase the mass transfer resistance considerably.

g) The membrane surface contacting the feed solution should be made of a material of high fouling resistance, although fouling effect in MD is not as strong as it is in pressure-driven membrane separation processes. Membrane surface modification can be achieved by either coating the surface with a thin layer of a fouling resistant material or following other possible membrane modification techniques depending on the feed solution to be treated.

h) The membrane should exhibit good thermal stability. Long term stability is required for MD membranes at temperatures as high as 100 °C.

i) The membrane material should have excellent chemical resistance to various feed solutions. If the membrane must be cleaned, resistance to acid and base components is necessary.

j) Finally, the membrane should have a long life with a stable MD performance (permeability and selectivity).

The above-mentioned features considerably determine the morphology and structure of the MD membranes and whether they have high transmembrane fluxes and rejection factors together with high heat efficiencies (i.e., low heat transfer by conduction). To summarize, the main requirements for the MD membrane are that the membrane must exhibit low resistance to mass transfer, must not be wetted by the aqueous solutions in contact with and only vapor and non-condensable gases are present within its pores during the MD operation. As water is usually the major component in the feed solution, the membrane must be hydrophobic and therefore must be made of polymers or inorganic materials with low surface energies. It is generally agreed upon, that the MD permeate flux will increase with an increase in the membrane porosity and pore size under some limitations, which means that the pore size should allow a sufficiently high LEP, and with a decrease of the membrane thickness and pore tortuosity. In other words, to obtain a high MD permeability, the hydrophobic layer that governs the MD transport should be as thin as possible and its porosity as well as pore size should be as large as possible. A relatively simple way to fulfill all the previously mentioned requirements is to use layered

porous hydrophilic and hydrophobic composite membranes. The hydrophobic thin layer will prevent the penetration of liquid solutions (i.e., water) into the pores, minimize the resistance to the mass transfer and both the hydrophobic and hydrophilic layers will contribute to the overall resistance to the heat transfer. Hydrophobic (non-wetting) microporous membranes are used in the MD process. These membranes are made from polytetrafluoroethylene (PTFE), polypropylene (PP) or polyvinylidene fluoride (PVDF). In general, the membrane used in the MD system should have low resistance to mass transfer and low thermal conductivity to prevent heat loss across the membrane. In addition, the membrane should have good thermal stability in extreme temperatures, and high resistance to chemicals, such as acids and bases.

2.3.1.1 Liquid entry pressure (wetting pressure). Liquid entry pressure (LEP) is a significant membrane characteristic. The feed liquid must not penetrate the membrane pores; so, the pressure applied should not exceed the limit, or LEP, where the liquid (i.e., aqueous solution) penetrates the hydrophobic membrane. LEP depends on the maximum pore size and the membrane hydrophobicity. It is directly related to feed concentration and the presence of organic solutes, which usually reduce the LEP. For example, LEP linearly decreases when ethanol concentration increases in the solution[38]. In addition, Garcia-Payo et al. [39] indicated that LEP is strongly dependent on the alcohol type, alcohol concentration in the aqueous solution, and solution temperature.

According to Franken et al. [40], LEP can be estimated from Equation 2.1:

$$\Delta P = P_f - P_p = -\frac{2\,\beta_{\gamma L} cos\,\theta}{r_{max}} \tag{2.1}$$

where P_f *and* P_p are the hydraulic pressure on the feed and permeate side, B is a geometric pore coefficient (equal to 1 for cylindrical pores), γ_l is liquid surface tension, θ contact angle and r_{max} is the maximum pore size. The contact angle of a water droplet on a Teflon surface varies from 108° to 115°; 107° for PVDF [41] and 120° for PP [42]. It is worthwhile indicating that a flat ceramic membrane made by S. Khemakhem and R. Ben Amar [43] had a contact angle varying from 177° to 179°. Moreover, ceramic zirconia and titania hydrophobic membranes were prepared with a 160° contact angle [44].

With regard to surface tension, Zianhua et al. [45] studied the impact of salt concentration (NaCl) on the water and found that surface tension for pure water surface tension at 25 °Cis 72 mN/m. As a result, membranes that have a high contact angle (high hydrophobicity), small pore size, low surface energy and high surface tension for the feed solution possess a high LEP value [46]. The maximum pore size to prevent wetting should be between 0.1–0.6 μm [47]. Moreover, the possibility of liquid penetration in VMD is higher than other MD configurations, so a small pore size is recommended [48].

2.3.1.2. Membrane thickness. The membrane thickness is a significant characteristic in the MD system. There is an inversely proportional relationship between the membrane thickness and the permeate flux. The permeate flux is reduced as the membrane becomes thicker, because the mass transfer resistance increases, while heat loss is also reduced as the membrane thickness increases. Membrane morphology, such as thickness and pore size distribution, has been studied theoretically by Lagana. et al. [49]. They concluded that the optimum membrane thickness lies between 30–60 μm. It is worth noting that the effect of membrane thickness in AGMD can be neglected, because the stagnant air gap represents the predominant resistance to mass transfer.

2.3.1.3. Membrane porosity and tortuosity. Membrane porosity refers to the void volume fraction of the membrane (defined as the volume of the pores divided by the total volume of the membrane). Higher porosity membranes have a larger evaporation surface area. Two types of liquid are used to estimate membrane porosity. The first penetrates the membrane pores (e.g., isopropyl alcohol, IPA), while the other, like water, and does not. In general, a membrane with high porosity has higher permeate flux and lower conductive heat loss. The porosity (ε) can be determined by the Smolder–Franken equation [50]

$$\in = \frac{1 - \rho_m}{\rho_{pol}} \tag{2.2}$$

where ρ_m and ρ_{pol} are the densities of membrane and polymer material, respectively.

Tortuosity (τ) is the deviation of the pore structure from the cylindrical shape. As a result, the higher the tortuosity value, the lower the permeate flux. The most successful correlation was suggested by Macki–Meares [51], where:

$$\tau = \frac{(2 - \epsilon)^2}{\epsilon} \quad (2.3)$$

2.3.1.4 Mean pore size and pore size distribution. Membranes with pore size between 100 nm to 1 μm are usually used in MD systems [34]. The permeate flux increases with increasing membrane pore size [52]. The mechanism of mass transfer can be determined, and the permeate flux calculated, based on the membrane pore size and the mean free path through the membrane pores taken by transferred molecules (water vapor). Generally, the mean pore size is used to determine the vapor flux. A large pore size is required for high permeate flux, while the pore size should be small to avoid liquid penetration. As a result, the optimum pore size should be determined for each feed solution and operating condition.

In fact, the membrane does not have a uniform pore size so more than mass transfer mechanisms occur simultaneously (depending to the pore size). There are several investigations examine the importance of pore size distribution in MD flux [53-55]. Khayet et al. [54] reported that, care must be taken when mean pore size is utilized to calculate vapor transfer coefficient instead of pore size distribution. However, Martinez et al [55] obtained a similar vapor transfer coefficient when the mean pore size and pore size distribution were used. Better understanding of membrane morphology such as pore size, pore size distribution, porosity, and thickness directs to have an accurate mass and heat transfer modelling. Regarding to the MD membrane, two types of characteristics can be analyzed, the structural characteristic and the actual separation parameters (permeation) [52, 56].

2.3.2. Membrane Modules

2.3.2.1. Plate and frame. The membrane and the spacers are layered together between two plates (e.g., flat sheet). The flat sheet membrane configuration is widely used on laboratory scale because it is easy to clean and replace. However, the packing density, which is the ratio of membrane area to the packing volume, is low and a membrane support is required. The flat sheet membrane is used widely in MD applications, such as desalination and water treatment.

2.3.2.2 Hollow fiber. The hollow fiber module, which has been used in MD, has thousands of hollow fibers bundled and sealed inside a shell tube. The feed solution flows through the hollow fiber and the permeate is collected on the outside of the membrane fiber (inside-outside), or the feed solution flows from outside the hollow fibers and the permeate is collected inside the hollow fiber (outside-inside) [42]. For instance, Lagana. et al. [49] and Fujii. et al. [57] implemented a hollow fiber module (DCMD configuration) to concentrate apple juice and alcohol respectively. Also, saline wastewater was treated successfully in a capillary polypropylene membrane [58]. The main advantages of the hollow fiber module are very high packing density and low energy consumption. On the other hand, it has high tendency to fouling and is difficult to clean and maintain. It is worth mentioning that, if feed solution penetrates the membrane pores in shell and tube modules, the whole module should be changed [42, 59].

2.3.2.3. Tubular membrane. In this sort of modules, the membrane is tube-shaped and inserted between two cylindrical chambers (hot and cold fluid chambers). In the commercial field, the tubular module is more attractive, because it has low tendency to fouling, easy to clean and has a high effective area. However, the packing density of this module is low, and it has a high operating cost. Tubular membranes are also utilized in MD. Tubular ceramic membranes were employed in three MD configurations: DCMD, AGMD and VMD to treat NaCl aqueous solution, where salt rejection was more than 99% [44].

2.3.2.4 Spiral wound membrane. In this type, flat sheet membrane and spacers are enveloped and rolled around a perforated central collection tube. The feed moves across the membrane surface in an axial direction, while the permeate flows radially to the center and exits through the collection tube. The spiral wound membrane has good packing density, average tendency to fouling and acceptable energy consumption.

It is worth stating that there are two possibilities for flow in a microfiltration system: cross flow and dead-end flow. For cross flow, which is used in MD, the feed solution is pumped tangentially to the membrane. The permeate passes through the membrane, while the feed is recirculated. However, all the feed passes through the membrane in the dead-end type [59].

2.3.3. Types of MD Membranes

The requirement of MD membranes is that at least one of the layers should be made of a hydrophobic material and be porous. The pore size range of MD membranes range from several nanometers to a few micrometers. The membrane should exhibit good thermal stability and long-term stability. The membrane material should have superior chemical

resistance to various feed solutions. The commercially used MD hydrophobic membranes are made of different polymers such as polypropylene (PP), polyvinylidene fluoride (PVDF), polytetrafluoroethylene (PTFE) and polyethylene (PE) available in tubular, capillary or flat sheet forms have been used in MD experiments. Detailed explanations of the used characterization techniques of some commercial membranes may be found elsewhere [60].

It is worth quoting that PTFE represents an ideal material for MD membrane fabrication owing to its super- hydrophobic nature among polymers and possess one of the best chemical resistance and thermal stability. The basic disadvantage of PTFE lies in its challenging process ability. Commercial PTFE membranes are usually manufactured through extrusion, rolling and stretching or sintering procedures [61]. Other polymers such as PP and PVDF can also be employed as MD membranes which are manufactured by either molten extrusion technique followed by stretching or by thermal phase separation process that requires dissolution of the polymer at high temperature in solvents[61]. PVDF on the other hand can be easily produced by phase inversion process, by simply immersing the cast solution film in a coagulant bath.

Compared to the synthetic membranes fabricated for different membrane processes such as reverse osmosis (RO), pervaporation (PV), ultrafiltration (UF), nanofiltration (NF) and gas separation, limited research has been performed on the fabrication and modification of membranes for MD process specifically. As defined earlier, the MD membrane architecture must display specific features and achieve specific requirements. Therefore, the study on the fabrication of MD membranes is very essential. Some noteworthy results have been accomplished over the last 6 years on the fabrication and

modification of polymeric membranes for MD applications leading to an increase in reliability for the MD process which will be discussed in this review.

Improved MD membranes with specific morphology and structure are highly required for commercialization of the process. Membranes with varied pore sizes, porosities, thicknesses, materials are required to carry out systematic MD studies for a detailed understanding of the mass transport in different MD configurations and thus improving the permeate flux and selectivity.

Hydrophobic porous membranes can be prepared by different methods depending on the properties of the chosen materials. Microporous membranes can be made by sintering, stretching, phase inversion or thermally induced phase separation (TIPS) [62, 63]. Moreover, various physical and chemical techniques have been performed for membrane surface modification including coating, grafting, plasma polymerization, etc. Recently, copolymers like poly(vinylidenefluoride-hexafluoropropylene) (PVDF-HFP) and polyvinylidenefluoride-tetrafluoroethylene (PVDF-TFE) are employed in the preparation of MD membranes in flat sheet or hollow fiber using the phase inversion technique[64-67]. Membrane surface modification using different technologies such as grafting, differential chemical etching, coating, or blending fluorinated surface modifying macromolecules (SMMs) with hydrophilic polymers have been also tested for different MD systems and configurations [44, 67-71]. In the recent past attempts were made to use nanofiber membranes prepared by electro-spinning method in AGMD desalination [72] and carbon nanotube bucky-paper membranes in DCMD desalination[73] which will be discussed in more details in the later sections of this thesis.

2.3.3.1. Carbon Nanotubes (CNTs) Membranes. Carbon nanotubes (CNTs) have gained significant interest since their discovery in 1991 [74] owing to their exceptional mechanical, optical, and electrical properties that make them suitable for a wide range of applications including catalysis, electronics, environmental applications and molecular sensing [75-77]. CNTs are made of cylindrical graphite sheets rolled up in a tube like structure [78]. Single-walled carbon nanotubes (SWCNTs) have cylindrical shape with single shell of graphene and multi-walled carbon nanotubes (MWCNTs) have multiple layers of graphene sheets. Both SWCNTs and MWCNTs have been used for direct water desalination [79-81] or indirectly to remove contaminants that complicate the desalination processes [82].CNTs are excellent materials for electrode production for use in desalination of water using a flow through capacitor [83, 84]. Single, double, and multi-walled carbon nanotubes have been made of various sizes, and modern fabrication techniques have facilitated the arrangement of tube alignment of controllable sizes [85-87] and within membranes [88-91] which has opened the door to potential filtration applications. Measurements have shown selective gas transport via carbon nanotube membranes [91] in support of preceding simulation studies [92].

Properly aligned CNTs can serve as robust pores in membranes for water desalination and decontamination based uses [93]. The hollow CNT structure delivers frictionless transport of water molecules, thus making them appropriate for the growth of high flux separation methods. Suitable pore diameters can establish energy barriers at the channel entrances, eliminating salt ions and allowing water to pass through the nanotube hollows [94]. CNT pores can be modified to selectively sense and reject unwanted solutes [95]. CNTs have antifouling, self-cleaning and reusable features. Efforts have been made

to demonstrate potential of CNT membranes to resolve water desalination and resource concentration and recovery. CNT-membranes deliver almost frictionless flow of water through them by retaining an extensive spectrum of water contaminants. The inner hollow cavities, high aspect ratios, smooth hydrophobic walls of CNTs allow super-efficient transport of water molecules.

2.3.3.1.1 Bucky paper Carbon Nanotubes.

Bucky paper (BP) CNTs refer to the randomly entangled CNTs into a non-woven, paper-like, structure with a porous 3D network, highly flexible, mechanically robust and has large specific surface area [96]. Owing to the simple preparation technique, Bucky-papers were one of the first macroscopic structures invented from CNTs and their mechanical, electrical, and thermal properties have been comprehensively investigated [73, 97-102]. CNTs tend to agglomerate due to van der Waals interactions, and it is these van der Waals interactions which also hold the CNTs together into a cohesive Bucky-paper. Longer, fewer walled and pure nanotubes usually lead to stronger Bucky papers with greater tensile strengths[98, 103]. Increasing the MWNT diameter reduces the attractive van der Waals forces between CNTs, leading to lower tensile strength and poor cohesiveness of the BPs. Functionalization of MWNTs or the addition of polymers can improve the tensile strength to some extent [98].

Commercial MD membranes such as PP, PVDF and PTFE are highly hydrophobic, expensive and difficult to process [104]. It is therefore vital to explore other choices as well as techniques for enhancing the process efficiency by altering the membrane properties and structure. CNT Bucky-Paper (BP) membranes, which is a paper-like structure of CNTs

processed by vacuum filtration [105] have been applied extensively in MD processes by Dumee et.al [73].

The CNTs were grown by chemical vapor deposition (CVD). A 1–5 nm thick iron catalyst film was deposited onto a silicon substrate bearing a thin silicon dioxide layer. A mixture of helium (95%)–acetylene (5%) was used as the carbon feedstock and heated to between 650 and 750 °C. The CNTs produced had an outer diameter of ∼10–15 nm and length of 150–300 μm.[106]. The CNT BP membranes were processed by vacuum filtration of CNTs dispersed in 99.8% pure propan-2-ol[73]. Well-dispersed CNT suspensions were obtained by repeated sonication for 15 min intervals at a power of 150 W. Vacuum filtration was performed with a 47 mm diameter Millipore filtration unit with house line vacuum. The CNTs were filtered onto a polyethersulphone (PES) membrane with 0.2-μm pore size and then peeled off to form a self-supporting membrane.

Another study reported the CNT-BP composite fabrication[107] where the grown CNTs were dispersed in propan-2-ol. The suspensions were sonicated up to 5 times, for 15 minutes and at 150 W, in a sonicating bath. Once well-dispersed, CNT suspensions were achieved which were filtered through a Millipore filtration unit. This study reported the fabrication of composite CNT BP membranes by three methods. The first method involved hot pressing the self-supporting BPs between two layers of porous PP supports making it a “sandwiched BP”. The three layers were maintained between two stainless steel plates and hot-pressed at low pressures for 15 min at 80^{o}C. The second method involved filtration of the suspensions of dispersed CNTs through a PP support with a PES membrane underneath with CNTs present on and within the pores of the PP support. The PP-CNT cake was sandwiched with another layer of PP support and the layers were hot-pressed

together under the same conditions as the first method. The third technique used partial embedding of self-supported BPs by vacuum filtration of a polymer/solvent solution, across the self-supporting membrane. Solutions at 5% of either Polystyrene (PS) or PVDF in Di-Methyl-Formamide (DMF) were used. After polymer infiltration, 99.99% pure DMF was filtered through the membrane to remove any non-bonded polymer.

Results showed that PTFE membranes are amongst the best available for MD[108] and as expected, the flux reached steady state after an initial settling period of ~15–20 min. The BPs on the other hand behaved differently where the flux initially increased over the first 15 min before stabilizing. However, it was observed that this stabilization was followed by a slow decline until the membrane broke. The origin of this declining flux is still uncertain. This could be due to several factors. It may be a result of temperature polarization as the BP membranes had a thermal conductivity 10 times higher than that of PTFE membrane. Different feed temperatures were investigated which showed that the temperature polarization coefficients for both the PTFE and BP membranes were always greater than 0.9. The authors indicated that temperature polarization is not a dominant effect. However further work is required to characterize the effects of temperature polarization more thoroughly and to determine its dependence on feed temperature and structure of the membrane.

Another study reported that the decline in BP membrane flux with time could be due to factors such as physical ageing of the membrane including micro-crack formation. The declining flux of the BP membranes may also result from gradual compaction of the membrane due to pressure from the hot and cold water streams [49, 109]. A previous study has shown that the permeate pressure plays a role in flux determination and membrane

behavior[110]. Self-supporting BP membranes were successfully operated in a DCMD setup to desalinate synthetic seawater achieving a flux on the order of 5–25 kg/m^2 h [73]. They also exhibited a high contact angle (113^0), high porosity (90%), and relatively low thermal conductivity of 2.7 kW/m^2 h with 99 % salt rejection. Results are encouraging as the BP membranes fabricated had no supports or binding agents and are a promising alternative to current polymeric membranes. The CNTs within the BP membrane were held together solely by Van der Waals interactions.

Gray et.al chemically modified high purity CNTs by UV/ozone treatment to create hydroxyl groups and substituted with alkoxysilane based groups [111]. The UV/ozone modified CNTs underwent a two-step alkoxysilane treatment to maintain hydrophobicity. This could possibly lead to increased hydroxyl group formation. Another alternative is coating with more hydrophobic additive materials such as fluoro-silane to engineer super-hydrophobic surfaces. However, different geometries or material supports should be taken into consideration for improving the performances of the membranes. Additional work is essential to completely comprehend their properties and behavior and to make the most of their potential in MD. Research is under way to fully characterize the BP thermal behavior and detect the role of heat diffusivity and heat conductivity on flux and temperature gradient. Other composite material membranes could be processed to optimize the performances of CNT BP membranes in MD.

2.3.3.1.2. CNT Mixed Matrix Membranes

Continues research and development is being carried out in both academia and industries on mixed matrix membranes due to their distinctive properties linking integral features of polymer and inorganic fillers. Mixed matrix membrane refers to incorporating

nanomaterials or solid particles into a continuous polymer dope solution. The application of these membranes is an excellent technique to achieve instrumental effects between the polymeric matrix and solid particles. Hollow fiber or the flat sheet membranes are prepared by the addition of solid particles into the polymer matrix via phase inversion. Solid particles include dispersed nanomaterials such as zeolite and carbon nanotubes in the polymer dope solution.

Compared to conventional MD membranes, the immobilization of CNTs in polymeric matrices (e.g. PVDF) results in the so-called MMMs, that has the potential to reduce the operating temperature of the MD process while increasing the water fluxes [112]. For instance, the advantageous effect of CNTs on MMMs has been described for polyamide membranes, and credited to the enhanced mechanical resistance of the membrane and both salt and organic matter rejection [113]. Despite their extraordinary properties, the CNT's tend to form bundles by van der Waals forces between the tubes[114], as well as their inert graphitic surface, may cause unwanted interaction with the polymer when composites are fabricated, thus limiting the CNTs effective dispersion.

In order to address this issue, functionalization of CNTs can enhance the sturdiness and stability of the membrane structure. A recent study employed MWCNTs in the fabrication of PVDF blended membranes, investigating various synthesis parameters such as the loading and surface chemistry of the MWCNTs and pore former loading. The resulting MWCNT/PVDF blended membranes were tested in DCMD of salty water and the membrane properties correlated with the performance obtained in terms of water permeation and salt rejection [115]. MWCNT/PVDF blended membranes were prepared by the phase inversion method where a suitable amount of MWCNTs was dispersed in 60

mL of NMP for 10 min by using an ultrasonic processor until achieving a uniform dispersion. PVP was added as pore forming agent. The PVDF polymer was passed through vacuum at high temperature overnight before dissolving in the NMP dispersion under continuous stirring at 70 °C for 2 h to form a homogeneous casting solution. The PVDF solution was cooled down to room temperature overnight to remove the air bubbles trapped within. The degassed solution was casted on a glass plate through spin-coating at high speed and then dipped immediately into a DI water coagulation bath at 22^0C to prompt precipitation of the PVDF by NMP/water mixture to make a defect free membrane. The membrane was peeled off from the glass dish and moved to another DI water bath to eliminate the residual solvent. Some authors have proposed natural drying after treatment to avoid pore collapse [116].

It was observed recently that on increasing the CNT loading up to an optimum of 0.2 wt. % resulted in membranes with large pore sizes, high pore density and sponge-like pores, also leading to the highest water flux obtained with salty water ($9.5 \times 10-3$ kg m^{-2} s^{-1}) while maintaining 100% salt rejection [115].

2.3.3.1.3. Electrospun CNT membranes

In recent years, electrospun membranes, a class of mixed matrix membranes have attracted significant interest for desalination and water reuse applications in membrane based processes [117]. Electrospinning involves the production of ultrafine fibers using high voltage electric field on a polymer solution [118]. Fabricated membranes demonstrate exceptional properties such as high hydrophobicity and porosity and high surface area to volume ratio compared to conventional membranes, thus making it an attractive alternative for MD applications [119]. Moreover, the properties of nanofibers such as layer thickness,

fiber diameter, and porosity can be altered by choosing materials and adding them into dope solution [119, 120].

Although the preparation of electrospun membranes for MD application has progressed in recent years, there are still limitations related to the durability, robustness, and mechanical stability of the membrane. Electrospun nanofiber membranes has already been prepared using many hydrophobic polymers [121-123] and they possess many excellent properties such as high porosity, interconnected open pores and hydrophobic surface [124-127]. The polymers used play a role in the hydrophobicity and cannot prevent wetting in long-term experimental studies. Thus, significant efforts have been devoted to render electrospun membrane surface more hydrophobic [128-131].

It has been stated that carbon-based composite membranes predominantly carbon nanotubes (CNTs) can significantly improve the performance as well as the membrane properties. Combination of the superior properties of electrospun membrane and the exceptional features of CNTs, a CNT/polymer composite nanofiber could result in ideal membrane properties required for MD performance enhancement. A recent study reported a one-step colloid electrospinning technique to develop robust, super hydrophobic nanofiber membranes for DCMD applications [132]. The upper thin layer was composed of CNT/polymer nanofiber and the thick bottom layer consisted of smooth, highly neat porous polymer nanofibers. The incorporation of pristine CNTs increased the surface roughness leading to a super hydrophobic surface (significant increase in contact angle compared to the commercial PVDF membrane). Incorporating CNTs increased the tensile strength of the fabricated membrane, improved permeate flux with a salt rejection of >

99.99 %, providing a scalable methodology for prospective mass manufacturing for MD applications.

Another study investigated the role of CNTs in the performance enhancement based on theoretical phenomena and modelling studies [133] [134]. The membranes were fabricated by dissolving the polymer dope (containing CNTs) into a mixture of DMF and acetone and electrospun at a rate of 0.7 mL/h with a voltage of 18 kV. The dope electrospinning stability was enhanced using lithium chloride. The residual solvent evaporated by putting the membrane surface under vacuum at 60 °C overnight. Results showed that although the improvement of the mass transfer can enhance the permeate flux; heat transfer modification is also required to explain the increase in the permeate flux of DCMD with the fabricated membranes.

Another study investigated CNT agglomeration as a result of incomplete distribution in aqueous environment [135] due to relatively long fabrication time. Thus, the electrospun CNT membranes become prone to beads formation and pore blocking. A spraying method was suggested to overcome this problem to form a homogeneous CNTs network on the membrane surface by spraying the CNTs/ethanol dispersion on membrane surface with rapid ethanol evaporation rate. The fabricated membranes were tested by VMD method and the results demonstrated that the CNT coated electrospun membranes possessed anti-wetting properties and higher water flux.

2.3.3.1.4. CNTs Immobilized on polymer surface

Recent studies have demonstrated immobilization of CNTs on different membrane surfaces that play a role in altering solute-membrane interactions, which is a predominant physicochemical factor affecting the permeability and selectivity of a membrane. The

CNTs serve as a sorbent and provide an additional pathway for transport of solute through the membrane. Surface coating of CNTs have been applied to solvent extraction and pervaporation [136] [137] and have demonstrated superior performance.

The CNT coating was prepared using hollow fiber as the starting material. MWCNTs were dispersed in a solution of acetone and PVDF (acts as a binder) and sonicated for 4 hours. The PVDF/CNTs dispersion was then forced under controlled vacuum into the pores of the polypropylene membrane [138]. Surface coating of CNTs (referred to as carbon nanotube immobilized membrane (CNIM)) resulted in a significantly higher flux and salt rejection for a wide range of salt concentrations over a conventional PVDF membrane.

Mitra.et.al reported the use of CNIM in SGMD that showed a significant enhancement in desalination [28]. Another recent study synthesized functionalized CNTs immobilized membranes on the hydrophobic porous PP support to generate pure water from high concentration brine mixtures. High water flux (36.8 kg/m^2 h) at 70 °C was achieved for CNT–COOH–PP membrane with salt rejection greater than 99.9%. This was credited to the fact that the CNTs serves as sorbent sites for vapor transport, rejecting the water [22]. The membranes showed stability over long period without any fouling and breakage. CNIM was also used in MD for concentrating pharmaceutical waste and simultaneously generating pure water [139] and in desalination applications via MD on PTFE membrane surface where the permeate flux reached a maximum of 77 kg/m^2 h [140]. Functionalized CNTs have been demonstrated in nanofiltration applications [141]. A recent study on MD investigated that effect of functionalization on the interaction of nanotubes with the polar water vapor which improved desalination efficiency [142].

Mitra.et al developed CNIM comprising of a two-layer structure with a layer of hydrophobic octadecyl amide group on the feed side and functionalized CNTs on the permeate side for water desalination by membrane distillation. It was observed that the hydrophobic CNTs led to higher water vapor permeation, while the hydrophilic CNTs enabled water vapor condensation leading to improved performance [143].Carbon nanotube immobilized membranes (CNIM) were also fabricated via phase inversion technique for water vapor diffusion. Significantly high water vapor flux (51.4 L/m^2 hr) was achieved with no salt leakage [144].

Enhanced ammonia separation using CNIM via DCMD has also been investigated. The flux with CNTs was 63% higher than the PTFE membrane, twice that of what has been reported before. Comparable trends were obtained for ammonia removal efficiency. The enhancement in ammonia removal is attributed to the favored chemisorption of ammonia on the CNTs [145]. Enhanced VOC removal from their aqueous mixtures via SGMD in the presence of CNTs where investigated [146]. The CNTs considerably altered the liquid–membrane interactions to promote solvent transport by impeding water penetration into the membrane pores. The solvent flux, separation factor and mass transfer coefficient were significantly higher with CNIM than the unmodified membrane at different experimental conditions with enhancement in separation factor reaching 350% at 70 °C. The enhancement in performance with CNIM was primarily due to the preferential sorption on the CNTs followed by rapid desorption from its surface. A very recent paper reported the scaling reduction in CNIM by the use of the antiscalants [147]. High salt concentrations were intentionally used to initiate scaling on the membranes where CNIM showed significantly improved antiscaling behavior. The CNTs enabled the removal of deposited

salts by washing and regained 97% of its initial water flux, whereas the polypropylene only regained 85% of the original value.

2.3.3.2 Graphene Based Membranes. Recently, graphene has been confirmed to be an excellent platform for developing size selective molecular separation membranes because of its atomic thickness, high mechanical strength, and chemical inertness [148, 149]. Graphene composes of a single layer of carbon atoms arranged in a sp^2 -bonded aromatic structure [150]. The delocalized electron clouds of π-orbitals occupy the voids of aromatic rings in a graphene sheet, thereby effectively preventing the permeation of even the smallest molecule, helium [151]. Therefore, graphene was tested to be an impermeable material in its pristine state. Nevertheless, protons were reported to be able to penetrate through monolayer graphene[152]. The impermeability of graphene for molecules makes it is applicable as a barrier layer for gases and liquids, or to protect metallic surfaces against corrosion [153, 154]. For molecular separation, a graphene-based membrane must be functionalized with nanopores or nanochannels through chemical or physical approaches. The typical graphene-based materials for this purpose are nanoporous graphene and graphene oxide (GO) membranes.

Graphene oxide (GO) nanosheets can be assembled into laminar structures via filtration or coating approaches, providing fast and selective 2D nano-channels for transporting small molecules. The pioneering work of Geim.et.al. found that submicrometer-thick laminates formed from GO can be completely impermeable to liquids, vapors and gases, but allow unimpeded permeation of water [155]. From then on, the assembled GO membranes have been reported for applications in water purification[156] and solvent dehydration [157, 158]. Meanwhile, graphene-based

laminates can also exhibit gas separation characteristics if their stacking structures are carefully controlled [159]. Apart from the all-graphene membranes, graphene-based composites [160, 161], which generally combined graphene or GO nanosheets with polymers or inorganics, have gained ground as a means of improving selective-permeation and/or anti-fouling properties of the pristine membranes. Graphene-based membranes constructed by different approaches possessed distinct microstructures and transport pathways, enabling them to be applied for various membrane processes such as pressure filtration (e.g., ultrafiltration [162] , nanofiltration [163], reverse osmosis[164], forward osmosis [165], pervaporation [157, 161, 166] and gas separation [159].

Graphene can be produced by four major methods: micro-mechanical exfoliation of graphite, chemical vapor deposition, epitaxial growth, and the reduction of graphene oxide (GO) [167]. The first three techniques can produce relatively perfect graphene structures; however, mass production of graphene from these methods is still questionable [168]. In comparison, GO can be produced by cost-effective methods with a high yield by using cheap graphite as the raw material. It shows attractive physical properties like those of graphene. In addition, GO possesses many functional groups such as hydroxyls and epoxides, which make it molecularly tunable on surface properties to ensure good compatibility with various polymer materials. However, since GO is inherently hydrophilic, incorporating GO into PVDF membranes would lower the contact angle and wetting resistance [169]. In addition, the different surface tensions between GO and PVDF may engender GO agglomeration and result in poor mixing in casting solutions. Therefore, surface modification of GO is necessary to increase its hydrophobicity and interaction with PVDF. Recently, some studies have successfully rendered hydrophobicity

to GO via alkyl amine functionalization [170]. The modified GO has been blended with polymers such as polyethylene to form nanocomposites with significantly high mechanical properties [171].

To enhance the mechanical properties and wetting resistance of poly (vinylidene fluoride) (PVDF) membranes for membrane distillation (MD) of seawater, a recent study added n-butylamine modified graphene oxide (GO-NBA) in PVDF flat-sheet and hollow fiber membranes. For the first time, it was found that the addition of GO-NBA leads to PVDF flat sheet membranes with greater mechanical properties than that of conventional GO because of better compatibility, dispersity, and crystalline structure. The addition of the GO-NBA also improved the mechanical properties of PVDF hollow fiber membranes in both tensile and hoop directions. With a small loading of 0.5 wt% GO-NBA in PVDF hollow fiber membranes, the maximum tensile stress, maximum tensile stain, and Young's modulus increase by 32%, 63% and 71%, respectively, while the liquid entry pressure (LEP) and burst pressure jump by 67% and 15%, respectively. Under direct contact membrane distillation (DCMD), the 0.5 wt% GO-NBA incorporated membrane shows a flux of 61.9 kg m-2 h-1 and a salt rejection of 99.9% using a model seawater as the feed at 80 °C [172]. Another study elucidated the influence of graphene (G) and graphene oxide (GO) content on the desalination performance and scaling characteristics of G/polyvinylidene fluoride (G/PVDF) mixed matrix and GO/PVDF composite-skin membranes, applied in a direct contact membrane distillation process (DCMD) [173]. Inclusion of high quality, nonoxidized, monolayered graphene sheets as polymer membrane filler, and application of a novel GO/water-bath coagulation method for the preparation of the GO/PVDF composite films, took place. Water permeability and

desalination tests via DCMD, revealed that the optimal G content was 0.87 wt %. At such concentration, the water vapor flux of the G/PVDF membrane was 1.7 times that of the nonmodified reference, while the salt rejection efficiency was significantly improved (99.8%) as compared to the neat PVDF. Similarly, the GO/PVDF surface-modified membrane, prepared using a GO dispersion with low concentration (0.5 g/ L), exhibited two-fold higher water vapor permeate flux as compared to the neat PVDF, but however, its salt rejection efficiency was moderate (80%), probably due to pore wetting during DCMD. The relatively low scaling tendency observed for both G and GO modified membranes was primarily attributed to their smoother surface texture as compared to neat PVDF, while scaling is caused by the deposition of calcite crystals, identified by XRPD analysis.

GO can be particularly attractive to MD for multiple reasons such as the selective sorption of water vapors, nanocapillary effect for selective sieving of pure water from brine and the reduction in temperature polarization. The pore chemistry of GO where the carbon atoms adjacent to the pores are preferentially hydroxylated or carboxylated are also expected to enhance flux [174]. Recent research has shown that GO can be used to fabricate high performance membranes either as the main constituent material or as an additive to other matrix materials. Owing to the abundant functional groups of GO, it can be readily functionalized with other molecules which can alter its properties [175]. Amongst these, is the functionalisation with silanes, which have been shown to improve the dispersability of GO in epoxy resins for composite materials [176] and improve the performance and mechanical strength of ultrafiltration membranes [177]. A recent study focused on the fabrication of high flux, robust membranes for the purification of artificial sea water by

incorporating graphene oxide functionalized with 3-(aminopropyl)triethoxysilane (APTS) into PVDF polymer solutions [178]. It was shown that the addition of GO and GO-APTS enhanced the permeate flux by 52% and 86%, respectively, compared to pure PVDF. These improvements were attributed to increased surface and bulk porosity, larger mean pore size and hydrophilic interactions owing to the functional groups of GO and GO-APTS.

2.4 MD Applications

MD is going to be an attractive technology for separation processes due to its unique properties. Dealing with water as a key component of chemical and physical processes and high separation factor are the most attractive characteristics of MD technology. Nowadays, MD is used in environmental, food, pharmaceutical, and nanotechnology industries. Also, MD can be used as a single-step process or can be combined with other separation techniques as a last stage [179]. Some applications of MD are the following:

1. Desalination of seawater, brackish water, groundwater, and brines brought from other units.
2. Industrial wastewater treatment including radioactive waste treatment, concentration of nonvolatile acids, volatile acid recovery from industrial effluents, salt recovery by membrane distillation crystallization (MDC), and textile industry effluents.
3. Preparation of distilled water, pure water, and ultrapure water for medical and pharmaceutical purposes.
4. Production of liquid food concentrates such as mandarin juice, sucrose solution, whey, and apple juice.
5. Volatiles removal from fruit juice, alcohols, halogenated VOCs, and benzene by VMD and SGMD.
6. Dealcoholization of fermented beverages and enhanced ethanol production using DCMD.
7. The most important MD application is desalination of wastewaters including high percentage of salt molecules for safe discharge into the environment or to produce drinkable, pure, and ultrapure water. The theoretical 100% rejection of nonvolatile

solutes, colloids, and biological matters by MD guarantees the elimination of all unwanted solutes that are often existing in water sources. The treated water by MD shows an electrical conductivity as low as 800 μS/cm with total dissolved solids (TDS) of 0.6 ppm [180].

CHAPTER 3

ENHANCED MEMBRANE DISTILLATION OF ORGANIC SOLVENTS FROM THEIR AQUEOUS MIXTURES USING A CARBON NANOTUBE IMMOBILIZED MEMBRANE

3.1 Introduction

Thermal distillation is one of the most common methods for the separation of liquid mixtures. However, this cannot be used to separate azeotropes where the composition remains unchanged in the vapor and liquid phases. Conventional distillation also has short comings such as high energy requirements, poor separation for close boiling liquids and heating to boiling point may lead to undesirable side reactions and deterioration to heat sensible materials. On the other hand, separation in membrane distillation (MD) is driven by a vapor pressure differential across a membrane which is created by having a hot feed and a lower permeate side temperature [181]. MD can be carried out at a temperature below the boiling point and shows high rejection of dissolved and non-volatile species. From a practical standpoint, the footprint of MD systems is smaller than the thermal distillation units and the hydrophobic porous membranes used in MD have relatively lower fouling than dense membranes used in other techniques such as reverse osmosis [182-185]. MD has been used in applications such as water desalination, solute concentration, and recovery of volatile compounds from aqueous solutions [46, 181, 186-189], and the low temperature operation has been facilitated by waste heat, low pressure steam and also solar energy [190, 191].

Among the different MD configurations, the sweep gas membrane distillation (SGMD) shows relatively low conductive heat loss and higher flux compared to direct

contact MD (DCMD), less energy consumption compared to vacuum MD (VMD), as well as simpler instrument design and higher flux compared to air gap MD (AGMD). SGMD typically shows lower flux in comparison to DCMD and VMD, however, since we are interested in removing a volatile species for later collection, having a sweeping gas in the permeate side allows relatively easier recovery of the organic solvent [192-194].

The enhancement of membrane performances by producing innovative membrane architecture is of significant importance for MD. Numerous membrane materials based on polypropylene (PP), polyvinylidene difluoride (PVDF) and Teflon have been used [45, 195]. Diversity in surface modification of MD membranes have been achieved by radiation graft polymerization, plasma polymerization, grafting ceramic membranes, hydrophobic or hydrophilic surface coating, casting hydrophobic polymer over flat sheet or porous fibers as supports, co-extrusion spinning and use of surface modifying macromolecules (SMMs) [68, 69, 144, 196-200]. A double-layer hydrophilic–hydrophobic polyacrylonitrile PVDF hollow fiber membranes has been reported [201] besides the combination of hydrophilic base polymer with a hydrophobic surface modifying macromolecules [202].

Carbon nanotube-based membranes have been used in a variety of separation applications that range from pervaporation, extraction to nanofiltration [141, 203-205]. The physicochemical interaction between the solutes and the membrane can be dramatically altered by immobilizing CNTs on the membrane surface [142, 143, 206]. First, CNTs are excellent sorbents that have surface areas between 100–1000 m^2/g [46, 207]. Many factors, such as the presence of defects, capillary forces in nanotubes, polarizability of graphene structure led to strong sorbate/sorbent interactions, the absence of a porous structure led to high specific capacity while facilitating fast desorption of large molecules [208-210]. A

more recent development in MD has been the development of carbon nanotube immobilized membrane (CNIM) for desalination where the CNTs increase the partitioning of the water vapor while rejecting hydrogen bonded salt-water phase leading to dramatic increase in flux [189, 211, 212]. We have already employed the CNIM successfully in sweep gas membrane distillation (SGMD) to show significant enhancement in desalination [28]. It was observed that the water vapor flux for SGMD remained constant with increasing salt concentration, reaching up to 19.2 $kg/m^2.hr$ [142].

Isopropyl alcohol (IPA) is a common industrial solvent used in many chemical and pharmaceutical industries. IPA forms an azeotrope with water at 14.7% weight percent of water, and is not easy to recover by the traditional distillation [213]. Although pervaporation has been used widely to separate azeotropes and can provide high selectivity, the flux and membrane stability remained poor [214, 215]. While MD has been used to separate water-isopropanol mixtures, it faces issues like high energy consumption which has been reported to be over 625 kWh/m^3 [12]. Since the CNTs are also excellent sorbents for organic molecules, it is conceivable that they can be used to enhance the separation of aqueous-organic solvent systems as well. The objective of this study is to investigate the separation of IPA-water mixtures using CNIM to enhance IPA separation in terms of flux and selectivity.

3.2 Experimental

3.2.1 Chemicals and materials

IPA and acetone used in these experiments were obtained from Sigma Aldrich (St. Louis, MO). Deionized water (Barnstead 5023, Dubuque, Iowa) was used in all experiments.

MWCNTs were purchased from Cheap Tubes Inc., Brattleboro, VT. The average diameters of the CNTs were ~30 nm and a length range of 15 μm.

3.2.2 CNIM Fabrication

Effective dispersal of CNTs and immobilization on the membrane surface was an essential step in CNIM fabrication. The CNT membrane was prepared using a polytetrafluoroethylene (PTFE) laminate supported on polypropylene composite membrane (Advantec, 0.2 μm pore size, 74% porosity). The CNTs dispersion was carried out as follows: 1.5 mg of CNTs were dispersed in a solution containing 8 g of acetone and sonicated for four hours. 0.2 mg of polyvinylidene difluoride (PVDF), which acted as a binder during immobilization of the CNTs was dissolved in 2 g of acetone and mixed with CNTs dispersion. The PVDF-nanotube dispersion was thereafter applied uniformly with a dropper over the membrane held on a flat surface to form the CNIM. The wet CNIM was kept under the hood for overnight drying.

The CNIM was characterized using scanning electron microscopy (SEM) (Leo 1530 VP, Carl Zeiss SMT AG Company, Oberkochen, Germany). Membrane hydrophobicity was measured via contact angle measurements using deionized water, isopropanol and their mixture. Droplets of different concentration of isopropanol were deposited using a micro syringe (Hamilton, 0–100 μL) on the base PTFE and the CNIM. The droplet positions were recorded, and the contact angle was measured using a digital video camera mounted at the top of the stage.

3.2.3 Experimental Set Up

The MD set up was used in a sweep gas MD (SGMD) mode where a cool inert gas swept the permeate side of the membrane and carried the vapor [52, 216]. A flat membrane module was used to make the SGMD test cell that was fabricated from polytetrafluoroethylene (PTFE). The experimental setup is illustrated in Figure 3.1. The disk-shaped module had an inner diameter of 4.3 cm and an active contact area of 14.5 cm^2. Peristaltic pump (Cole Parmer, model 77200-52) was used to circulate IPA-water mixture through the membrane module and the feed was recycled. The hot isopropanol water mixture was circulated on one side of the membrane, and the cold sweep gas on the other side. The temperature of the feed was controlled by a water bath. The gas velocity was measured by a flowmeter (model no EW-03217-02, Cole Parmer). Temperature was measured with thermistor thermometers (K-type, Cole Parmer) placed on the inlet and outlet of the stream.

Laboratory air supplied from the fume hood was passed through the permeate side of the membrane at room temperature (22^{o}C). Impurities such as moisture or dust in the sweep air were reduced by passing it through a drierite laboratory air and gas drying unit (W. A. Hammond Drierite, Xenia, OH) and a Barnstead D3750, Hollow Fiber Filter (Barnstead International, Beverly, MA). The relative humidity of the dry air was found to be zero. The permeate side air flow rate was kept constant at 1 L/min in all experiments. Each experiment was repeated five times and the relative standard deviation was found to be less than 1%.

The volumes were measured using a graduated measuring cylinder. The final volume at the end of the experiment was measured after it was cooled down to room

temperature. Using an enclosed feed chamber ensured that no sample was lost via evaporation. The compositions of the feed mixture before and after the experiment were analyzed by a UV Spectrophotometer (UV-1800 UV-Vis Spectrophotometer, Shimadzu) to calculate the flux and separation factor. Isopropyl alcohol showed a λ_{max} at 195 nm. A calibration curve of IPA concentration vs absorbance at room temperature is shown in Figure 3.2. This calibration curve was used to evaluate the IPA concentration in the feed mixture before and after the experiment.

The liquid entry pressure (LEP) was measured using a method described before[217]. A stainless-steel chamber (Alloy Products Corp, 185 Psi Mawp) was filled with the IPA-water feed solution at different concentrations. The membrane held in a test cell was connected to the liquid chamber. A gas cylinder was used to increase the pressure above the liquid, which was increased till the liquid started to enter through the membrane pores. The onset of the liquid entry into the membrane was the LEP. The measurement was repeated three time to ensure reproducibility.

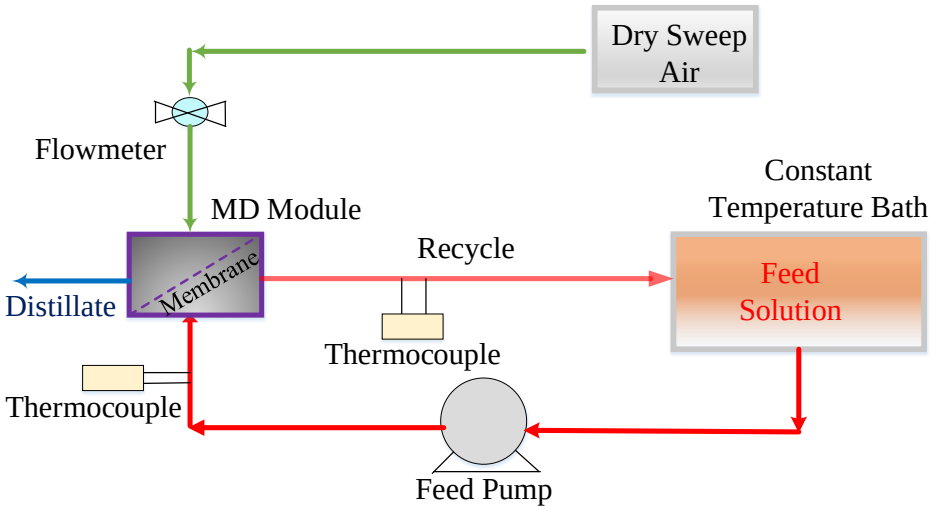

Figure 3. 1 Experimental Setup for Sweep Gas Membrane Distillation.

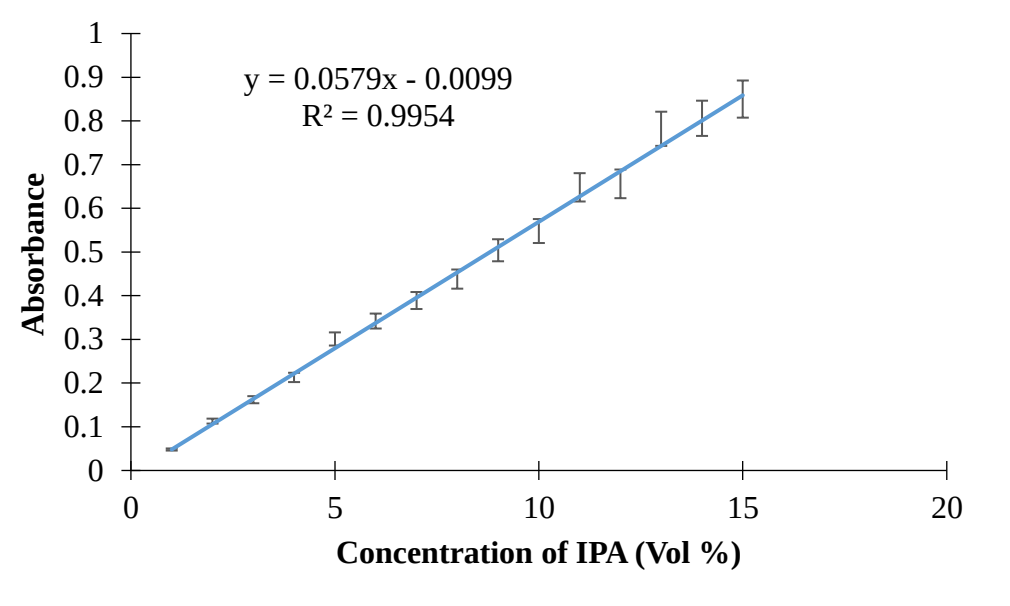

Figure 3.2 UV absorbance calibration curve of IPA at different concentrations.

3.2.4 Gas Permeation Test

The effective surface porosity over the effective pore length was calculated by gas permeation test as described in literature [218]. The total molar flux per unit transmembrane pressure difference across the porous membrane can be described as

$$\frac{J_i}{\Delta P} = \frac{2}{3}\left(\frac{8RT}{\pi M}\right)^{0.5} \frac{1}{RT} \frac{r\varepsilon}{L_p} + \frac{\bar{p}}{8\mu RT} \frac{\varepsilon r^2}{L_p} \qquad (3.1)$$

Where r is mean pore radius of the membrane, ε is surface porosity, μ is gas viscosity, M is molecular weight of gas, $\bar{p}$ is the average of feed and permeate side pressure, R is gas constant, L_p is effective pore length and T is temperature (K). The first term in this equation denotes the Knudsen flow and the second term refers to Poiseuille

flow. The gas permeation flux per unit driving force ($J_i/\Delta p$) can be calculated using the equation below

$$\frac{J_i}{\Delta P} = \frac{N_{t,i}}{A_t} \tag{3.2}$$

where, $N_{t,i}$ is total molar gas permeation rate in mol s^{-1}, ΔP is the transmembrane pressure difference across the membrane area A_t. The total gas permeation rate through the membrane was measured using a bubble flow meter.

3.3 Results and Discussion

The SEM images of the CNIM and the unmodified PTFE membrane are shown in Figure 3.3 a) and b). SEM image shows porous structure of the pristine PTFE membrane and presence of CNTs on the CNIM surface. The distribution of CNTs was relatively uniform over the entire membrane surface. Based on the gas permeation test, the effective porosity over pore length was found to be 1.12×10^5 m^{-1}. This value did not change with CNT incorporation because only a small amount of CNTs had been used to fabricate the CNIM. The thermal stability of the unmodified and CNIM membrane was studied by thermogravimetric analysis (TGA). The TGA curves of unmodified and CNIM membranes are shown in Figure 3.3c. It is clear from the figure that the thermal stability of CNIM was enhanced due to the presence of CNTs.

We have carried out long term stability tests and there was decrease in flux, no CNTs have been detected in the feed solutions that have been recycled. CNIM was also heated in aqueous solutions for days and then inspected to see is there was loss of CNTs. We did not observe any appreciable loss of CNTs.

The liquid entry pressure (LEP) of the membrane was observed to be a function of IPA concentration in the feed mixture. The LEP of 5% IPA solution was found to be 41 and 37 psig, which changed to 27 and 21 psig at 15% IPA, and gradually dropped to 21 and 13 psig at 20% IPA solution for unmodified PTFE and CNIM, respectively. The prolonged use of feed concentration higher than 15% could lead to membrane wetting and leakage of the feed mixture into the permeate side as also evident from the contact angle measurement described below.

The contact angles of the unmodified PTFE and CNIM at different IPA-water concentrations are shown in Figure 3.4a, b and c. Droplet size of 4 mm was used to measure contact angles. The presence of CNTs dramatically altered the contact angle. With 100% water in the feed, the contact angle for CNIM was higher than the unmodified PTFE membrane. Since organic molecules including alcohols are known to have strong sorption onto CNTs [219], the presence of IPA led to strong interactions with the CNTs. Therefore, the contact angles of the mixtures were lower in the CNIM. For example, the photograph of the water droplet on unmodified PTFE membrane showed a contact angle of 83° with 10% isopropanol, however, after CNT immobilization, the contact angle reduced to 50° which showed higher affinity to the membrane. CNIM provides higher adsorption of the IPA molecules thus enhancing the flux. Improvement of IPA affinity of the CNIM membrane over unmodified PTFE is one of the ways to enhance the separation performance and mitigate concentration polarization.

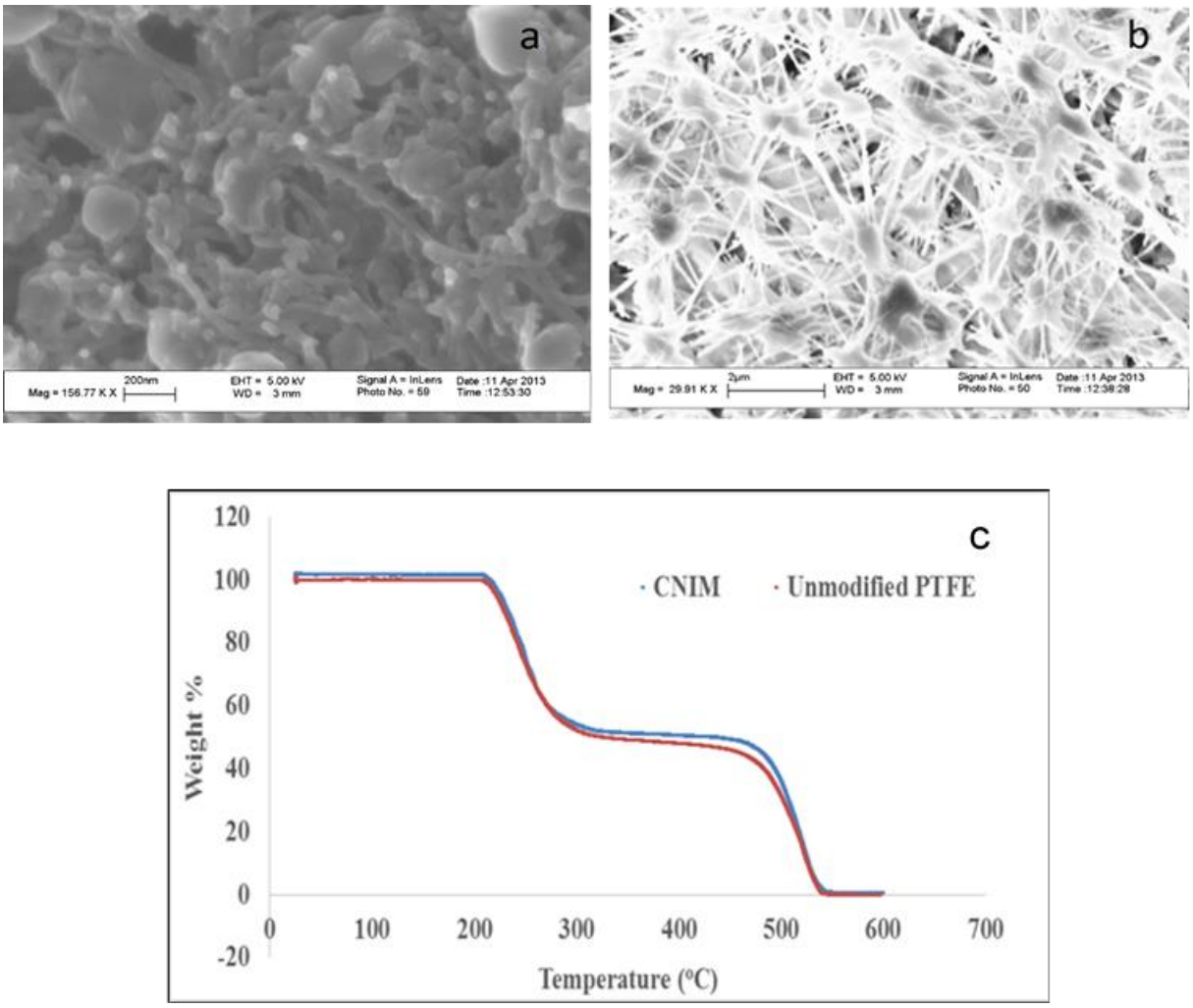

Figure 3.3 Scanning electron micrograph of **(a)** CNIM and **(b)** unmodified PTFE **(c)** thermogravimetric analysis of PTFE and CNIM.

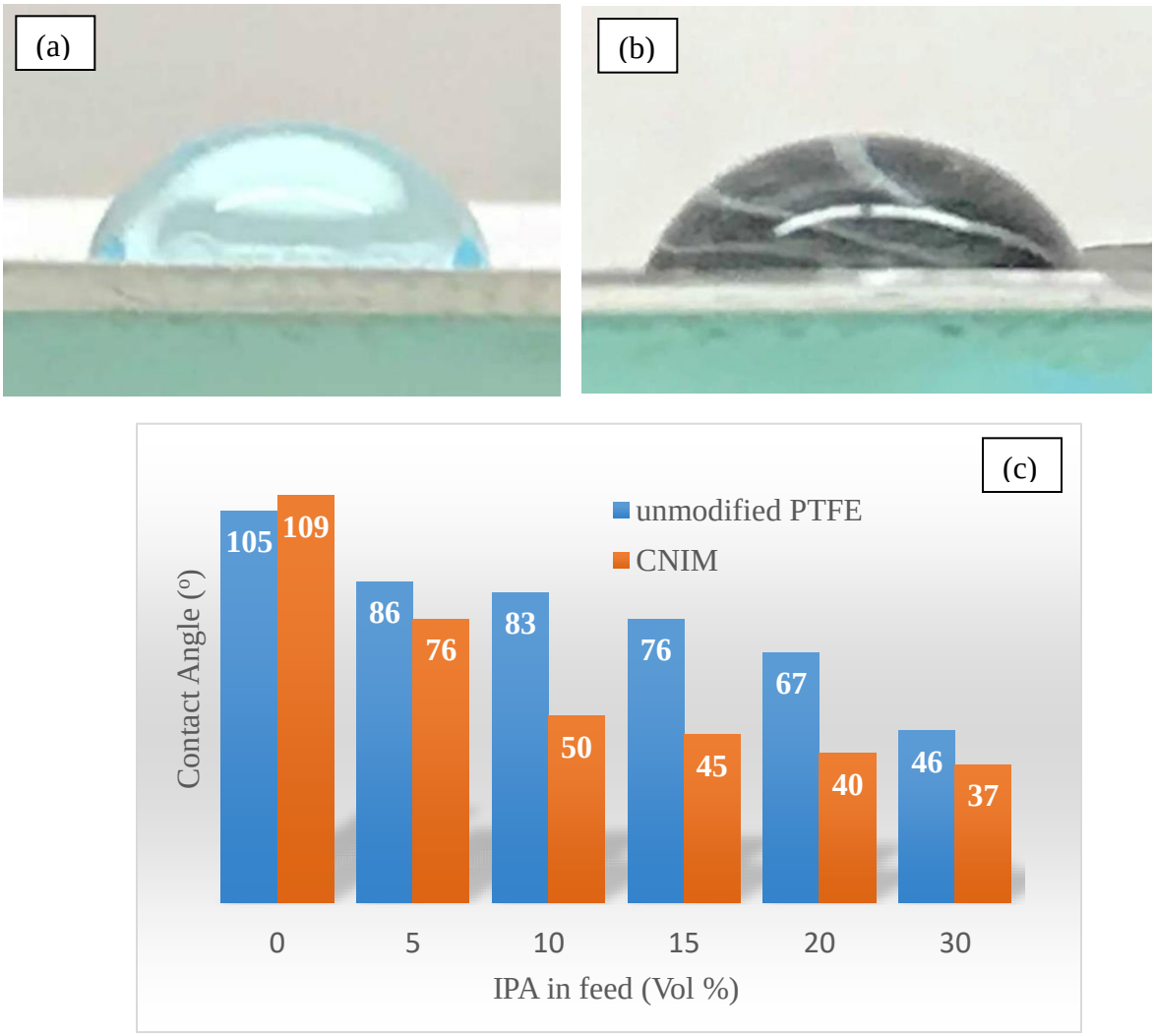

Figure 3.4 (a) Photograph of isopropanol- water mixture (10 volume %) drop on unmodified PTFE and **(b)** CNIM; **(c)** contact angle measurements on unmodified PTFE and CNIM membrane.

3.3.1 SGMD Performance Using CNIM and Unmodified Membrane

The separation characteristics of the membrane is described in terms of flux and separation factor. The performance of CNIM was compared to the unmodified PTFE membrane. The flux of species '*i*' (J_{wi}), across the membrane was expressed as:

$$J_{wi} = \frac{Wpi}{t*A} \tag{3.3}$$

Where, W_{pi} was the total mass of species '*i*' in the permeate, *t* is the permeate collection time and *A* is the effective membrane surface area. The separation factor (α_{i-j}) is the measure of the efficiency of separation and is determined from the ratio of the concentrations of the species '*i*' (more permeable) and the species '*j'* (less permeable) in the permeate divided by the same ratio in the feed side. The separation factor of IPA can be described as:

$$\alpha_{IPA-water} = \frac{y_{IPA}/y_{water}}{x_{IPA}/x_{water}} \tag{3.4}$$

Where y_i and x_i are weight fraction of component '*i*' in permeate and feed, respectively.

The Figure 3.5a shows a plot of IPA flux and separation factor as a function of IPA concentration in the feed. Three different feed concentrations namely 5, 10, and 15 (volume %) of IPA were tested. The feed flow rate was kept constant at 112 mL/min and the temperature was maintained at 50^0C. The IPA flux increased with increase in the concentration of IPA in feed for both membranes. However, the IPA flux was higher when CNIM was used. The presence of CNTs increased the partition coefficient of the IPA which

is the equilibrium ratio of IPA concentration on the CNIM surface to its concentration in the liquid phase and its effect was more distinct at higher IPA concentration. The separation factor reduced with increase in concentration for both membranes. However, CNIM gives a higher separation factor than the unmodified PTFE membrane at all concentrations.

The effect of feed temperature on IPA flux and separation factor of the CNIM and the unmodified PTFE membrane is shown in Figure 3.5b. The feed flow rate was fixed at 185 mL/min and the feed concentration was 10 volume %. The permeate fluxes of both membranes increased with increase in feed temperature. Permeate flux reached their maximum at 70 ^{0}C with maximum flux for CNIM reaching 13 L/m^{2}.hr., which was significantly (over 5 times) higher than what has been reported before [220]. Overall, CNIM showed consistently higher flux at all temperatures, although the enhancement seemed to be most pronounced at lower feed temperatures. At 40^{o}C the enhancement reached as high as 130% compared to the unmodified membrane. Therefore, operations could be carried out at significantly lower temperature on the CNIM thereby making it a more energy efficient process. The vapor pressure of IPA increased in an exponential manner. This trend may be explained by the Antoine equation which predicts an exponential relationship between the driving force (vapor pressure difference) and temperature (true for water as well). The sharp increase in vapor pressure from 40 to 50°C is reflected in the correspondingly increase in flux. The evaporation of the mixture at the pore entrance was affected by vapor–liquid equilibrium of IPA–water mixture which depends upon temperature and concentration. From the figure, the IPA separation factor for CNIM was constantly higher at all temperatures compared to the unmodified membrane. The enhancement in separation factor of CNIM over unmodified PTFE reached

as high as 350% at 70^{o}C. The IPA separation factor for both membranes decreased with feed temperature, which was attributed to the negative effects of viscosity [220].

Effect of feed flow rate on IPA flux is illustrated in Figure 3.5c. The feed flow rate was varied from 42 to 185 mL/min. The feed temperature was 50^{0}C and IPA concentration was 10 volume %. The permeate flux increased as high as 12 L/m^{2}.hr with 112 mL/min feed flow rate and the separation factor was three times higher in CNIM over unmodified PTFE membrane. The increase in flux was much more in the case of CNIM than the unmodified PTFE and enhancement reached as high as 174%. This can be explained by the temperature and concentration polarization phenomenon. Increasing the flow rate reduces the difference between the bulk and membrane surface concentration. At low flow rates, IPA concentration was depleted at the liquid–membrane interface resulting in lower flux. Increased turbulence caused by the higher feed flow rate increases the IPA concentration and the vapor pressure on the feed-membrane interface resulting in an increase in the permeate flux. In this case, as expected, the higher feed flow rate promoted both heat and mass transfer from the bulk feed to the membrane surface, thus resulting in higher IPA removal efficiencies [221]. It is evident from the figure that the CNIM exhibited higher separation factor at all feed flow rates compared to the unmodified membrane. Higher separation factor is mainly attributed to the partitioning of the IPA on the CNTs in the CNIM. At high flow rates the residence time is short and relatively less amount of IPA partitions on the CNIM. This leads to a drop in the separation factor at higher flow rate.

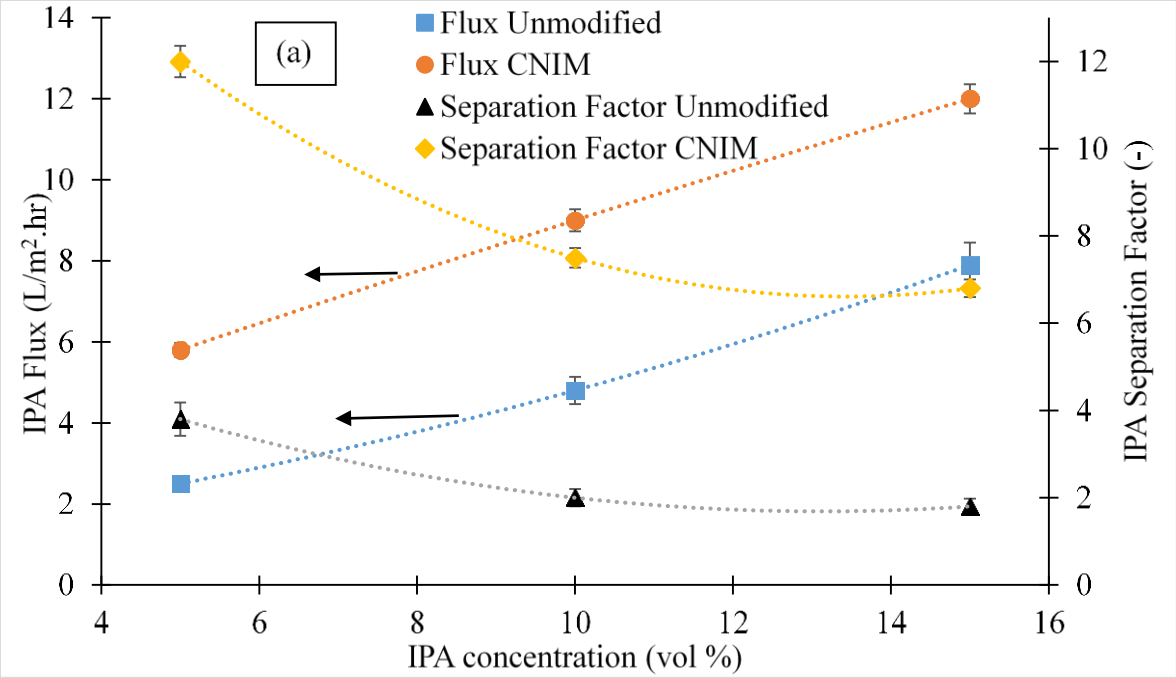

Figure 3.5 (a) Effect of feed concentration on IPA flux and Separation factor.

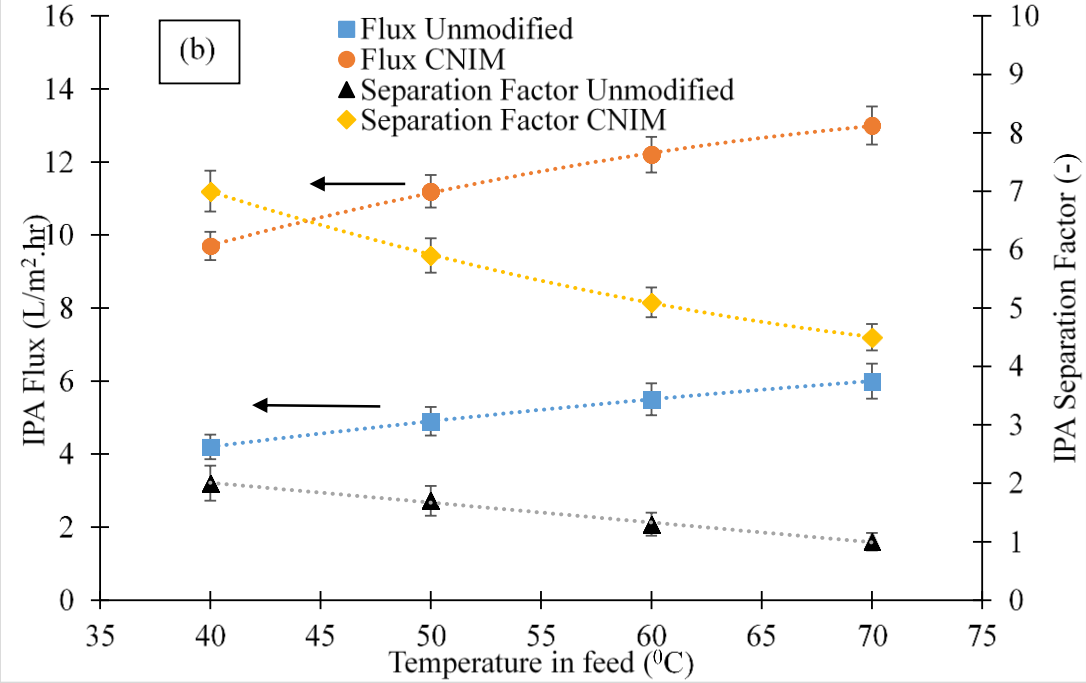

Figure 3.5 (b) Effect of feed temperature on IPA flux and separation factor.

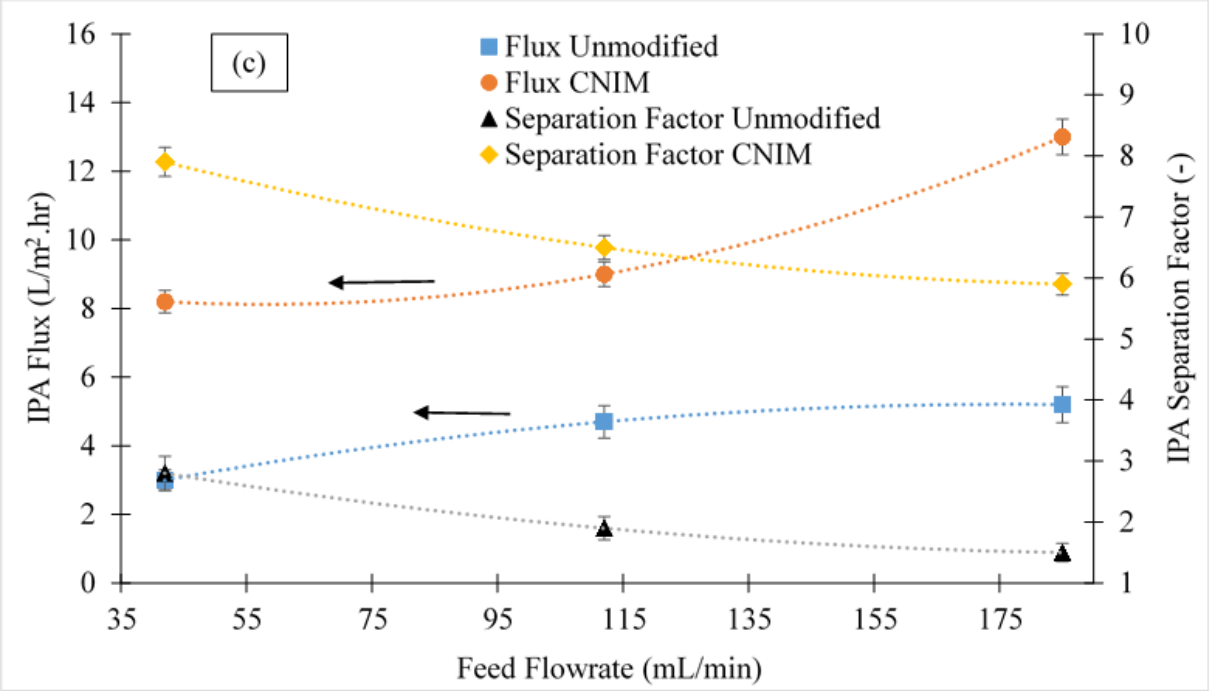

Figure 3.6 (c) Effect of feed flowrate on IPA flux and separation factor.

3.4 Mass Transfer Coefficient

The flux (J_{wi}) can also be denoted as:

$$J_{wi} = k\left(P_{fi} - P_{pi}\right) \tag{3.5}$$

$$k = \frac{J_{wi}}{P_{fi}} \tag{3.6}$$

Where, k is the mass transfer coefficient, P_{fi} and P_{pi} are the partial vapor pressure of species 'i' in feed and permeate side, respectively. The feed side vapor pressure at a

particular temperature was obtained from the literature [222] and the permeate side vapor pressure was considered close to be zero, since dry air was used as the sweep gas.

Table 3.1 shows the mass transfer coefficients of IPA at different temperatures and at 112 mL/min feed flow rate. The mass transfer coefficients were observed to decrease with increase in feed temperature for both membranes. The CNIM showed higher mass transfer coefficients than the unmodified membrane at all feed temperatures. The CNTs are known to provide rapid sorption/desorption properties, which contributed to high mass transfer coefficients. The enhancement of mass transfer coefficient reached as high as 131% at 40^{o}C. The overall mass transfer coefficient depended upon the partitioning of the IPA on the CNIM surface as well as the diffusion through the membrane. While the former decreased with temperature, the latter increased with temperature. In this case, the overall coefficient was the highest at 40^{0}C. This may be due to the decrease in sorption capacity at higher temperatures, which led to a reduction in enhancement of separation factor at higher temperatures.

Table 3.2 depicts that the mass transfer coefficients increased with increase in feed flow rate and the values were significantly higher for CNIM with the enhancement reaching up to 132% at 42 mL/min and 50^{o}C for 10 vol% IPA. The overall mass transfer is controlled by diffusion through the boundary layer. Higher flow rate led to higher turbulence which in turn reduced the boundary layer and consequently the resistance to mass transfer [223]. It was observed that with increase in flow rate, the mass transfer coefficient increased significantly for both membranes. Rapid mass transfer on the CNTs surface led to the enhancement in the mass transfer coefficient in CNIM. However, the reduction in IPA partition on CNIM surface due to the shorter residence time at high flow rates and the

competition between IPA and water lead to a drop in the percent enhancement with increase in flow rate.

Table 3.1 Mass Transfer Coefficient of IPA and Enhancement % at Various Feed Temperature at 15 Volume % Feed and 112 mL/min

Temperature (^{0}C)	**Mass Transfer Coefficient (m/s.mm-Hg)**		**%Enhancement for CNIM**
	Unmodified PTFE	**CNIM**	
40	1.1E-08	2.55E-08	131.0
50	7.7E-09	1.76E-08	128.6
60	5.3E-09	1.17E-08	121.8
70	3.66E-09	7.94E-09	116.7

Table 3.2 Mass Transfer Coefficient of IPA and enhancement% at Various Feed Flow Rate and 10 volume % IPA at 50 °C

Feed Flow rate (mL/min)	**Mass Transfer Coefficient(m/s.mm-Hg)**		**%Enhancement for CNIM**
	Unmodified PTFE	**CNIM**	
42	3.93E-09	9.11E-09	132.0
112	7.54E-09	1.41E-8	87.5
185	1.24E-08	1.89E-08	51.9

3.5 Membrane Stability

To investigate the stability of the membranes, SGMD was carried out for 60 days (approximately 8 hr per day) with 15 volume % IPA concentration at 60°C. The IPA flux was measured from time to time. No significant change in IPA flux as well as the membrane wetting were observed even during prolonged use for both CNIM and the PTFE membranes. It is believed that there was no appreciable loss of CNTs as none were detected in feed solutions that were recycled. Similar stability tests in the past were also performed where CNIM was used in hot aqueous solutions for days and then inspected for CNT loss [206].

3.6 Proposed Mechanism

The proposed mechanism for enhanced IPA transport in the presence of CNTs is shown in Figure 3.6. Previous studies with CNTs have demonstrated that CNTs are excellent sorbents that enhance partition coefficient of the solutes leading to higher flux in membranes [136, 137, 224-228]. The significant enhancement in IPA flux with CNIM is attributed to the preferential sorption and fast desorption to the permeate side via CNTs serving as nanosorbents. The organophilic CNT surface is selective towards IPA due to its organic nature. IPA also has a higher vapor pressure of 288.356 mm Hg at 60^{o}C which is almost double of that of water (149.038 mm Hg at the same temperature). In summary, the higher vapor pressure of IPA, preferential sorption, and permeation of the IPA via CNTs offer higher enhancement in flux and separation factor.

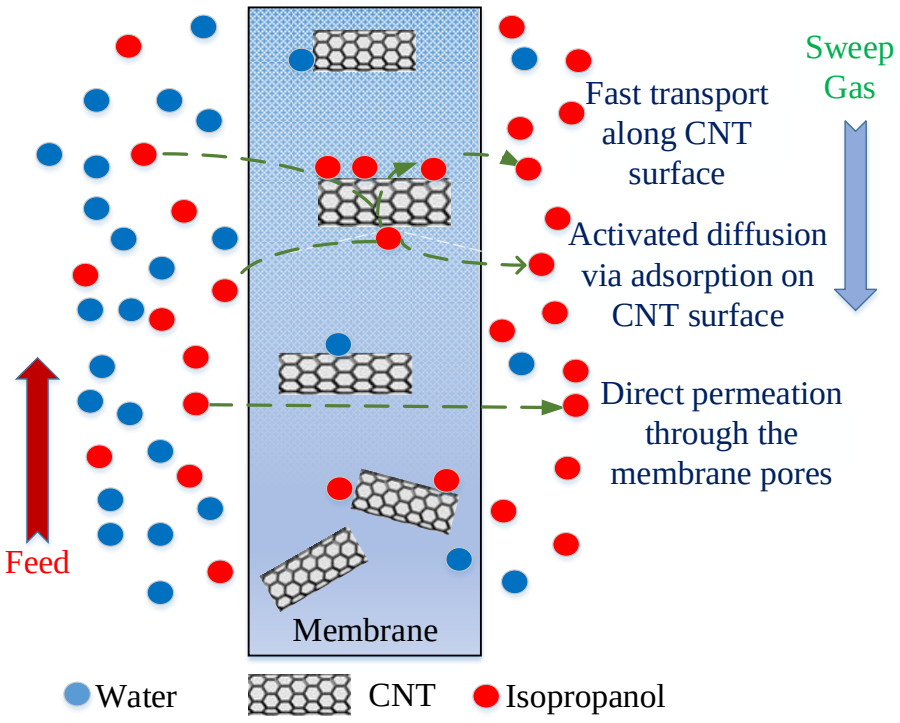

Figure 3.7 Schematic of proposed mechanism for CNIM.

3.7 Concluding Remarks

SGMD with CNIM provides a potential application for very efficient recovery and recycling of organic solvents and in this case IPA. Operating variables such as feed temperature, feed flow rate and feed concentration were found to have significant influences on the efficiency of IPA removal with CNT membrane. The presence of CNTs alter the IPA-membrane interaction which is evident from the contact angle measurements. A higher feed temperature and feed flow rate promoted IPA removal efficiency and permeate flux in the sweep gas MD mode. Feed temperature, concentration and flowrates were important process parameters that can be used to optimize a balance between flux and separation factor. The mass transfer coefficient of CNIM was found to be higher than that of unmodified PTFE membrane. The CNIM showed stability over longer periods of operation without any membrane wetting and solvent leakage. The CNIM membrane also showed better thermal stability than unmodified PTFE membrane. Since only a small amount of CNTs were used (~1mg/cm^2 membrane area) and the CNTs remained on the surface of the membrane, it did not contribute to heat conduction across the membrane. The gas permeation tests showed that the presence of CNTs did not affect the effective surface porosity over the effective pore length. These results encourage the incorporation of CNTs to provide an easy alternative of hydrophilic–hydrophobic SGMD membrane modification with enhanced flux and separation factor.

CHAPTER 4

MICROWAVE INDUCED MEMBRANE DISTILLATION FOR ETHANOL-WATER SEPARATION ON CARBON NANOTUBE IMMOBILIZED MEMBRANES

4.1 Introduction

The separation for liquid mixtures is commonly carried out by thermal distillation. However, the process is energy intensive, shows poor separation for azeotropes and higher operating temperature up to the boiling point may cause unfavorable side reactions. Membrane distillation (MD) has been used to circumvent some of these limitations and is being explored as an alternative for large scale techniques like multi-stage flash (MSF) and multiple effect distillation (MED) which also tend to be very capital intensive [229]. MD is driven by a vapor pressure gradient through a porous hydrophobic membrane where the vapor selectively transports across the membranes [34, 50, 230]. The variation in vapor pressure between the feed side and the permeate side occurs due to the difference in temperature across the membrane [34, 52]. Relatively lower temperature operations often below the boiling point make MD an attractive alternative for conventional distillation [40, 231-233]. Other advantages include a "greener" approach with reduced greenhouse gas emissions and a process design with minimal space requirement [234, 235]. MD has been employed in various applications including desalination and water purification, concentration of feed streams, removal and recovery of low boiling components from its aqueous mixtures [12, 46, 140, 142, 143, 206, 236-241], and the low temperature process can be conducted utilizing industrial waste heat and renewable energy resources [242-245].

Anhydrous ethanol is extensively used in chemical manufacturing as a solvent, a raw material in chemical production [246] and as fuels in gasoline-ethanol mixtures [247,

248]. Besides conventional distillation, ethanol water mixtures have been separated by azeotropic distillation [249, 250], adsorption on molecular sieves and pervaporation (PV) [251, 252]. All these processes have been used in industry and have limitation such as high operating and energy costs. MD has been used in the separation of organic molecules from water [220, 253, 254] and also water ethanol mixtures[253, 255]. Air gap, vacuum and sweep gas MD have been used for ethanol-water separation using conventional MD (heating the feed side using a regular heater) and membranes made of Polypropylene (PP), Polyvinylidene fluoride (PVDF) and Polytetrafluoroethylene (PTFE) [38, 57, 253-259]. The enhancement of MD performance in water ethanol separation is significant to make this process commercially viable. Recently, the use of carbon nanotube immobilized membrane (CNIM) for the separation of water-isopropyl alcohol mixtures has been reported by our group, where the nanotubes served as sorbents that improved the partition coefficient of the alcohol on the membrane and increased both flux and separation factor[146]. Therefore, it is anticipated that the CNIM would also enhance water-ethanol separation.

Microwave induced heating has been employed in various manufacturing methods such as drying, synthesis of chemical compounds, and in homes for cooking [260-265]. When a dielectric material is placed in an alternating electric field, the dipoles attempt to maintain alignment with the variable field and change direction at high frequency [266]. An alternating electric field through a microwave active material causes the energy to be dispersed as the molecules try to arrange themselves with the varying alternating field. The dielectric loss occurs as a result of the delay between the dipole alignment and the applied electromagnetic field that leads to heat generation [267, 268]. Microwave processes are

also associated with non-thermal effects such as localized super heating, reduction in activation energy, breakdown of structures formed through hydrogen bonding in aqueous medium, and the generation of nano bubbles [269-275]. The effects of microwave heating has been stated to persist for several hours after the removal of the microwave field [276, 277]. While microwaves have been used extensively in conventional distillation [278, 279], there are only a limited amount of studies on their application in membrane separation processes. Microwave heating has been used in gas separation and vacuum-based membrane distillation where the entire distillation units was placed in a microwave oven [280]. Recently, the development of MIMD has been reported in the direct contact mode for water desalination [281]. MIMD can potentially be used in many different separations but it is sensitive to the interaction of the microwave with the solute.

The objective of this paper is to investigate the effects of microwave heating in membrane distillation for the separation of ethanol-water mixture in sweep gas mode (SGMD), where an enhancement in performance can be expected due to non-thermal effects resulting in higher flux and separation factor for both membranes. Yet another objective is to see if the microwave treated ethanol-water mixture interacts differently with different types of membranes especially those immobilized with carbon nanotubes (CNTs).

4.2 Materials and Methods

4.2.1 Chemicals and Materials

Ethanol and acetone (Sigma Aldrich, St. Louis, MO), multiwalled CNTs (dia: ~30 nm, lemgth: 15 μm, Cheap Tubes Inc., Brattleboro, VT), high purity deionized water (Barnstead 5023, Dubuque, Iowa) was used in this experiment. The membrane employed for this MD

experiment was a PTFE membrane on PP support (Advantec MFS, Inc.; Dublin, CA, 0.2 μm pore size, 74% porosity).

4.2.2 CNIM Fabrication

Homogeneous dispersion of CNTs in organic solvents and its distribution on PTFE membrane surface uniformly are vital steps in CNIM preparation. The CNIM fabrication technique was performed according to the procedure described elsewhere[146]. The wet CNIM was dried overnight at room temperature.

4.2.3 Experimental Setup

Figure 4.1 shows the experimental setup for MIMD. Here, a microwave was used to heat the feed mixture containing ethanol-water before entering the membrane module. An inert gas at room temperature was used to sweep the permeated vapor. The effective membrane surface area was 14.5 cm^2. The heated ethanol-water mixture was recirculated using a Peristaltic pump (Cole Parmer, model 77200-52) and collected in the same feed chamber as the retentate. The temperature of the feed reservoir was controlled with a temperature regulated water bath. A flowmeter (Cole Parmer EW-32460-42) was used to determine the gas velocity on the permeate side of the membrane module. Microwave powers were adjusted to maintain the temperature in the feed solution.

Laboratory air supplied was passed through the permeate side of the membrane from the fume hood at room temperature (22^oC). The sweep air was dried and purified using a procedure described before[146]. In all experiments the air flow rate was maintained at 4.5 L/min. The experiments were performed thrice, and the relative standard deviation was observed to be below 1%.

The reduction in feed volume was measured after 1h of the experiment and the ethanol-water mixture composition before and after the experiment were evaluated using a UV Spectrophotometer (UV-1800 UV-Vis Spectrophotometer, Shimadzu). At 190 nm ethanol exhibited maximum absorbance (λ_{max}). A calibration curve was plotted for ethanol concentration vs absorbance at room temperature to measure the unknown concentration of ethanol after each experiment.

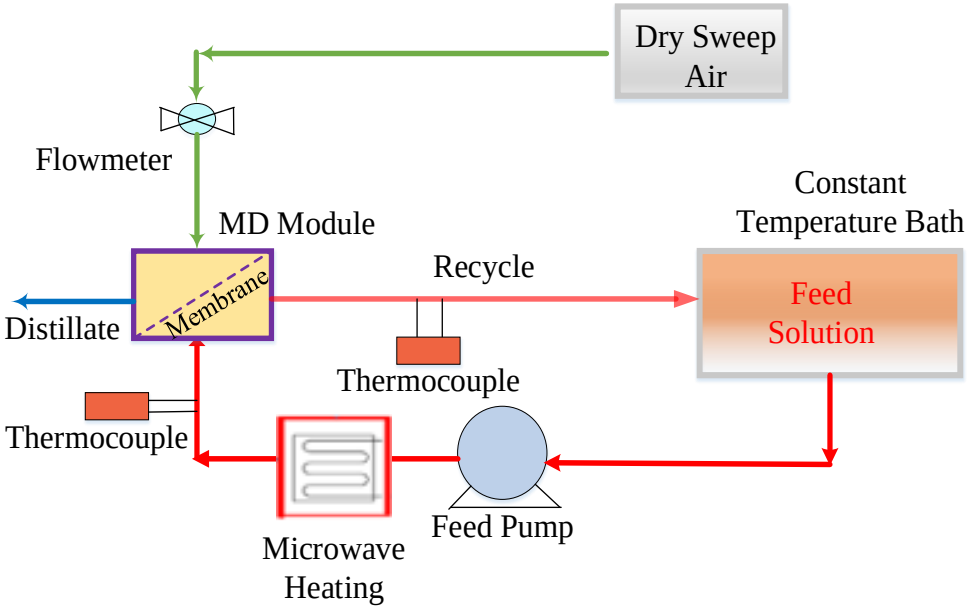

Figure 4.1 Experimental Setup

4.3 Results and Discussion

Ethanol-water separation was quantified based on flux and separation factor. The performance of CNIM and a commercial PTFE membrane by conventional heating were compared to the microwave heating. The ethanol vapor flux, J_w, across the membrane was defined as

$$J_w = \frac{W_p}{t \times A} \tag{4.1}$$

where, W_p was the total mass of the permeate, t is the time and A is the effective membrane surface area. Selectivity was quantified as separation factor which was a measure of preferential transport of ethanol and was defined as

$$\alpha_{ethanol-water} = \frac{y_{ethanol}/y_{water}}{x_{ethanol}/x_{water}} \tag{4.2}$$

where y_i and x_i are the weight fraction of the component 'i' in permeate and feed, respectively.

Various feed concentrations (5, 10, and 15 volume %) of ethanol were used in these experiments. Feed concentration greater than 15% resulted in membrane wetting and penetration of the feed solution through the membrane. The Figure 4a and b illustrates the ethanol flux and separation factor at various ethanol concentration in the feed with CNIM and PTFE membranes, respectively. It is evident from the figures that for both membranes, the flux increased as the partial vapor pressure increases with increase in ethanol concentration in the feed mixture. The flux as well as separation factors were significantly higher when CNIM was used. This is in line with what has been published before [146]. The CNTs enhanced the partition coefficient of ethanol on the membrane due to its higher affinity towards organic moiety and its influence was more evident when the ethanol concentration was high for both conventional and microwave heating. However, both membranes showed a decline in ethanol separation factor with increase in ethanol

concentration. It can also be seen from Figures 4.2a and b that under the same experimental conditions, MIMD consistently showed significant enhancements over conventional MD in terms of both ethanol flux and separation factor. Ethanol flux in MIMD reached as high as 8.6 and 11.3 L/m^2.hr with PTFE membrane and CNIM, respectively, which were 86% and 70% higher than conventional MD under the same conditions of 15 volume % of ethanol in feed at 50^0C. The separation factors in MIMD were also significantly higher than conventional MD and enhancement via microwave heating reached 263% and 124% for PTFE and CNIM, respectively.

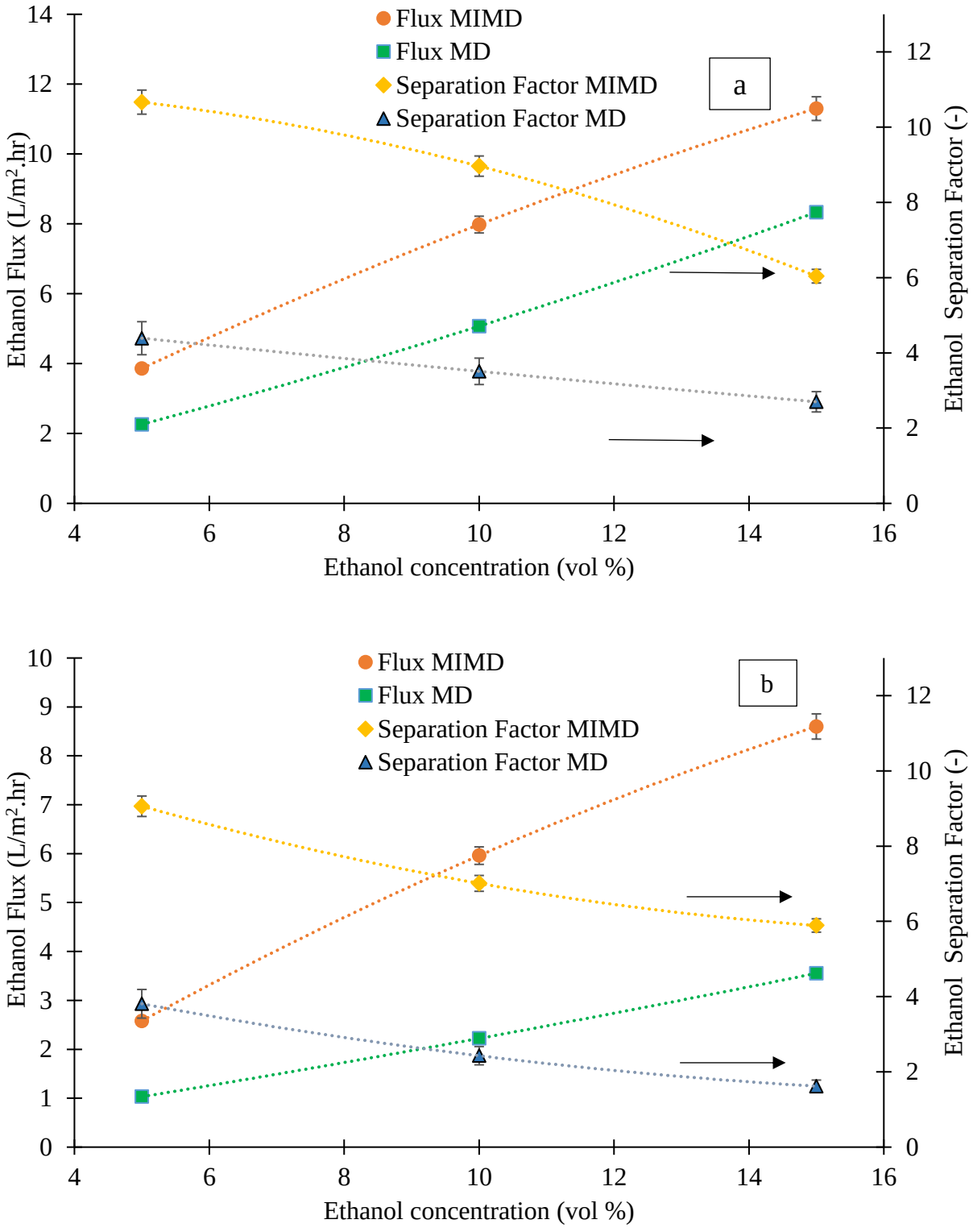

Figure 4.2 The influence of feed concentration on ethanol flux and separation factor with **(a)** CNIM, and **(b)** PTFE membrane. The experiments were carried out at 50°C.

Figure 4.3a and b show the influence of temperature on ethanol flux and separation factor in conventional MD and MIMD with CNIM and PTFE membrane at a feed flow rate of 112 mL/min and sweep gas flow rate of 4.5 L/min. The ethanol concentration in the feed was kept constant at 10% (v/v). From the figure, the ethanol flux increased with increase in feed temperature, because at a higher feed temperature the driving force for solvent vapor transport increased due to higher vapor pressure difference across the membrane. Improved ethanol flux was observed in MIMD compared to conventional MD for both membranes. Based on Figures 4.3a and b, at 60 °C, the ethanol vapor fluxes reached 7.6 and 10.6 $L/m^2.h$ for PTFE and CNIM respectively, in MIMD, which were 108% and 92% higher than conventional MD.

Mechanistically speaking, the selective adsorption of the ethanol on the CNTs played a significant role in enhancing the performance dramatically. Consequently, the flux and separation factor enhancements from microwave heating as compared to conventional heating were higher for the PTFE membrane than CNIM. The enhancement in ethanol flux did not show any trend with increase in temperature, however, an increment in separation factor was observed for both membranes. In general, the flux enhancement in MIMD with CNIM was anywhere between 70-92 % and separation factor enhancements were between 101-206 %. The corresponding enhancements for the PTFE membrane were 106-195% and 126-220 %.

Overall, while enhancements were a bit higher in the PTFE membranes, at all temperatures CNIM displayed consistently improved ethanol vapor flux and better selectivity. The effects were more apparent at reduced feed temperatures. Thus, the MIMD technique using CNIM could possibly make the ethanol separation process more energy

efficient by operating it at substantially lower temperature. The flux and separation factors based on CNIM and MIMD were between 65% and 156% times higher than what has been published before by either MD or PV [253, 255, 256, 282, 283]. Therefore, the MIMD approach represents a major improvement in the state of the art.

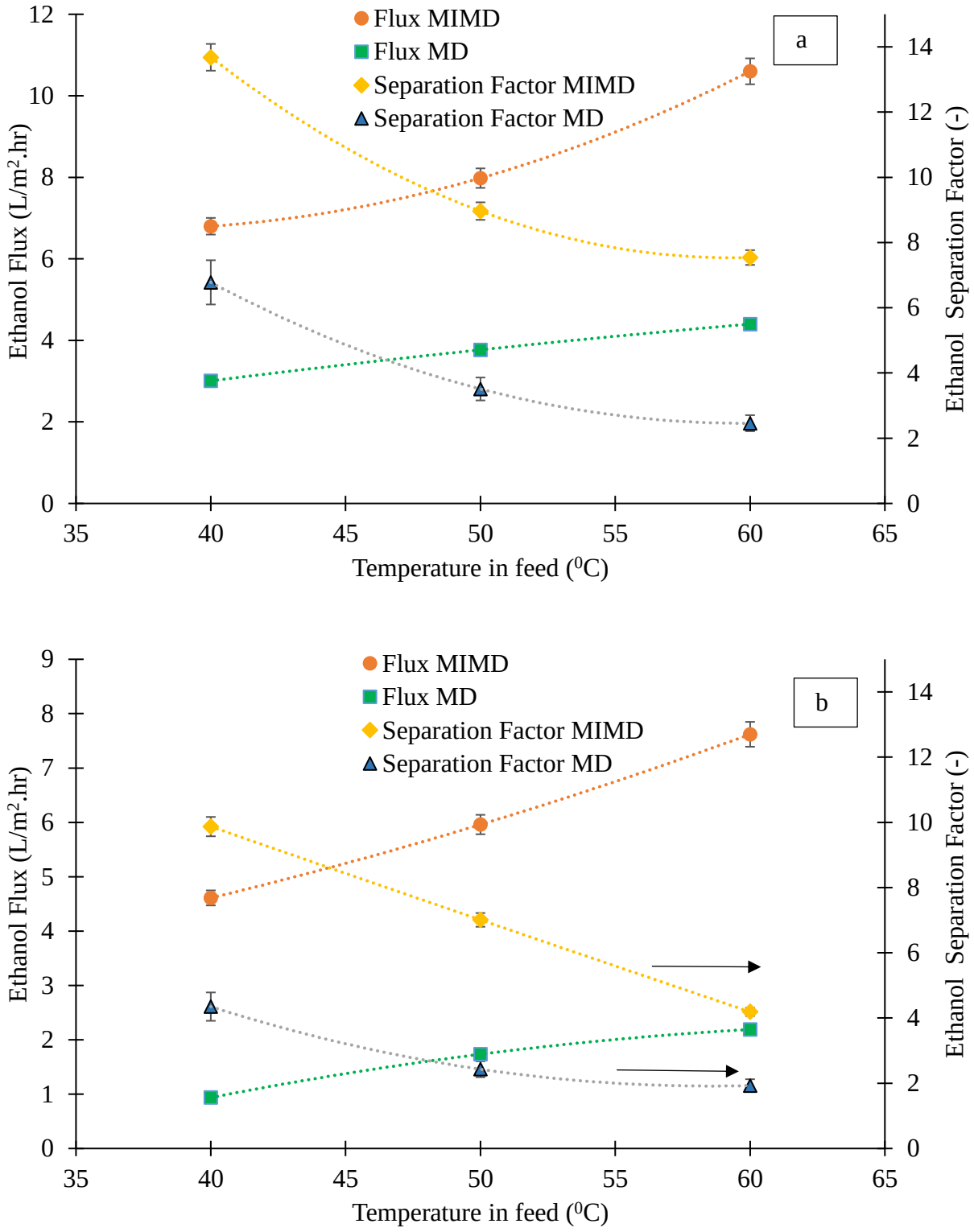

Figure 4.3 **(a)** The influence of feed temperature on ethanol flux and separation factor with CNIM, and **(b)** with PTFE membrane. The experiments were carried out at a feed concentration of 10% ethanol.

4.3.1 Mass Transfer Coefficient

The mass transfer coefficient k was calculated from flux J_w as:

$$J_w = k\left(P_f - P_p\right) \tag{4.3}$$

where, P_f and P_P are the partial pressure in feed and permeate side. Usually, P_p is considered as zero since dry air was used as sweep gas. Table 4.1 shows the variation in mass transfer coefficient in MIMD and conventional MD at different feed temperatures. It can be seen from the table that the mass transfer coefficients decreased at higher temperatures. This can be attributed to the fact that the effect of concentration and temperature polarization increase at higher temperatures. Compared to conventional MD at 40^{o}C, the enhancements in mass transfer coefficient in MIMD for PTFE membrane and CNIM were ~195% and 81%, respectively. These were due to certain non-thermal effects that decreased the temperature/concentration polarization and boundary layer resistance [267, 284].

Table 4.1. Mass transfer coefficients with conventional and microwave heating for PTFE and CNIM

Temperature (^{0}C)	Mass Transfer Coefficient (Conventional MD) (m/s mm-Hg)		Mass Transfer Coefficient (MIMD) (m/s mm Hg)		Enhancement (%)	
	PTFE	CNIM	PTFE	CNIM	PTFE	CNIM
40	9.49E-2	2.11E-1	2.58E-1	3.81E-1	171.86	80.85
50	8.75E-2	1.60E-1	2.02E-1	2.71E-1	130.85	69.42
60	7.81E-2	1.17E-1	1.61E-1	2.05E-1	106.14	74.54

4.3.2 Power Consumption in MIMD

Since MD is a thermally driven process, power requirement is an important factor. The power required to heat the feed solution containing ethanol-water mixtures was measured by using a power meter. Compared to conventional heating, where a heat exchanger or temperature regulated bath is used to conduct the heat followed by convection to the bulk, the microwave heating involves direct localized heating. The energy requirement to operate the MD at different temperatures and 112 mL/min feed flow rate for 1 h is shown in Figure 4.4. The MIMD was observed to be more energy efficient than conventional MD. As compared to conventional MD, the MIMD required 19−23% less energy, which can be further improved by distributing the microwave irradiation uniformly. The difference in energy requirement, although was reduced at higher temperatures. The combination of direct energy saving along with better performance make MIMD approach quite attractive.

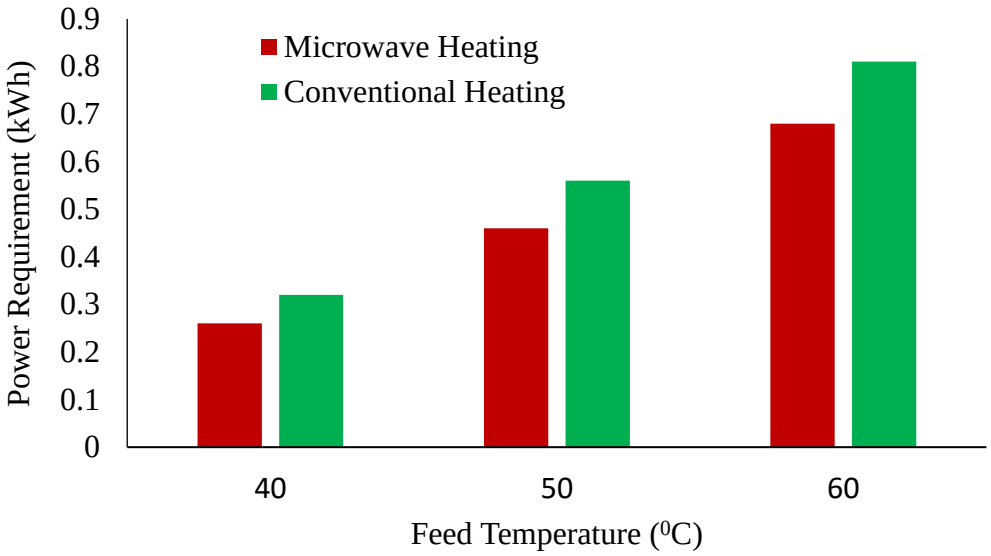

Figure 4.4 Power Consumption with conventional and microwave heating.

4.4 Proposed Mechanism

During microwave heating, the dipoles from polar molecules continuously reorient themselves within the microwave field. This not only leads to heat generation [285] but also break down the hydrogen-bonded structures in an aqueous medium. The latter increases molecular mobility and alters water-solute (ethanol) interactions [286]. Therefore, the MIMD was expected to behave differently than conventional MD.

Contact angle measurements were made to study the effect of microwave heating. The contact angles of ethanol/water mixture (10% v/v) heated via conventional and microwave heating on PTFE and CNIM are shown in Figure 4.5a, b, c and d respectively. Droplet size of 4 mm was used to measure the contact angles. Table 4.2 shows the contact angle data with pure water, 10% and 20% ethanol in feed at room temperature and two kinds of heating systems with the two membranes. It can be seen from the table that pure

water at room temperature had the highest contact angle followed by 10% and 20% ethanol mixtures for both PTFE and CNIM. The contact angle decreased with heating and microwave heating showed the lowest contact angle for all concentrations. At lower (room) temperature, there were stronger intermolecular forces between water molecules, thus the molecules tended to hold together more strongly. As the temperature increased, the kinetic energy of molecules is increased thus reducing the surface tension. These factors led to a decrease in contact angle. Ethanol contains hydroxyl groups, which forms hydrogen bonded clusters with water molecules and under microwave heating these dipole rotations leads to the breakdown of these clusters which led to further reduction of contact angle. The organic species including alcohols exhibited high sorption phenomena on CNT surface, which could be responsible for altering the contact angle of the membrane surface in presence of CNTs [211, 219]. Therefore, the contact angles of the mixtures were observed to be lower for CNIM than for the original PTFE membrane. The contact angles decreased with temperature and ethanol concentration and decreased further when the heating was carried out by microwave. In general, the contact angles were lowest for the CNIM with microwave heating.

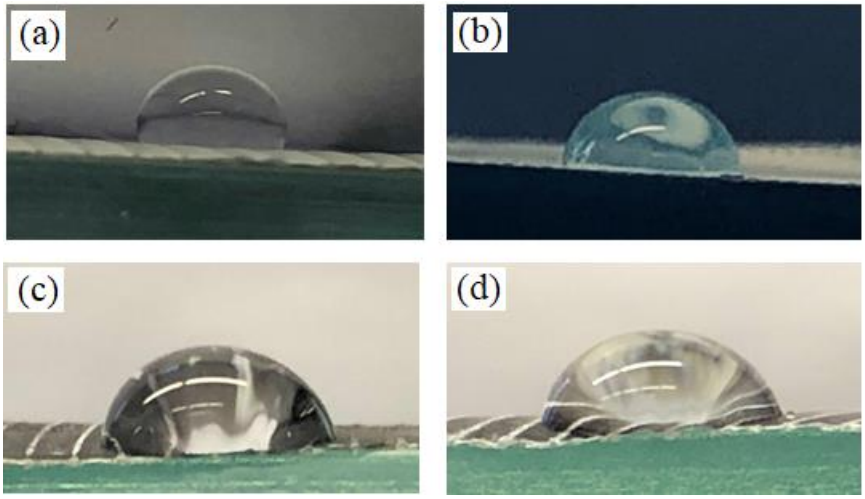

Figure 4.5 Contact angle of **(a)** PTFE with conventional heating, **(b)** PTFE with microwave heating, **(c)** CNIM with conventional heating, and **(d)** CNIM with microwave heating. (10% ethanol in feed).

Table 4.2. Contact Angles in Degrees with PTFE Membrane and CNIM (^{0})

Solvent	**Room Temperature**		**Conventional Heating**		**Microwave Heating**	
	PTFE	**CNIM**	**PTFE**	**CNIM**	**PTFE**	**CNIM**
Pure Water	130	120	108	98	105	89
10 % ethanol	110	101	101	87	88	80
20% ethanol	80	72	61	58	53	50

Figure 4.6 represents the FTIR spectra of ethanol-water mixture under various conditions. The alteration in interactions between water−water and ethanol−water clusters under various heating environments lead to variation in IR absorption of ethanol-water molecules. The hydrogen bonding was seen to be much weaker for microwave irradiated mixture as evident from the bending frequency at around 1654 cm^{-1}. The peak at ~3450 cm^{-1} was attributed to the primary stretching band for ethanol-water molecules. The peak

broadening signified the slightly different extent of the H-bonding in ethanol-water clusters. This indicates stretching of the O-H bonds which was stronger for conventional heating as microwave heating weakened the hydrogen bonding in ethanol-water mixture. The peaks at 1045 cm^{-1} and 2970 cm^{-1} were from C-O and C-H stretching, respectively.

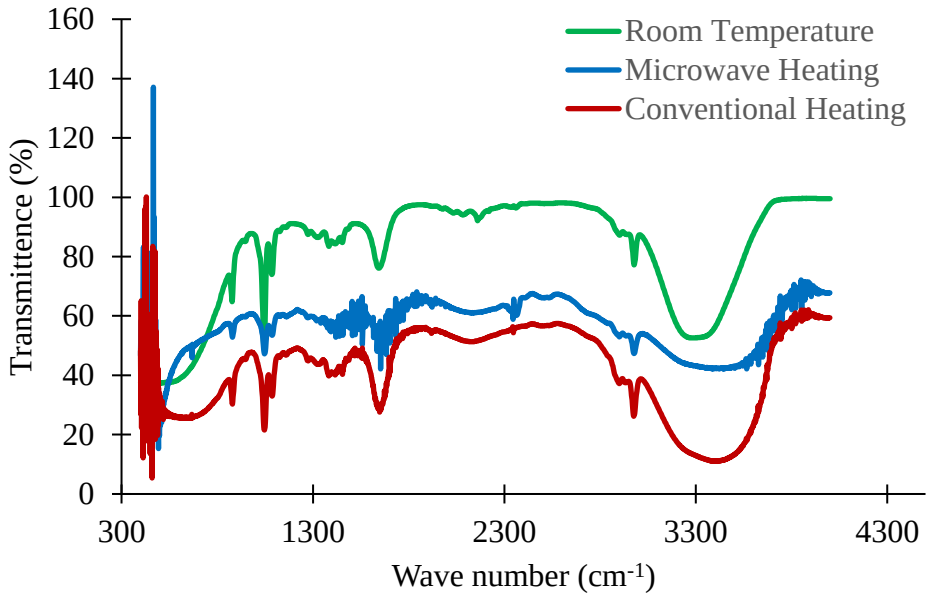

Figure 4.6 FTIR spectra of ethanol-water solution (50% v/v).

The proposed mechanism is shown in Figure 4.7. During conventional heating, the entire volume of the feed stream is uniformly heated. On the contrary, microwave heating involves direct heating of the feed mixtures resulting in localized superheating [269, 272]. The dielectric loss of ethanol is known to increase with temperature whereas for water it decreases with temperature, therefore the microwave dissipation can be more significant in hot areas and can lead to local turbulence and spatial temperature gradients [287, 288]. The localized super heating and breaking of hydrogen bonded ethanol-water clusters are

bound to enhance the tendency of ethanol molecules to escape from the feed mixture resulting in improved flux and better separation efficiency.

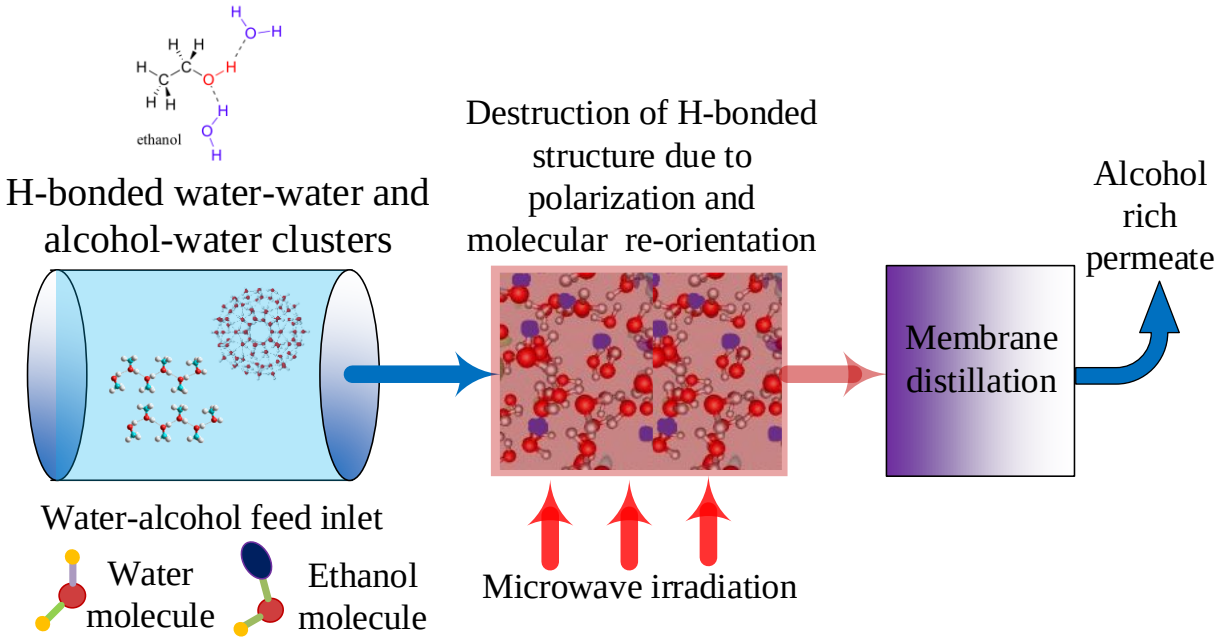

Figure 4.7 Schematic of the proposed mechanism of microwave heating.

4.5 Conclusions

This process involved successful implementation of microwave irradiation to heat the ethanol- water mixture in SGMD using PTFE membrane and CNIM. Experiments were conducted at three different feed stream temperatures (40, 50 and 60 °C), and three feed compositions (5, 10 and 15 vol% ethanol in water). The contact angles on of ethanol-water mixtures after microwave heating dropped by 12.8% – 13.1 % for PTFE membrane and 8.1%-13.09% for CNIM as compared to conventional heating. As compared to conventional SGMD, the increase in ethanol flux, separation factor and mass transfer coefficient during MIMD were 69%, 155% and 70%, respectively, with CNIM at 50 ^{0}C and 10 (v/v%) ethanol in feed. The flux and separation factors based on CNIM and MIMD were between 65% and 156% higher than what has been published before by either MD or pervaporation. Therefore, the combination of CNIM and MIMD represents a major improvement in the state of the art. Factors such as localized super heating and the breakdown of ethanol−water clusters led to the performance enhancement in MIMD. The MIMD was also observed to be less energy intensive compared to the conventional MD process.

CHAPTER 5

LOW TEMPERATURE RECOVERY OF ACETONE-BUTANOL-ETHANOL (ABE) FERMENTATION PRODUCTS VIA MICROWAVE INDUCED MEMBRANE DISTILATION ON CARBON NANOTUBE IMMOBILIZED MEMBRANES

5.1 Introduction

The cost-efficient production of biofuels from biomass has the potential to address global problems such as energy security and climate change. An important process in the biofuel industry is the generation of acetone-butanol-ethanol (ABE) mixture as fermentation products which has garnered huge attention in recent times [289]. There is significant interest in the efficient ethanol recovery from fermentation broths for clean fuel and chemical feed stock production [290, 291]; acetone and butanol are important solvents that also have many other industrial applications[292, 293]. As a biofuel, butanol has high energy content, is compatible with prevailing gasoline supply channels and has low vapor pressure [294]. In a typical ABE fermentation system, the produced acetone, butanol and ethanol maintain a fixed ratio of 3:6:1. Maximum amount of total solvents usually varies between 16-20 g/L with concentration of butanol at 10-12 g/L being a limiting factor due to end production inhibition resulting from its toxicity. This leads to high energy cost for ABE recovery from the low concentration fermentation broth via thermal distillation [295]. Currently an equivalent of 50% of the heat of combustion of butanol is used up in the ABE distillation process itself, therefore the development of cost-effective separation technologies that can perform a substantial role in increasing productivity and improve the economics of ABE production is of great importance [295-297].

Alternate ABE separation approaches such as adsorption [298], gas stripping [299], liquid–liquid extraction[300], perstraction [301], pervaporation [302], membrane distillation[303] and reverse osmosis[304] have been explored. Membrane distillation (MD) is a thermally driven process where separation of two phases (a hot feed side phase and a colder receiving phase) occurs through a hydrophobic microporous membrane. The difference in temperature between the feed and permeate side of the membrane creates the vapor pressure gradient, triggering the transport of the vapor across the membrane. Some of the major advantages of MD are comparatively low energy requirement, capital cost and operation temperatures compared to distillation [305], and significantly higher flux than pervaporation . While modelling studies showed that MD has much potential in ABE separation[306, 307], to the best of our knowledge, only limited experimental studies have been published in this field [303, 308].

A range of separation applications such as pervaporation, extraction, protein separation, breaking oil-water emulsion, nanofiltration and membrane distillation have been carried out on carbon nanotubes based membranes [141, 146, 203, 206, 252, 309-311]. We have demonstrated that on immobilizing CNTs on the membrane surface, the physicochemical interaction between the solutes and the membrane can be significantly altered [142, 143, 206]. A rapid progress in MD has been achieved with the incorporation of carbon nanotube immobilized membrane (CNIM) for desalination where the CNTs enhance the preferential passage of the water vapor molecules while repelling the liquid salt-water feed mixture resulting in a remarkable increase in pure water flux. Super-hydrophobic CNT loaded PVDF membrane synthesized by one-step electrospinning technique has shown improved desalination performance[312]. CNIM has been

successfully implemented in membrane distillation using sweep gas to carry out the permeated species (SGMD) for enhanced organic solvent recovery [142]. Another study investigated the performance of vertically aligned (VA) and open-ended CNT arrays filled polydimethylsiloxane (PDMS) composite membrane for pervaporative recovery of butanol from ABE fermentation broth[313].

Microwave induced heating has been employed in several methods including drying, chemical synthesis and in-home kitchens. Microwave processes are associated with nonthermal effects such as localized super heating, activation energy reduction, breakdown of hydrogen bonded structures in aqueous medium, and the generation of nano-bubbles[274, 276]. Recently, a MD process induced by a microwave has been reported by our group for desalination where microwave heating led to the breakdown of hydrogen bonded salt water clusters leading to high flux[314]. Comparison of MD by conventional and microwave heating has been published before with ethanol-water system. Microwave induced membrane distillation has shown significant advantages including higher flux, selectivity and lower energy consumption[315]. Since ABE consists of polar molecules, it is anticipated that they will absorb microwave energy and their interactions will lead to the breakdown of water-organic clusters to enhance the removal of ABE[316, 317]. The aim of this project was to incorporate CNIM along with microwave heating to enhance ABE separation via SGMD.

5.2 Materials and Methods

5.2.1 Chemicals and Materials

The solvents (acetone (AR ≥ 99.5%), butanol (anhydrous, 99.8%) and ethanol (anhydrous, ≥ 99.5%)) used in this experiment were procured from Sigma Aldrich (St. Louis, MO).

Cheap Tubes Inc. (Brattleboro, VT) has supplied the MWCNTs (~30 nm dia, 15 μm long). Octadecyl amide (-CO-NH-$C_{18}H_{37}$) functionalization (CNT-ODA) was performed in our laboratory following a method published before [318]. In all experiments, deionized water (Barnstead 5023, Dubuque, Iowa) has been used.

5.2.2 CNIM Fabrication and Characterization

Proper dispersion of CNTs and CNT-ODA in organic solvent and the fabrication of uniformly distributed CNTs throughout the membrane surface was the main concern. A commercial PTFE membrane (Advantec, 0.2 μm pore size, 74% porosity, polypropylene supported) was used as base membrane and the CNIMs were prepared on it. The CNTs as well as CNT-ODA dispersion were carried out using a procedure described in our previous paper [146]. Our previous studies have indicated that functionalization of CNTs enhanced its dispersibility in the solvent phase, which eventually helped in film-formation [318]. Scanning electron microscopy (SEM) (JEOL; model JSM-7900F) was utilized to characterize the CNIM and CNIM-ODA. The hydrophobic nature of the membranes used was measured via contact angle and liquid entry pressure (LEP) measurements with DI water and ABE mixture. Drops of a fixed ABE concentration were placed on the membrane with the help of a micro syringe (Hamilton, 0–100 μL). The contact angles of the drops on the membrane surface were measured using a digital video camera placed at the top of a stage.

5.2.3 Experimental Setup

Figure 5.1 illustrates the experimental setup. The MIMD in sweep gas mode was used in all experiments where dried air at room temperature was passed through the permeate side of the membrane module that assisted in removal of the permeated vapor. A module made

of polytetrafluoroethylene (PTFE) was used in the SGMD test cell. Details have been described elsewhere [146]. The inner diameter of the module was 4.3 cm with an operational contact area of 12.5 cm^2. The ABE-water feed mixture was pumped (Cole Parmer, model 77200-52) through the SGMD module and was recirculated. The ABE-water feed temperature was controlled using a microwave oven and the power level of the microwave was adjusted as needed to get the desired temperature. The feed reservoir temperature was maintained by regulating the temperature of a constant temperature bath. A flowmeter (model no EW-03217-02, Cole Parmer) was used to monitor the sweep gas flow rate. Two thermistor thermocouples (K-type, Cole Parmer) were placed on the stream inlet and outlet to measure the temperature of the feed solution entering and exiting the membrane module.

5.2.4 Experimental Procedure

To remove impurities in the dry sweep air such as dust or moisture, laboratory air from the fume hood was circulated through a drying unit (W. A. Hammond Drierite, Xenia, OH) and hollow Fiber Filter (Barnstead International, Beverly, MA) prior to flow into the permeate side. The drying unit helps to lower the relative humidity close to zero. In all experiments, the sweep airflow rate on the permeate side was maintained 4.5L/min. Experiments were performed thrice to estimate precision. The experimental data show lower than 1% relative standard deviation.

The liquid entry pressure (LEP) is the minimum pressure at which liquid penetrates the membrane pores. In MD, LEP measurement is important as a liquid–vapor interface develops at the membrane pore entrance and the permeated species vaporizes through it. The LEP was measured using a method described before[146]. A stainless-steel chamber

(Alloy Products Corp, 185 Psi Mawp) was filled with the ABE-water feed solution (1.5, 3, 0.5 vol% ABE, respectively). The membrane held in a test cell was connected to the liquid chamber. A gas cylinder was used to increase the pressure above the liquid, which was increased till the liquid started to enter through the membrane pores.

A graduated measuring cylinder was used to measure the volume of the feed solution before and after experiments. After each experiment, the recycled feed mixture was cooled down to room temperature and the final volume was measured. An airtight feed solution chamber was used to confirm that sample was not lost due to evaporation of volatile components. The flux and separation factor were calculated by analyzing the initial and final feed mixture compositions using a Gas Chromatography (HP-5890) equipped with an FID detector. The gas chromatograph was operating with injection port temperature of 200°C, column temperature of 150°C and detector temperature of 250 °C. Analyses were carried out on an EzChrom Elite Chromatography data system used for GC control, data acquisition and processing.

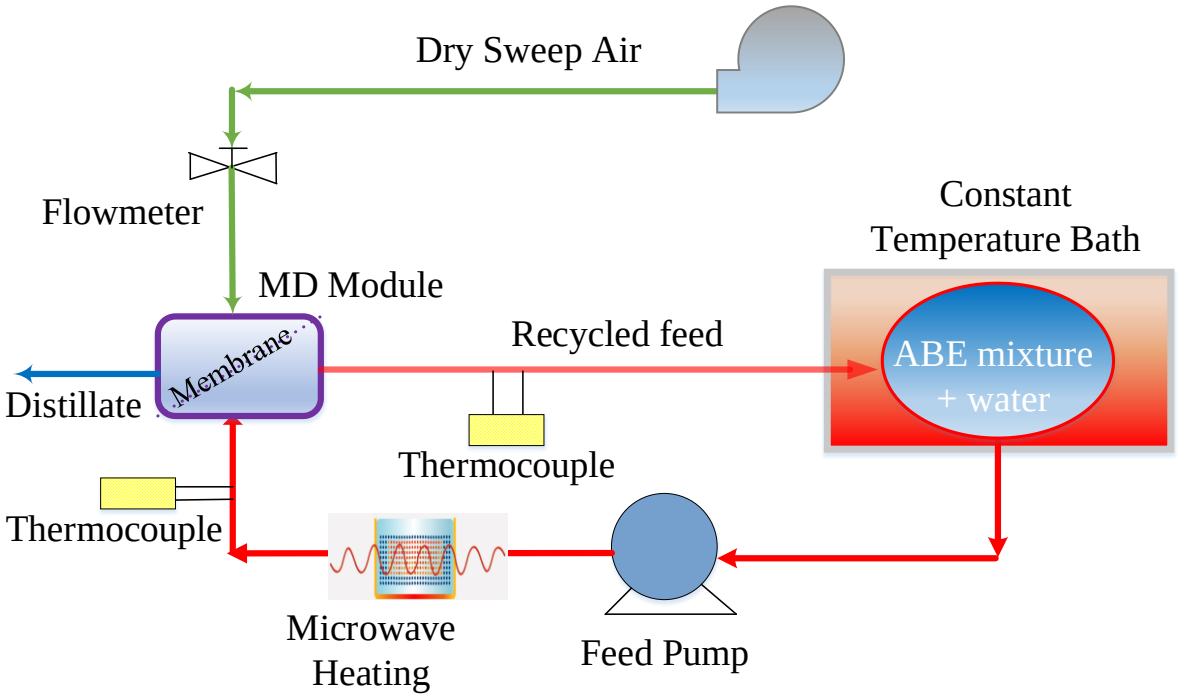

Figure 5.1 Schematic diagram of the experimental setup for the SGMD.

5.3 Results and Discussion

5.3.1 Membrane Characterization

The SEM images of the PTFE, CNIM, and CNIM-ODA are shown in Figure 5.2a, b and c. The porous structure of the pristine PTFE membrane and presence of CNT and CNT-ODA on the CNIM and CNIM-ODA surfaces are clearly visible. Uniform distribution of CNTs over the entire membrane surface was also observed. In our previous studies, gas permeation test showed no significant change in effective porosity over pore length of the membrane as very small amount of CNTs had been used to fabricate the membrane[206].

Thermogravimetric analysis (TGA) (10 0C/ min heating rate in air) was used to analyze the stability of the PTFE membrane, CNIM and CNIM-ODA at higher

temperature. The TGA and differential TGA curves are shown in Figure 3a and b, respectively. It is observed that the initial thermal decomposition of the membrane began at ~260 0C (degradation of PP support layer), followed by the degradation of PTFE active layer at 500 °C. From the figure, it is evident that CNIM and CNIM-ODA were thermally stable within the operating temperature ranges.

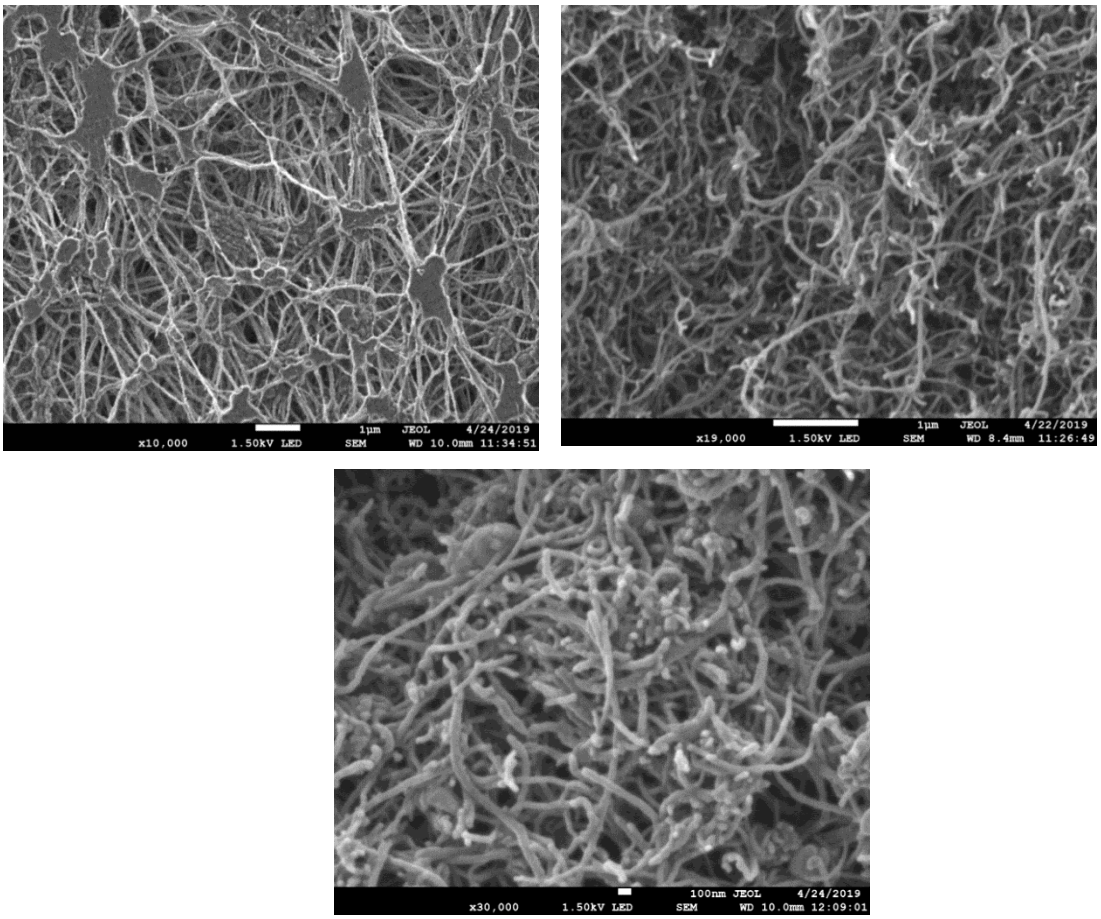

Figure 5.2 SEM images of **a)** unmodified PTFE membrane, **b)** CNIM, **c)** CNIM-ODA.

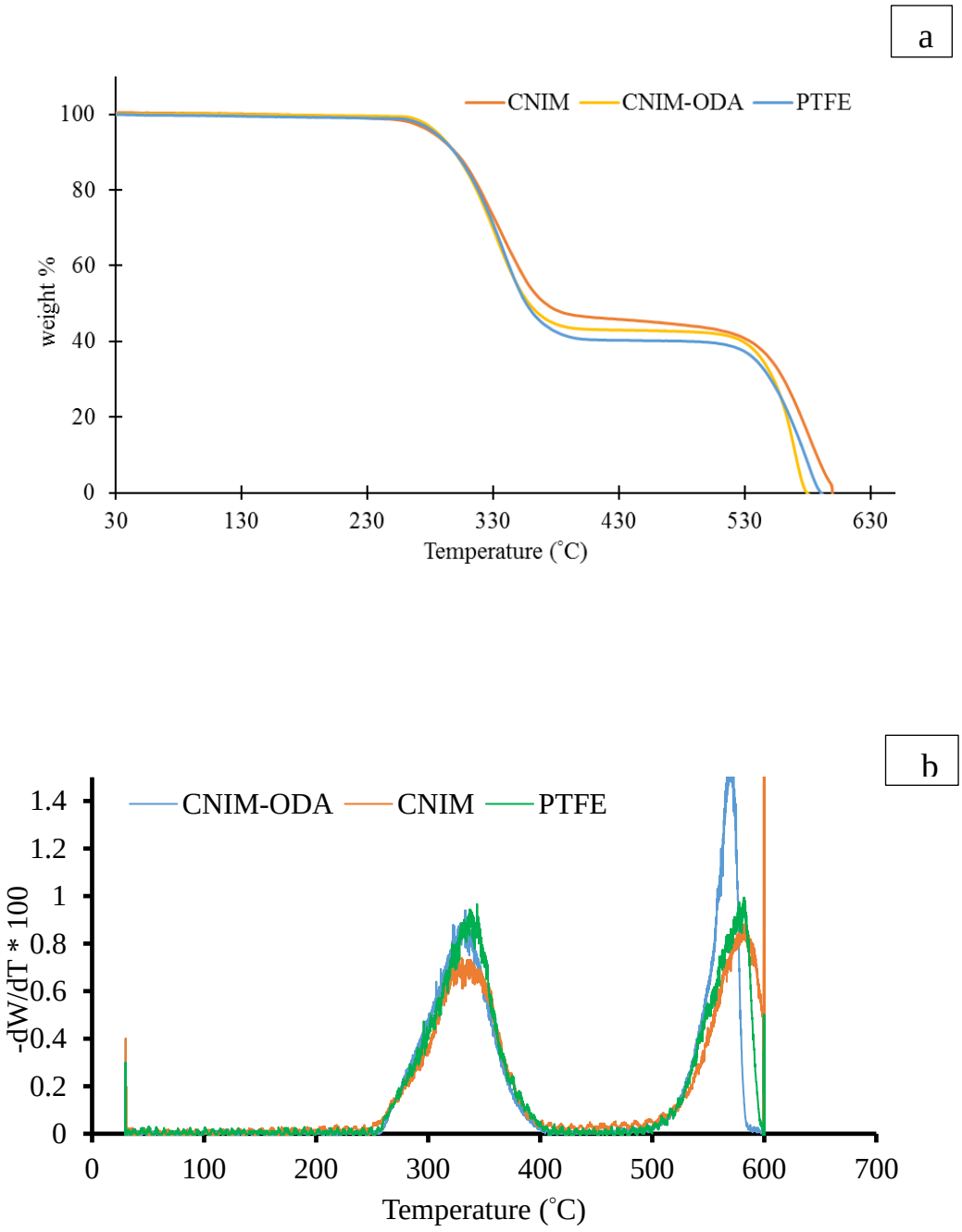

Figure 5.3 a) Thermogravimetric analysis of unmodified PTFE. CNIM and CNIM-ODA, **b)** differential TGA curves of the corresponding membranes.

The contact angle measurements provide a measure of wettability of the membrane surface. The contact angle depends upon the intermolecular interactions between the

membrane surface and the liquid placed on it. Table 5.1 demonstrates the contact angle values for pure water and ABE mixtures on different membrane surfaces. As can be seen from the table, the contact angles for pure water were much higher on CNIM and CNIM-ODA due to their higher hydrophobicity which were like what has been reported previously [140, 143, 146]. The contact angles on the PTFE, CNIM and CNIM-ODA membranes at 0.6, 1.2 and 0.2 vol % of ABE and 97.8 % water are shown in Figure 5.4a, b and c. The presence of CNTs dramatically altered the contact angle for CNIM. The presence of organic molecules in aqueous solution reduced the contact angle for all membranes. However, since the alcohols and other organic solvents possess an affinity for CNTs, the contact angles of the ABE mixtures decreased significantly in CNIM and CNIM-ODA (Table 1). The contact angles for ABE mixture decreased in the following order: PTFE> CNIM-ODA> CNIM. For instance, the droplet of ABE-water mixture on CNIM indicated a contact angle of 84° vs a contact angle of 103^{0} for PTFE and 108^{0} indicating strong interactions with the CNTs and relatively less with CNT-ODA. The increasing ABE affinity to CNIM and CNIM-ODA over PTFE are potential means to increase the removal efficiency and reduce concentration polarization[319].

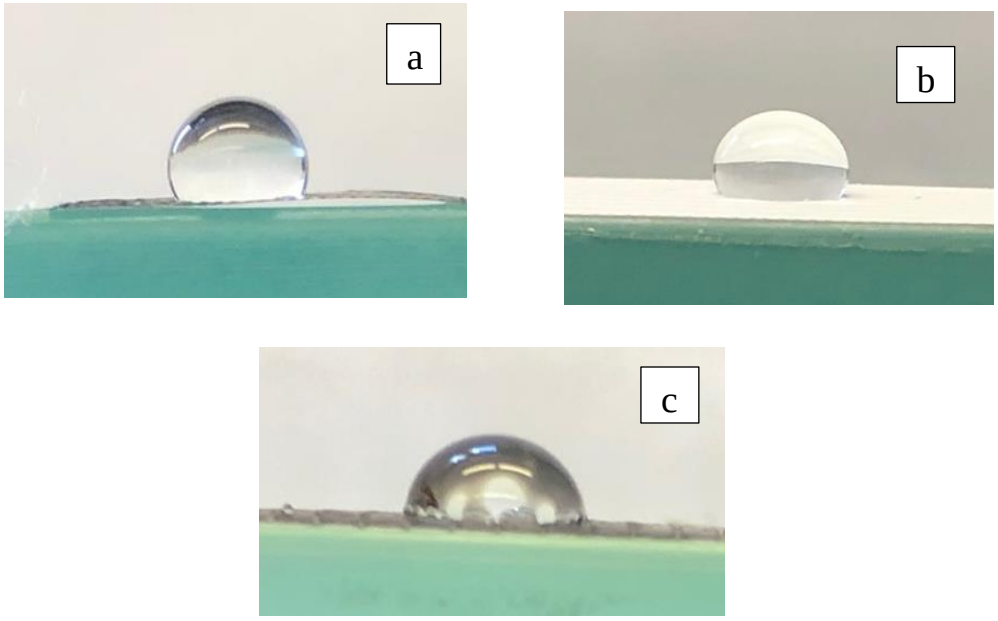

Figure 5.4 Picture of ABE- water solution (0.6, 1.2 and 0.2 vol % respectively) droplet on **a)** CNIM-ODA, **b)** PTFE, **c)** CNIM.

Table 5.1 Contact Angles of pure water & ABE mixture

Solvent	**Contact angle (º)**		
	PTFE	**CNIM**	**CNIM-ODA**
Pure water	105	109	116
ABE mixture	103	84	110

The LEP of pure water for PTFE, CNIM and CNIM-ODA were found to be similar, ~455.1 kPa, for all membranes, which further decreased to 220.7, 144.8 and 179.3 kPa, respectively for ABE mixture (1.5, 3 and 0.5 vol% of ABE in water). The high LEP values indicate the low wettability of the membranes as also evident from the contact angle measurement described above.

Figures 5.5a, b and c show the AFM images of pristine PTFE membrane, CNIM and CNIM-ODA, respectively. The average surface roughness (Ra) values were measured over an area of 10μm × 10 μm of the corresponding membrane samples and was found to be 127 nm, 142 nm and 138 nm, respectively. It is clear from the figure that the

incorporation of small amount of CNTs change the surface topography significantly and alters the characteristics of the fabricated membrane surface.

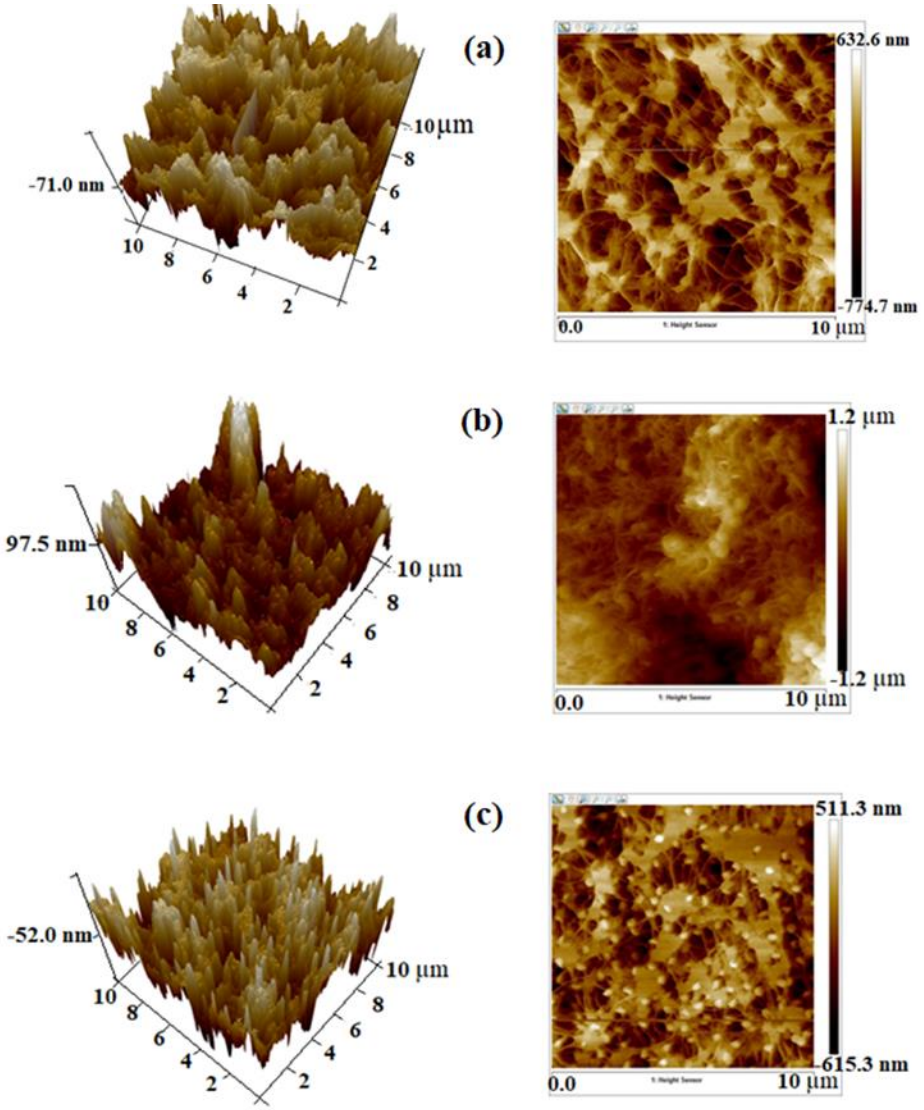

Figure 5.5 AFM images featuring the topography of the **a)** unmodified membrane surface (PTFE), **b)** CNIM and **c)** CNIM-ODA.

5.3.2 MD separation performance

The separation performances of various membranes were characterized with respect to ABE permeation rate and selectivity. The fabricated membranes' performance was

compared with the pristine membrane. The individual flux of '*i*' component (J_{wi}), was described as:

$$J_i = \frac{W_{pi}}{A * t} \tag{5.1}$$

Where, W_{pi} was the amount of permeated mass of species 'i' within a period 't' through a membrane of area 'A'. The measure of separation efficiency was denoted by separation factor ($\beta_{i\text{-}j}$), and is calculated from the following relation:

$$\beta_{ABE-water} = \frac{y_{ABE}/y_{water}}{x_{ABE}/x_{water}} \tag{5.2}$$

where y_i and x_i represent the permeate and feed side weight fraction of 'i' component.

Apparent activation energy (Eapp) of solvent transport in the membrane processes can be expressed as [320]

$$J = J_0 \ exp\left(-\frac{E_{app}}{RT_f}\right) \tag{5.3}$$

Where J and J_0 are fluxes (mol m^{-2} h^{-1}), R is gas constant (J mol^{-1} K^{-1}), T_f denotes feed temperature (K).

The Figures 5.6a, b and c display the effect of feed concentration on acetone, butanol and ethanol flux and separation factor. The ratio of ABE in the aqueous feed mixtures was kept constant at 3:6:1 (vol %). Three different feed concentrations namely 0.6, 1.2, and 1.5 (vol %) of acetone were tested and the butanol and ethanol in the feed solutions were adjusted accordingly. The feed temperature and feed flow rate were maintained at 40^0C and 112 mL/min, respectively. It can be observed from the figures that with increase in acetone, butanol and ethanol concentration in feed, the ABE flux increased for all membranes. The CNIM and CNIM-ODA showed improved flux compared to the PTFE membrane, which was due to the enhanced solvent affinity with the nanotubes. Total solvent flux was in the order of CNIM> CNIM-ODA> PTFE. The highest total solvent flux for CNIM may be attributed to the higher solvent sorption capacity, as also supported by the contact angle values. The presence of bulky ODA groups on CNT-ODA may have limited the direct sorption and fast transport of the organic compounds on the CNT framework.

The solvent flux reached as high as 0.82, 1.36 and 0.19 L/m^2.h for acetone, butanol, and ethanol, respectively, at 40 ^{0}C and 1.5, 3 and 0.5 vol % of ABE in the feed. The CNTs influenced the acetone, butanol and ethanol partition coefficient, and its effects were more pronounced at higher concentrations. The enhancement in acetone flux reached as high as 130.3 % for CNIM and 60.6 % for CNIM-ODA over PTFE membrane at 1.2 volume % of acetone. Enhancement in butanol and ethanol flux followed similar pattern with enhancement reaching up to 127% and 375% respectively for CNIM. Figures 5.6 d, e, and f show plots of separation factor of ABE with respect to feed concentration. As can be seen from the plots, the separation factor was inversely proportional to the concentration for all

the membranes. However, a higher separation factor for CNIM than CNIM-ODA and PTFE membrane was observed at all feed concentrations tested here. Enhancement over PTFE membrane for acetone reached as high as 79.92% for CNIM and 41.5% for CNIM-ODA. Similar trends were observed for ethanol and butanol separation factor.

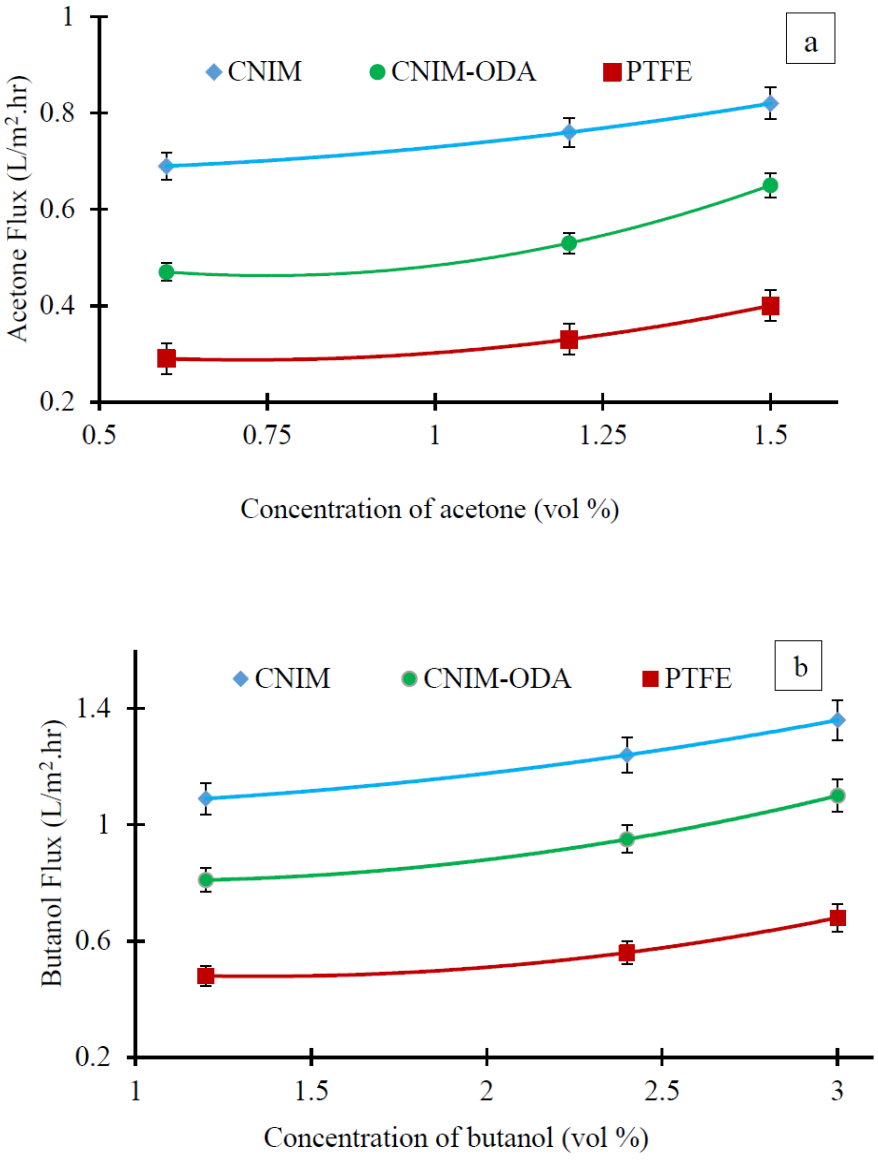

Figure 5.6 Effect of feed concentration on flux for **a)** acetone, **b)** butanol.

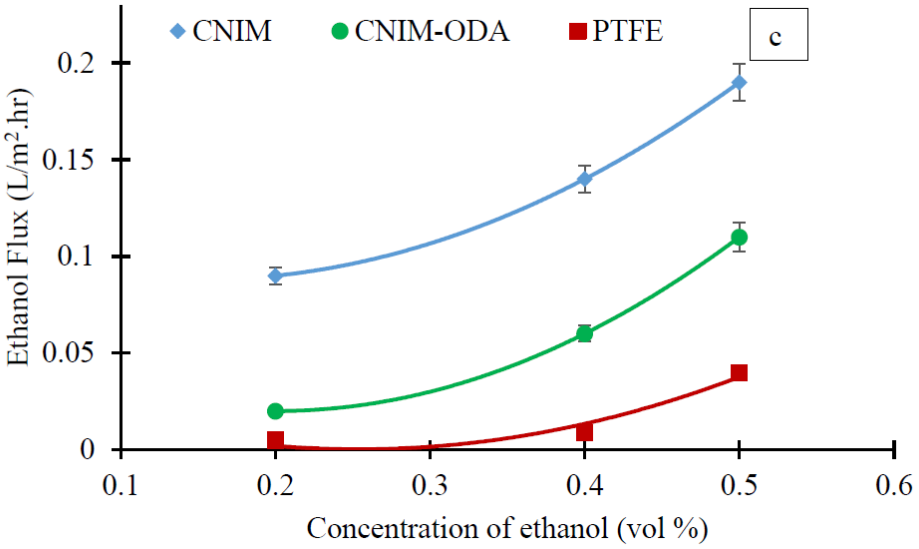

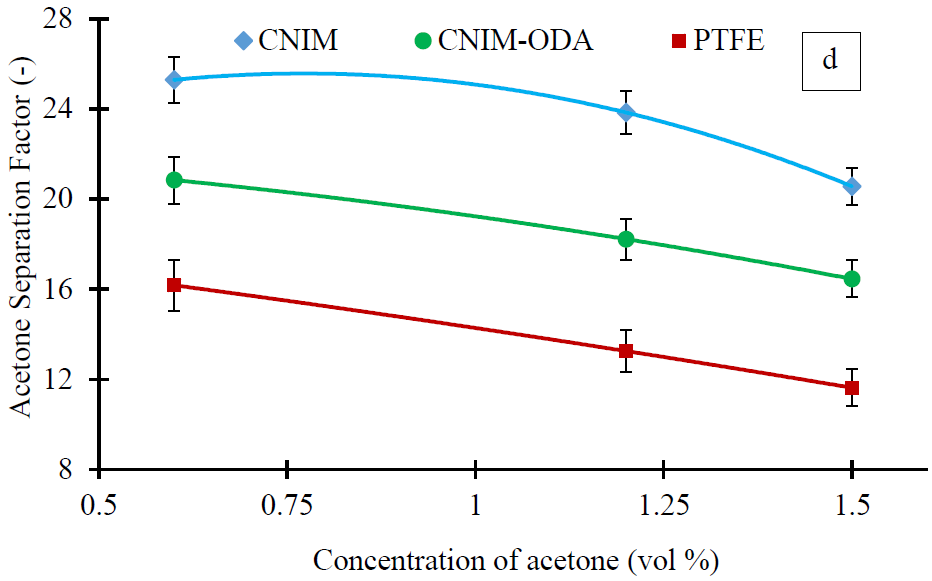

Figure 5.7 Effect of feed concentration on flux **c)** ethanol, and on separation factor for **d)** acetone.

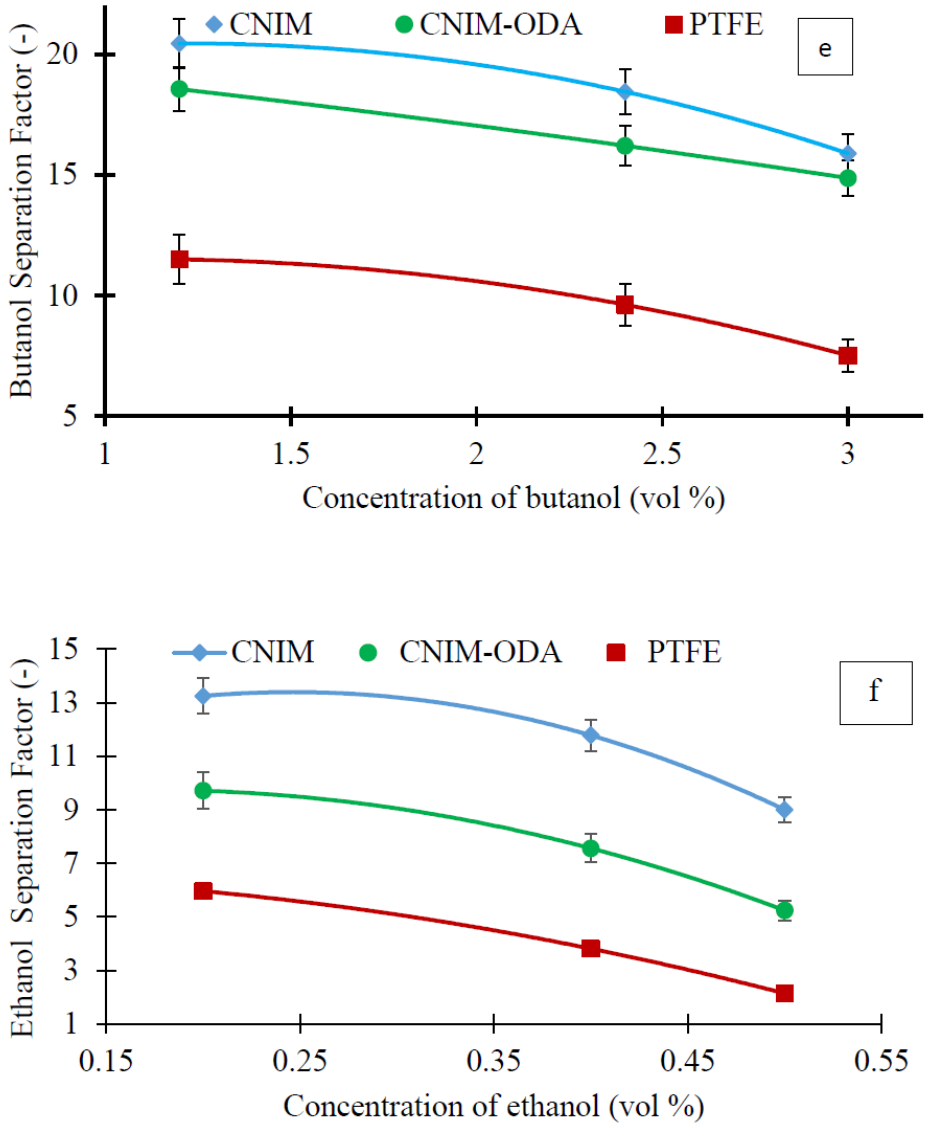

Figure 5.8 Effect of feed concentration on flux for **e)** butanol and **f)** ethanol.

The acetone, butanol and ethanol flux and separation factor on the CNIM, CNIM-ODA and the PTFE membrane as a function of feed temperatures are demonstrated in Figures 5.7 a, b, c, d, e and f. A feed concentration of 1.5, 3 and 0.5 vol % of acetone, butanol, and ethanol, respectively, was maintained and the feed flow rate was kept constant

at 112 mL/min. The permeate fluxes for all membranes showed a direct relationship with feed temperature. At 60 ^{0}C, the CNIM flux reached up to 1.15 L/m^2.h, 1.54 L/m^2.h and 0.58 L/m^2.h for acetone, butanol and ethanol, respectively, which were considerably (around ten times) higher than previously reported data for pervaporation[321, 322]. In general, higher fluxes at all temperatures for CNIM were observed followed by CNIM-ODA, although the enhancement was distinct at reduced temperature. At 40^{o}C the improvement in acetone, butanol and ethanol flux reached to 105, 100 and 375%, respectively, in comparison with pristine PTFE membrane. Hence, it is possible to perform the experiments at a relatively lower temperature thereby making it a less energy intensive process. It is well known that the vapor pressure increases exponentially with temperature and the sharp increase in vapor pressure from 40 to 60°C was reflected in the corresponding increase in ABE flux. From Figures 5.7 d, e, and f, it can be observed that at all the operating temperatures; CNIM's separation performance was significantly better compared to the commercial PTFE membrane. The separation factor enhancement of CNIM compared to PTFE membrane reached to 103, 129 and 324% at 50^{o}C for ABE. As a result of negative effects of viscosity, a decline in ABE separation factor was observed with increase in operating temperatures for all membranes [220]. The water flux is presented in Figure 5.7g which showed an increase with feed temperature due to higher vapor pressure at elevated temperatures.

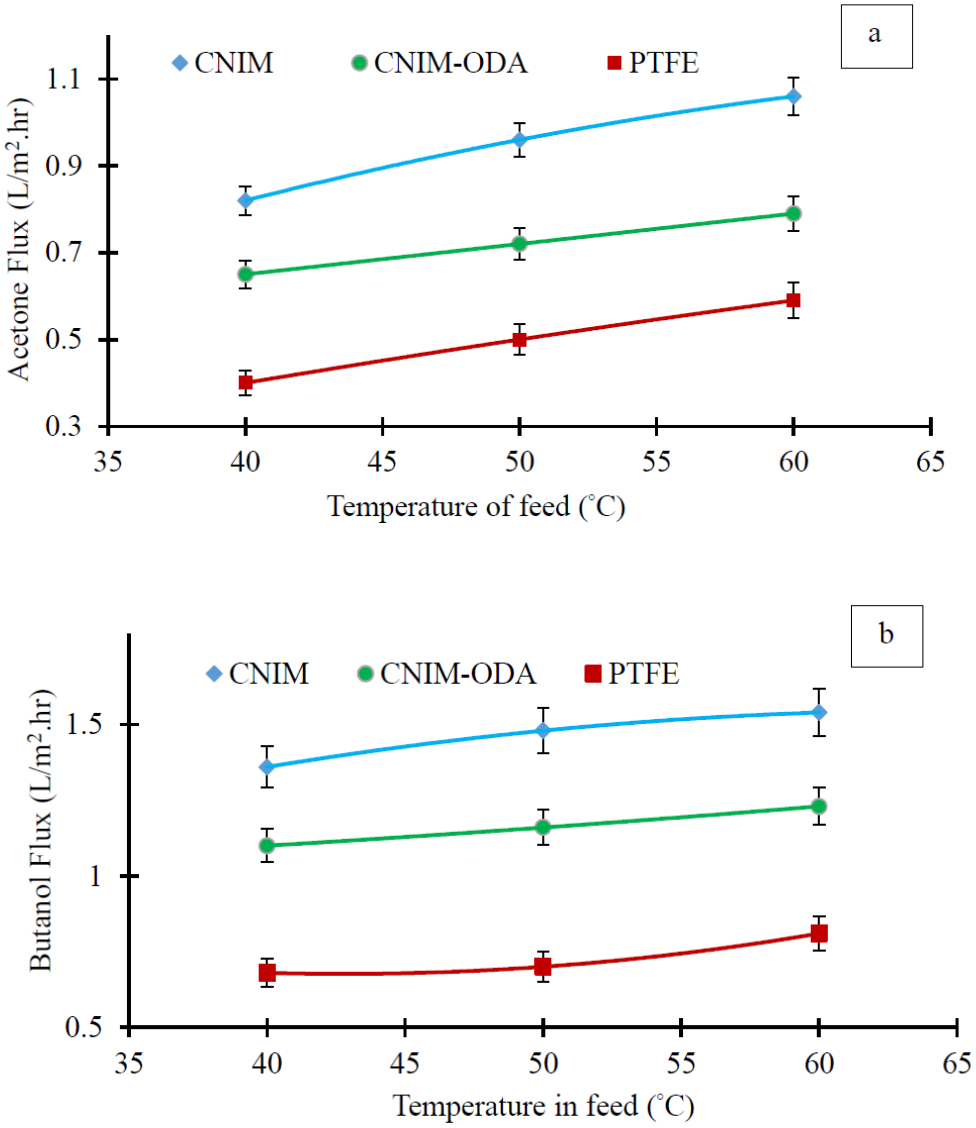

Figure 5.9 Effect of feed temperature on flux for **a)** acetone, **b)** butanol.

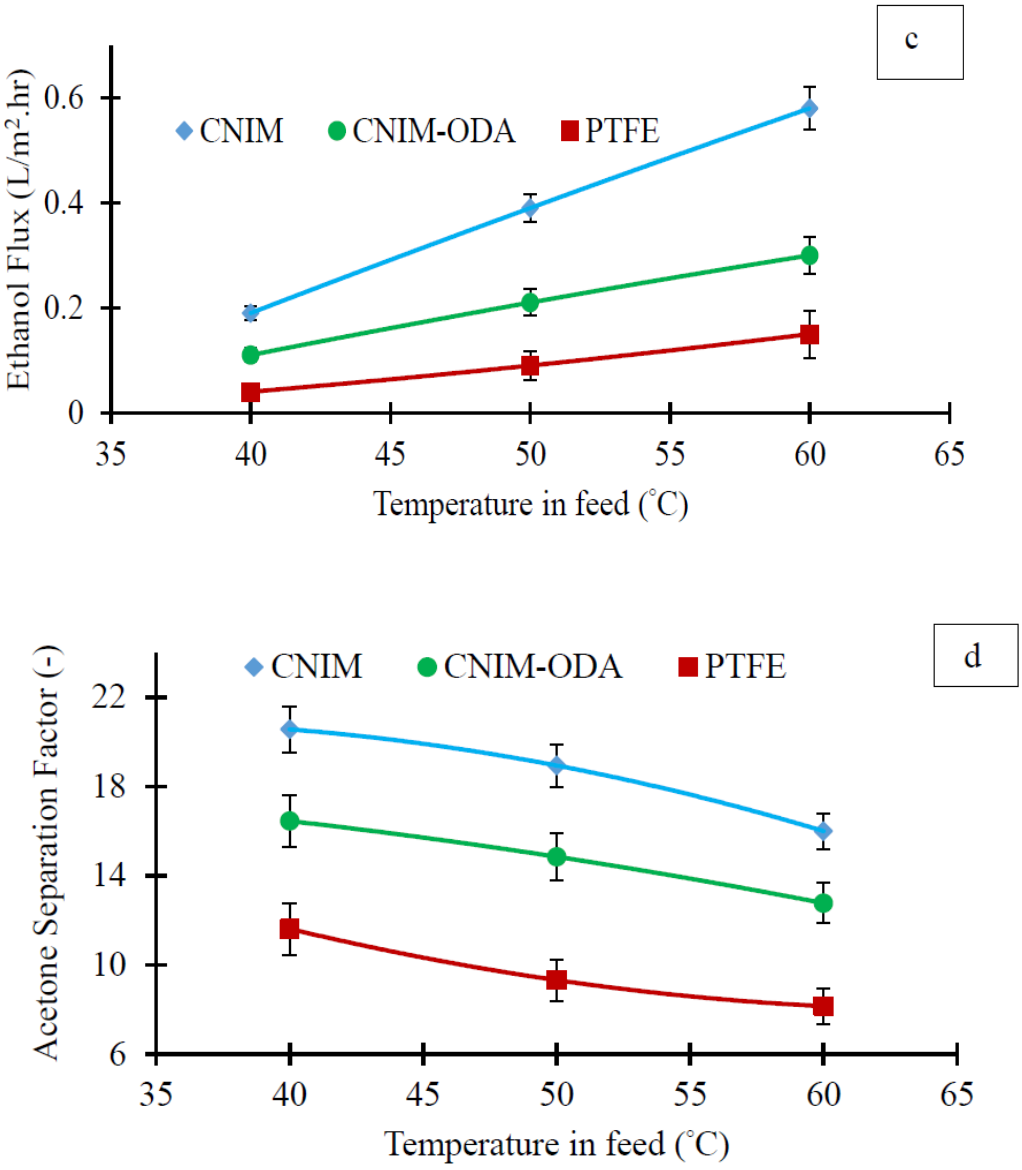

Figure 5.10 Effect of feed temperature on flux **c)** ethanol, and on separation factor for **d)** acetone.

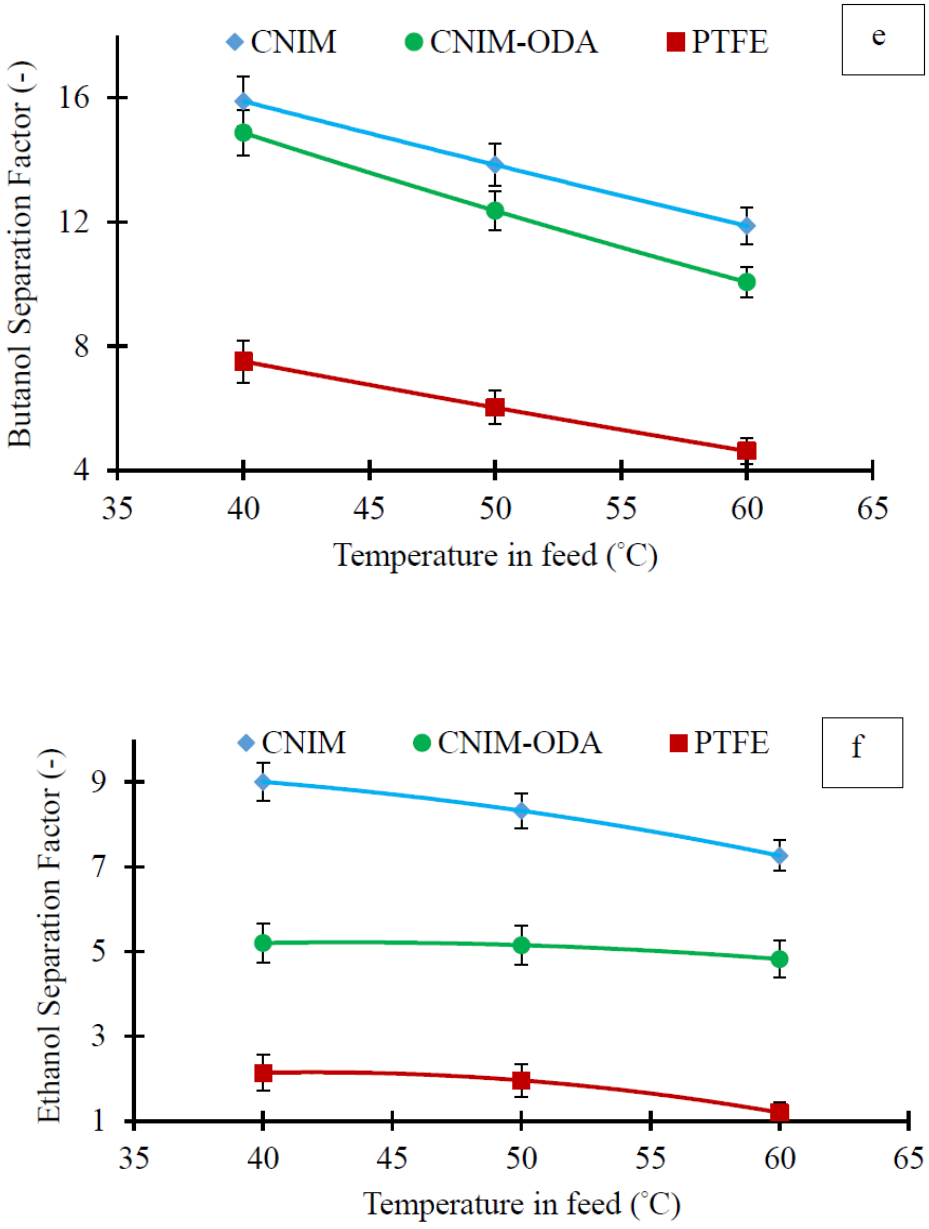

Figure 5.11 Effect of feed temperature on flux for **e)** butanol, **f)** ethanol.

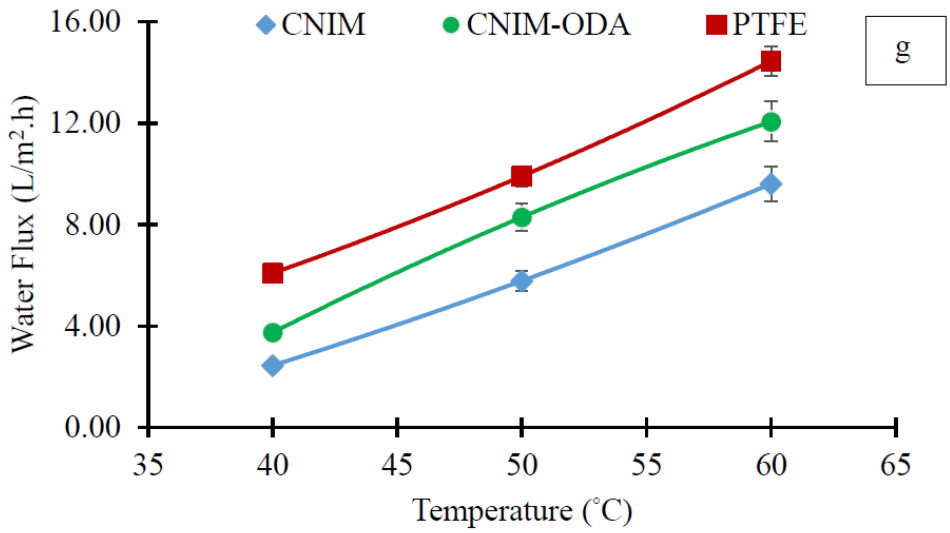

Figure 5.12 g) effect of feed temperature on water flux.

Apparent activation energy (E_{app}) for organic solvent transport through porous membranes in SGMD mode was calculated from Eq. (5.4). The concentration of the acetone, butanol and ethanol mixture was kept constant (1.5, 3, 0.5 vol %, respectively). The E_{app} values for PTFE, CNIM & CNIM-ODA are shown in Table 5.2.

Table 5.2 Apparent Activation Energy (E_{app}) Values forAacetone (1.5 vol%), Butanol (3 vol%), Ethanol (0.5 vol%) and Water (95 vol %) in Feed

Membranes	**Apparent activation energy (kJ/mol)**			
	Acetone	**Butanol**	**Ethanol**	**Water**
PTFE	16.9	17.5	57.4	37.6
CNIM	11.2	5.4	48.5	59.5
CNIM-ODA	8.5	4.8	43.6	50.9

It is clear from the table that the presence of CNTs significantly reduced the apparent activation energy for all ABE components. Among three solvents, butanol exhibited the lowest E_{app} value followed by acetone and ethanol with all membranes. However, the activation energy of water was much higher which may be due to the

exponential increment of water vapor pressure at elevated temperatures in case of modified membranes. This also results in reduction of separation factor with increase in feed temperature.

It was important to investigate if separation of each ABE component was affected by the presence of the other solvents. Therefore, binary mixture of each compound with water was also studied using PTFE and CNIM. The data related to the binary mixtures is presented in Figures 5.8a, b and c, where the flux of each component and separation factor are presented as a function of solvent concentration. The feed flow rate and the operating temperature was maintained at 112 mL/min and 40 °C, respectively. It is clear from the figure that with increase in feed concentration, the flux increased for each compound in both membranes. Butanol which had limited miscibility with water showed higher flux than ethanol that was significantly more miscible. As expected, higher flux was obtained for all solvents when CNIM was used. It was observed that the individual solvent flux in the binary mixtures were higher compared to the ABE mixture under similar condition. For example, the acetone flux was obtained to be 1.36 L/m^2.hr for CNIM at 40 ^{0}C and 1.5 vol % of acetone in water, which was 65.8% higher than the corresponding ABE mixture. Similar trend was also observed for butanol and ethanol mixture. The flux decline in the case of a mixture may be attributed to the mutual interaction and competition between the different compounds that reduced partitioning as well as permeability[323].

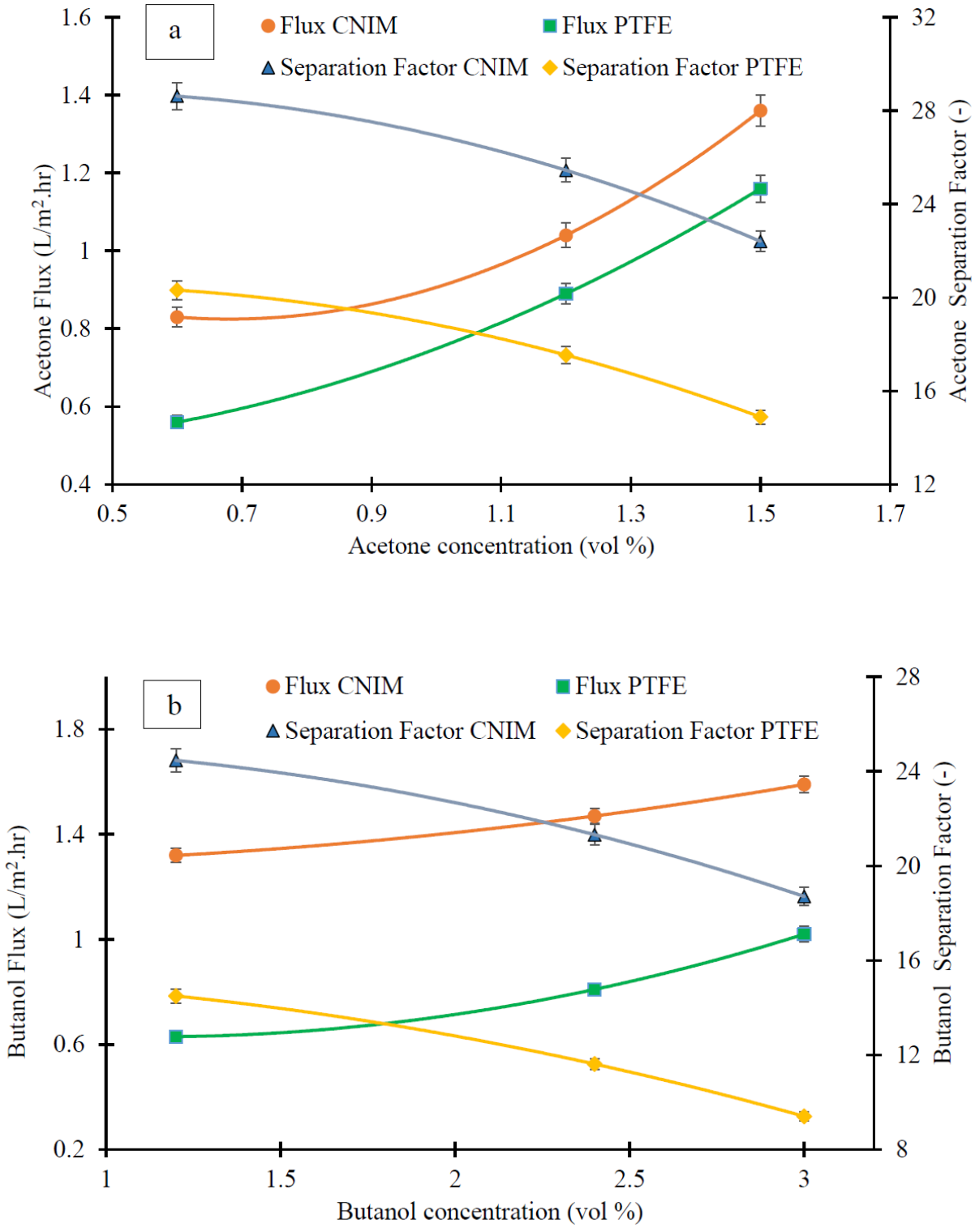

Figure 5.13 Effect of feed concentration on flux and separation factor for **a)** acetone, **b)** butanol.

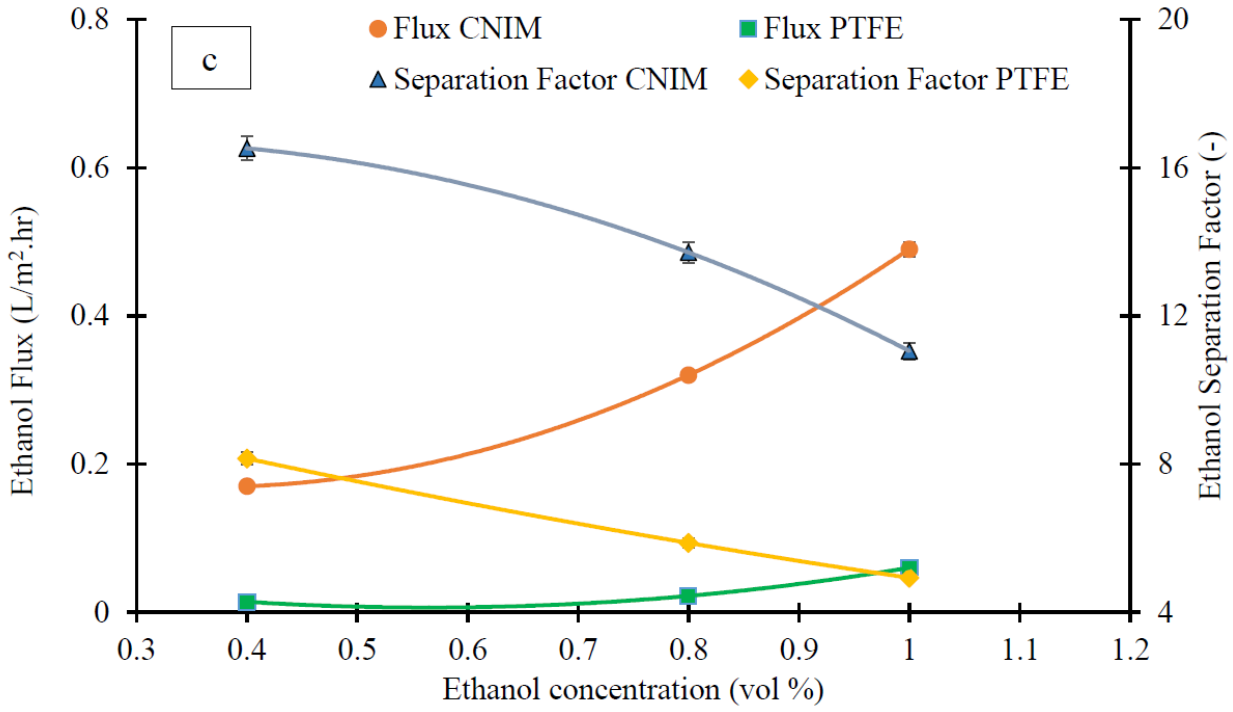

Figure 5.14 Effect of feed concentration on flux and separation factor for **c)** ethanol.

5.3.3 Mass Transfer Coefficient

The mass transfer coefficient (k) can be calculated from the following equation:

$$k = \frac{J_i}{(P_f - P_p)} \tag{5.4}$$

Where, J_{wi} is the flux of species 'i' and the feed side and permeate side partial vapor pressure is denoted as P_{fi} and P_{pi}, respectively. The vapor pressure of the different feed components at a particular temperature was attained from other sources [222] and the P_{pi}, was considered to be almost zero as the sweep air was dried completely prior to entering the permeate side of the membrane.

The 'k_i' values of different components in ABE mixture at varied operating temperatures and a constant feed flowrate of 112 mL/min are presented in Table 5.3. The mass transfer coefficients decreased or remained almost constant with increase in operating temperature for CNIM, CNIM-ODA and PTFE membranes. At all feed temperatures, the CNIM exhibited higher 'k_i' than the pristine PTFE membrane and CNIM-ODA. The enhancement of mass transfer coefficient over PTFE reached as high as 105% for CNIM and 62.5% for CNIM-ODA for acetone, 100 % and 61.8% for butanol and 375% & 175% for ethanol at 40 ^{0}C. For Butanol, the mass transfer coefficient follows an inverse relationship with temperature for all membranes. Also it is known that at higher temperatures the temperature polarization increases significantly, resulting in a lower membrane mass transfer coefficient [324].

Table 5.3 Mass Transfer Coefficient of ABE at Different Temperature and 1.5, 3 & 0.5 Vol % ABE Feed at 112 mL/min

Temp (ºC)	**Mass transfer coefficient (x 10^{-3} L/m^2.h.mm-Hg)**								
	PTFE			CNIM			CNIM-ODA		
	Acetone	Butanol	Ethanol	Acetone	Butanol	Ethanol	Acetone	Butanol	Ethanol
40	0.95	35.9	0.30	1.94	71.9	1.42	1.54	58.1	0.82
50	0.97	20.2	0.41	1.57	42.7	1.77	1.18	33.5	0.95
60	0.68	13.4	0.43	1.23	25.4	1.65	0.73	20.3	0.86

5.3.4 Membrane Stability

To explore the stability of the membranes in presence of these strong organic solvents, SGMD experiments were performed for 8 h a day for 60 days with 1.5, 3 and 0.5 vol % of ABE concentration, respectively. The temperature was maintained at 60^{o}C. The ABE flux was measured periodically. No substantial alteration in flux and membrane wetting were detected even during extended use for all membranes. It can be assumed that there was no significant CNTs loss from the membrane surface as it was not detected in the recycled feed solutions. Comparable stability checks in the past had been implemented where CNIM was used in high temperature aqueous solutions for extended periods and then examined for CNT loss [206].

5.4 Proposed Mechanism

Figure 5.9b demonstrates the enhanced ABE transport mechanism with CNIM. Earlier research published with CNTs have validated that CNTs are exceptional sorbents that increase solute partition coefficient generating higher permeation rate through the membranes [211, 225, 226, 325]. The CNTs are also known to facilitate fast mass transport in both separation processes including chromatography, sorbents, and membranes [210, 326, 327]. The higher vapor pressure of acetone, butanol and ethanol compared to water helped in selective sorption and penetration of ABE mixture through the porous membrane at low temperature. Apart from vapor-liquid equilibrium, the separation performance of CNTs incorporated membranes is due to improved sorption and activated diffusion of organic species on the frictionless CNTs. In addition it is worth noting that during conventional heating, the entire volume of the feed stream is uniformly heated whereas microwave heating results in localized superheating of the feed mixtures[272]. The dielectric loss of organic molecules is believed to increase with temperature whereas for water it decreases with temperature. This results in microwave dissipation being more significant in areas that are more heated and can lead to local turbulence and spatial temperature gradients[288]. A schematic of breakdown of the H-bonded solvent-water clusters is shown in Figure 5.9a. The localized super heating and breakdown of hydrogen bonded ABE−water clusters are likely to improve the tendency of solvent molecules to escape from the system, thus improving flux and separation efficiency. The significant enhancement in ABE flux and separation factors in CNIM and CNIM-ODA are attributed to these multiple factors.

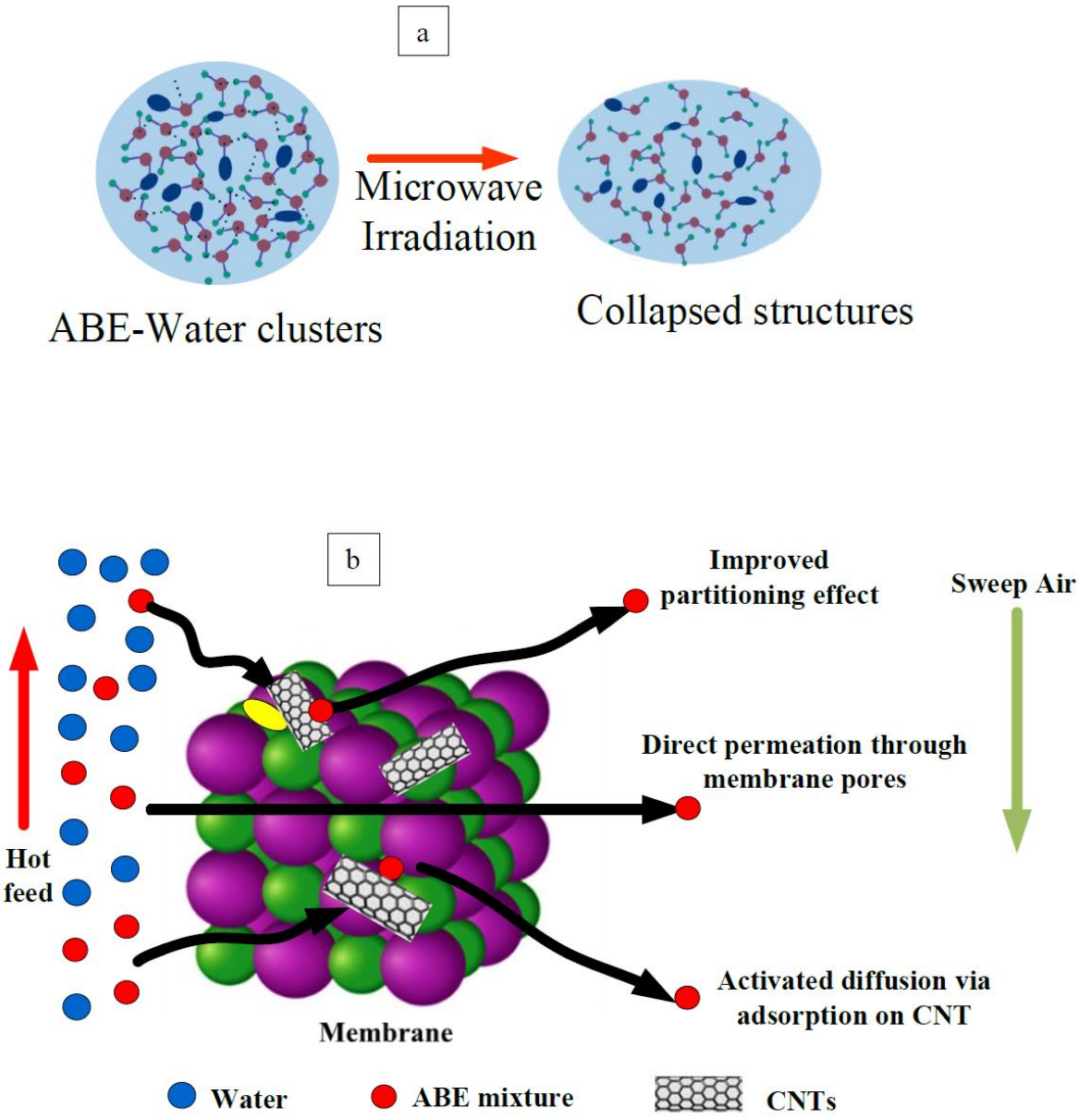

Figure 5.15 a) H-bonded ABE-water clusters, **b)** Proposed mechanism schematic.

5.5 Concluding Remarks

ABE separation is an important process in the economic development of biofuels with a goal of building a sustainable world economy. Several downstream processing techniques

have been employed to recover ABE from its fermentation broth, however all these techniques suffer from various limitations. MIMD was investigated using CNT modified membranes, which showed significantly superior performance. Convectional thermal distillation is an expensive and energy intensive process and the MIMD based on CNIM is clearly a viable alternative. The separation of binary acetone-water, butanol-water and ethanol-water by the membranes were carried out initially to evaluate the membrane performance, which was found to follow the order of butanol>acetone> ethanol. The modified membranes were shown to be preferentially permeable to the ABE components. Improved partitioning and activated diffusion via CNT surface were factors that played important role in performance enhancement of the CNIM and CNIM-ODA. While modeling studies have shown some interesting results, this study for the first time demonstrates the viability of this technology in ABE recovery. As compared to the plain PTFE membrane, significant enhancement in ABE flux and separation factor were obtained with CNIM and CNIM-ODA membranes. The ABE flux obtained here is about ten times higher than that reported before for pervaporation, which is the only other reported membrane-based technology for ABE recovery. Fermentation product recovery from the fermentation broth can be an important application for the modified CNT membranes.

CHAPTER 6

NANOCARBON-IMMOBILIZED MEMBRANES FOR SEPARATION OF TETRAHYDROFURAN FROM WATER VIA MEMBRANE DISTILLATION

6.1 Introduction

Energy requirements and carbon foot print of current solvent recycling processes tend to be quite high, and the incineration of the solvents for waste disposal produces toxic air emissions [328]. The commercial technique for solvent separation is thermal distillation and accounts for over 90% of the commercial operations [329]. However, the process is expensive, has large foot print and is energy intensive [330]. Conventional distillation is also limited by azeotrope formation. Processes such as solvent extraction, carbon adsorption or air stripping have also been used for solvent recovery from aqueous wastes, however restriction of the feed condition, byproduct generation, and high cost of post-treatment limit their economic feasibility [331, 332]. Over the last few decades, membrane-based processes, such as, reverse osmosis (RO), nanofiltration (NF), pervaporation (PV) have undergone rapid growth. Although, organic solvent nanofiltration (OSN) has much potential in terms of cost and applicability to industrial processes [333, 334], the availability of suitable NF OSN and RO membranes have restricted their applicability [335]. In recent years, PV using dense membranes have shown tremendous potential as a solvent separation method however it shows low permeate flux [220]. Therefore, novel technologies are needed for solvent recovery that can benefit diverse industries such as in pharmaceutical, cosmetics and paint.

Membrane Distillation (MD) is a relatively new and promising separation technology for organic solvent removal from aqueous medium. The process selectively

passes vapor molecules through a porous hydrophobic membrane. The driving force for separation is the difference in vapor pressure among the solvents at a particular temperature and a concentration gradient between the feed and permeate side [233]. MD has numerous benefits over traditional distillation such as low operating temperatures and capital investment, and it can be combined with other membrane processes such as Ultrafiltration (UF) [336], PV and RO [337]. Furthermore, the heat required in MD can be obtained from alternate energy sources, such as solar energy[338, 339] or microwave energy [281, 340] to make it more energy efficient. While MD has been extensively studied for water desalination, very few studies have reported the applications related to solvent recovery and have been limited to ethanol and isopropyl alcohol (IPA) [146, 220, 255-257].

At this point high performance membranes and advanced process development are needed to make MD commercially viable. Several membrane modifications have been implemented via graft polymerization, hydrophobic/hydrophilic coating of membrane surfaces, casting of polymer over a porous membrane support or a flat sheet to enhance hydrophobicity [68, 69, 196-198] , addition of zeolite and clay nanocomposite nanofiber to the surface of membranes [341, 342], silane grafting [343] and hydrophobic porous alumina [344] for performance enhancement in MD. We have demonstrated the effect of carbon nanotube (CNT) immobilization for enhancing permeability and selectivity [345] in MD where the CNTs not only serve as a sorbent but also provide an additional pathway for solute transport. IPA separation from their aqueous medium has also been explored through CNTs' immobilization on porous PTFE membranes for a sweep gas MD process. Superior performance was achieved with an enhancement in separation factor of 350% and an enhancement in mass transfer coefficient of 132%, credited to the enhanced adsorption

and rapid desorption by CNTs [146]. Additionally modelling studies show that MD has the potential to separate solvent mixtures for use as biofuels [306]. Graphene oxide (GO) and reduced GO (r-GO) are other important nanocarbon where the atomic-level thickness with controlled pore size makes them viable options for membrane modifiers for various applications [161, 346-351]. Recently, GO-based membranes have been validated to be operational barriers for gas and liquid separation [155]. A recent study showed that imperfections within GO flakes produced by the oxidation reaction and the inter-layer spacing between GO flakes play a dominant role in transportation of molecules through the GO membrane [352]. The comparatively higher hydrophobicity of r-GO compared to GO makes it a favorable material for performance enhancement of hydrophobic membranes in MD. Additionally, the narrow size distribution of rGO nanochannels lead to precise molecular sieving than those of commonly used polymeric membranes [353].

THF is an important solvent that is widely used in organic synthesis [354, 355] and also in the manufacture of poly-tetra-methylene glycol (PTMEG). Besides preventing water pollution, its separation from an aqueous medium is industrially significant as it's an expensive solvent [356, 357]. THF-water mixture forms a minimum boiling azeotrope with water at 95 wt. % water and reacts spontaneously with oxygen during contact with air and leads to the production of an unstable hydro peroxide. An increase in peroxide concentration occurs during distillation of the THF containing peroxide, resulting in a severe explosion risk [358]. PV has been used for the dehydration of THF using hydrophilic membranes [359-363]. However, the more efficient recovery of trace amount of THF from water using an organophilic membrane [364, 365] is of significant interest, and to the best of our knowledge has not been studied before. It is conceivable that CNTs, GO and r-GO

can be used to enhance the separation of THF from water via MD. That is the objective of this study.

6.2 Materials and Methods

6.2.1 Chemicals and Materials

THF (Sigma Aldrich, St. Louis, MO), Deionized water (Barnstead 5023, Dubuque, Iowa), MWCNTs (Cheap Tubes Inc., Brattleboro, VT), Zinc (Fluka) were used in all experiments. The average diameter and length of the CNTs were ~30 nm and 15 μm, respectively. Graphene oxide was procured from Graphenea Inc. Reduction of GO to r-GO was performed following a method published elsewhere [366]. rGO used in this study contained 9% oxygen by weight [367].

6.2.2 CNIM Fabrication and Characterization

Uniform dispersion of CNTs, GO and r-GO on the membrane surface was the primary stage in membrane fabrication. A porous composite PTFE membrane on a PP support layer (Advantec, 0.2 μm pore size, 74% porosity) was used in this study. The nanomaterial dispersion was performed in accordance to a method stated elsewhere[146]. Very small amount of nanomaterials (1.5 mg) were dispersed in a solution containing 10 g of acetone along with 0.2 mg of polyvinylidene difluoride (PVDF) and sonicated for four hours. The PVDF solution acted as a binder during nanomaterials' immobilization. The PVDF-nanomaterial dispersion was thereafter coated uniformly over the membrane surface to incorporate the nanocarbons, and then allowed to dry overnight under the hood for the acetone to evaporate. Reduction of GO to r-GO was performed by adding different amount of Zinc (Zn) to the solution in a stepwise process and details have been published by our group [368]. Reducing the amount of Zn resulted in the formation r-GO containing

different percentage of oxygen (31, 19 and 9%). 9% oxygen was the most hydrophobic and was thus chosen for THF separation experiments. r-GO and CNT mixture (1:1 by wt.) was used to fabricate the combined r-GO plus CNT membrane. The fabricated CNT, GO, r-GO, r-GO/CNT membranes are designated as CNIM, GOIM, rGOIM and rGO-CNIM, respectively. Since very small amount of nanocarbon was used for membrane fabrication, no noticeable change in thickness was observed.

The CNIM, GOIM, rGOIM, rGO-CNIM were characterized using scanning electron microscopy (SEM) (JEOL; model JSM-7900F) and thermogravimetric analysis (TGA) (Perkin–Elmer Pyris 7). Determination of membrane hydrophobicity was performed via contact angle and liquid entry pressure (LEP) measurements using deionized water, THF and their mixtures. Droplets of a fixed concentration of THF-water mixtures (5 w/w% THF in water) using a micro syringe (Hamilton, 0–100 μL) were placed on the unmodified PTFE, GOIM, rGOIM, CNIM and rGO-CNIM. The contact angle of the droplet positions with the membrane surface were recorded using a digital camera to determine the hydrophobicity. Experiments were performed three times and the average of the contact angle values obtained has been reported here. The onset of the liquid entry into the membrane is the LEP and was measured using a method described before [217]. The measurements were repeated thrice to ensure reproducibility.

6.2.3 Experimental Setup

A flat PTFE membrane module was used for this SGMD experiments. The experimental setup used has been shown in Figure 6.1. An inert sweep gas on the permeate side of the membrane transported the vapor as expected in the sweep gas MD configuration [52, 216]. Peristaltic pump (Cole Parmer, model 77200-52) was used to pump the THF-water feed

mixture through the membrane module and was recirculated and collected as the retentate. The temperature of the THF-water feed mixture was controlled using thermistor thermometers (K-type, Cole Parmer). The sweep gas flow rate was 4.5 L/min as measured and was monitored by a flowmeter (model no EW-03217-02, Cole Parmer). The relative humidity of the dry sweep air was estimated to be zero. Experiments with varying conditions were performed three times for reproducibility and the relative standard deviation was calculated to be less than 1%.

6.2.4 Experimental Procedure

The weight of the feed solution before and after experiments were measured using a digital balance and the change in feed weight over time was used to estimate flux and separation factor. An airtight feed chamber was used to eliminate chances of sample loss due to evaporation. Compositions of the unknown mixture after each experiment were analyzed by Refractive Index meter (EW 81150-55, Cole Parmer) to obtain the unknown concentration of the THF-water mixture after each experiment. A calibration curve showing refractive index vs concentration was thereafter used to calculate the THF flux and separation factor.

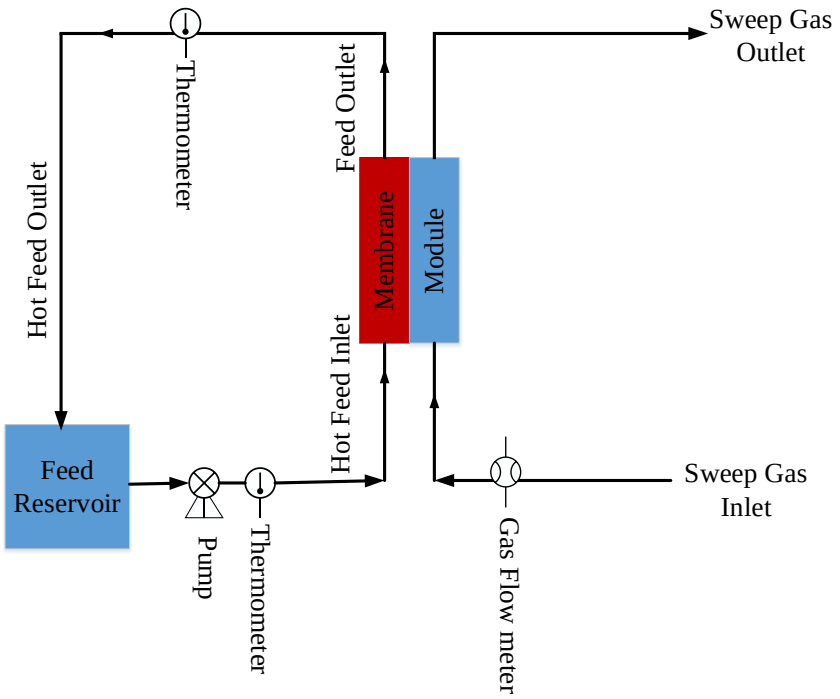

Figure 6.1 Schematic diagram of the experimental setup for the DCMD.

6.3 Results and Discussion

6.3.1 Membrane Characterization

The SEM images of the original PTFE, GOIM, rGOIM, CNIM and rGO-CNIM are shown in Figure 6.2a, b, c, d, and e. The porous structure of the PTFE membrane and presence of the nanocarbons can be clearly seen with uniform nanocarbon distribution. From Figure 6.2b, the surface of GO had a layered sheet structure that can be attributed to layer-by-layer stacking of GO. The GO sheets had smooth surface with few folded regimes and wrinkles [369]. The structural image of rGO-CNTs is shown in Figure 6.2e. From the image graphene and carbon nanotubes were well adhered to each other. Based on the SEM images, the size of GO and rGO particles on the membrane were between 5μm and 10 μm and between 150 nm and 250 nm, respectively. It is noted that the GO and rGO had laminate structures with multiple layers making up each particle.

The thermal stability of the unmodified PTFE, GOIM, rGOIM, CNIM, rGO-CNIM were studied using thermogravimetric analysis (TGA). All the modified membranes exhibited improved thermal stability over the unmodified PTFE membrane. The TGA and differential TGA curves of unmodified PTFE and rGO-CNIM are shown in Figure 6.3a and 6.3b, respectively. It is observed that the initial thermal decomposition of the membrane began at ~250 ^{0}C (degradation of PP support layer), followed by the degradation of PTFE active layer at 530 °C.

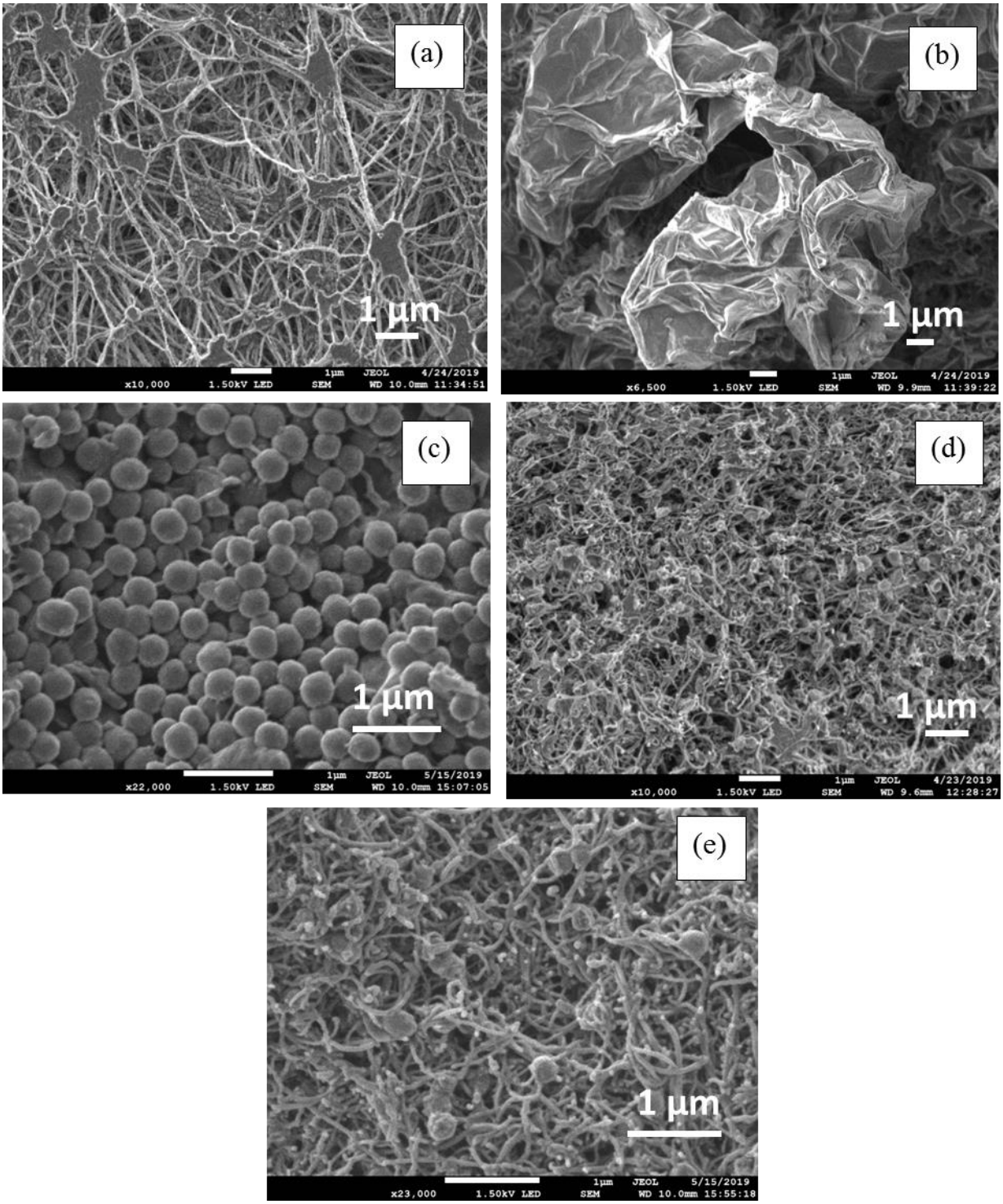

Figure 6.2 SEM images of **a)** unmodified PTFE membrane, **b)** GOIM, **c)** rGOIM, **d)** CNIM and **d)** rGO-CNIM.

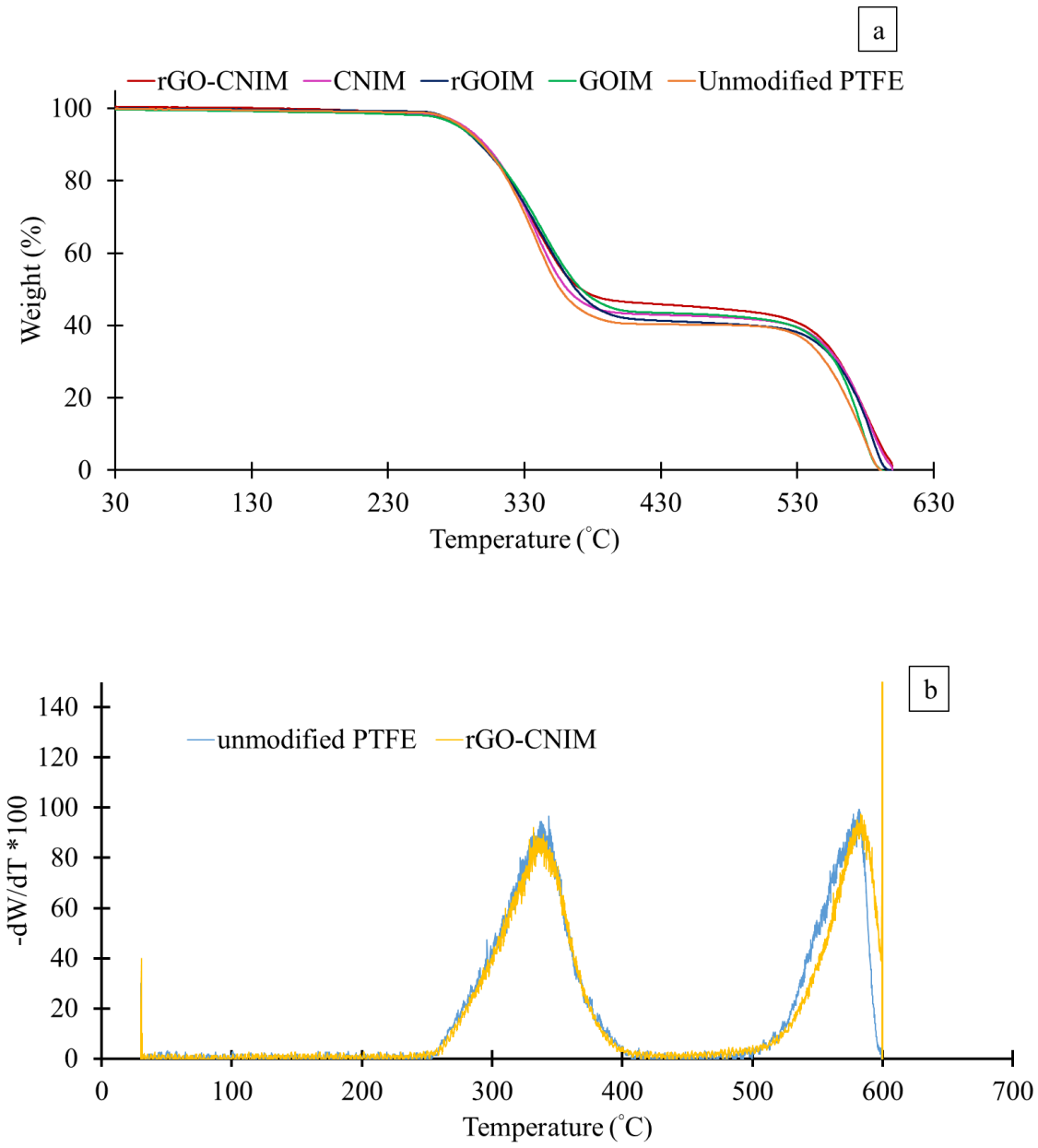

Figure 6.3 a) Thermogravimetric analysis of unmodified PTFE and rGO-CNIM, **b)** differential TGA curves of the corresponding membranes.

It is well known that organic solvents have strong affinity for hydrophobic surfaces [219]. The presence of THF resulted in strong interactions with the rGO-CNIM, CNIM and rGOIM. The bar graph (Figure 6.4) shows the contact angle values for pure

water and 5 (w/w %) THF in water. For rGO-CNIM, the contact angle with pure water and aqueous THF solution was observed to be 112^0 and 80^0 respectively, showing a reduction of 28.6%, the highest among all the fabricated membranes. The respective reduction in contact angle for the samples were15.8 % and 8.4 % for rGOIM and GOIM, respectively. The increased hydrophobicity of rGO led to stronger affinity for the organic solvent, indicating improved THF separation performance of rGOIM over GOIM. In general, increase in THF affinity to the r-GOIM, CNIM and rGO-CNIM over unmodified PTFE and GOIM were observed and was expected to improve the separation performance [319].

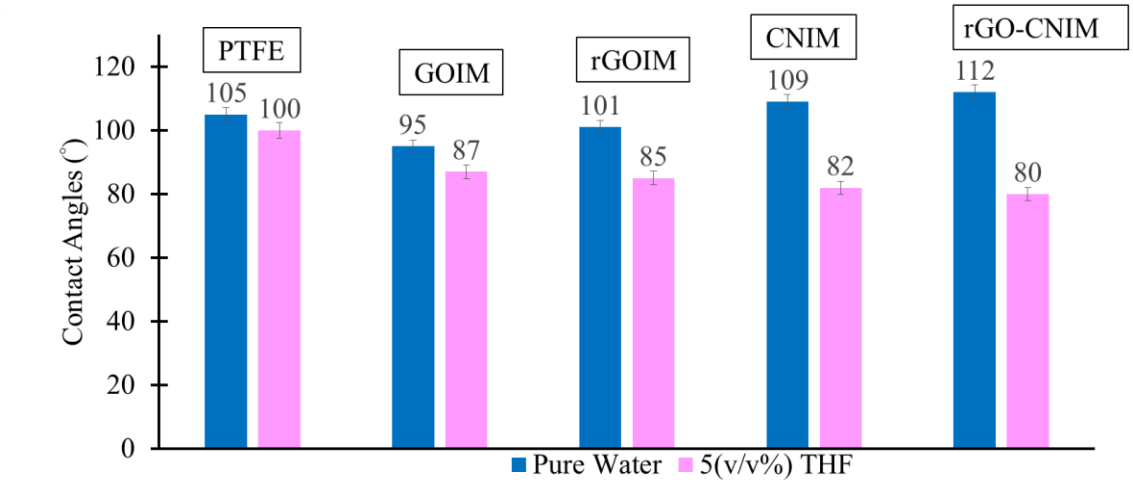

Figure 6.4 Contact angle measurements of pure water and 5 (w/w %) THF membrane surfaces.

The LEPs of pure water for PTFE, rGOIM, CNIM and rGO-CNIM were found to be ~66 psig, respectively, and for GOIM, the value was ~58 psig. These decreased by 59, 68, 71, 75, and 58%, in PTFE, rGOIM, CNIM, rGO-CNIM and GOIM respectively for 15 (w/w %) THF-water mixture. The high LEP values indicate reduced membrane wettability as was observed from the contact angle measurements described above. It is a well-known

that LEP depends on contact angle (hydrophobicity), pore size of the membrane surface, surface energy and surface tension of the feed mixture [46], and the presence of organic materials in feed solution lowers the LEP of hydrophobic membrane. The contact angle reduced with increasing THF concentration, thus resulting in a lower LEP. A further lowering of LEP with THF in the feed solution was credited to the reduction in the surface tension of the liquid and the contact angle. It is well known that LEP has a direct relationship with the surface tension of the feed mixture and the contact angle values [370].

6.3.2 MD Separation Performance

The fabricated membranes' performance was compared with the unmodified PTFE membrane. The flux of component '*i*' (J_{wi}), was described as:

$$J_i = \frac{W_{pi}}{A * t} \tag{6.1}$$

Where, W_{pi} represents the amount of mass permeated for species 'i' within a specific time period't' through an active membrane area 'A'. The efficiency of separation for each membrane studied was represented by separation factor ($\alpha_{i\text{-}j}$), and is estimated from the following mathematical relation:

$$\alpha_{THF-water} = \frac{y_{THF}/y_{water}}{x_{THF}/x_{water}} \tag{6.2}$$

where y and x represent the permeate and feed side weight fraction of the corresponding component. Apparent activation energy (E_{app}) of solvent transport in the membrane processes can be expressed as [320, 371, 372]

$$J = J_0 \, exp\left(-\frac{E_{app}}{RT_f}\right) \tag{6.3}$$

Where J and J_0 are fluxes (mol m^{-2} h^{-1}), R is gas constant (J mol^{-1} K^{-1}), T_f denotes feed temperature (K).

Figure 6.5 a and b represents the influence of feed concentration on THF flux and separation factor, respectively. THF feed concentration of 2.5, 5 and 10 (w/w %) was studied. The temperature in the THF-water feed mixture and feed side flow rate was kept constant at 40^0C and 112 mL/min, respectively. It can be observed from the figures that with increase in THF concentration in feed, the flux increased for all membranes. All the nanomaterial immobilized membranes exhibited improved separation performance compared to PTFE membrane. The THF flux reached as high as 4.8, 5.9, 7.6 and 8 g/m^2.h, for GOIM, rGOIM, CNIM and rGO-CNIM respectively, at 5 (w/w %) of THF in the feed, which were 20%, 47.2 %, 91.2 and 101 % higher, respectively compared to the PTFE membrane. The highest THF flux for rGO-CNIM can be attributed to the higher THF affinity, as also supported by the contact angle measurement, and activated diffusion via frictionless CNTs surfaces through the membrane pores. The presence of oxygenated functionalities (hydroxyl, carboxyl, epoxy) on GO may have limited the preferential interaction with the organic moiety and quick transport of the THF on the GO frameworks thus reducing the improvement in flux.

Figure 6.5 b shows plots of separation factor of THF as a function of feed concentration. It is evident from the plot that the separation factor has an inverse relationship to the THF concentration for all membranes studied here. However, a higher separation factor for rGO-CNIM and CNIM than rGOIM, GOIM and PTFE membranes were observed at all tested THF feed concentrations. Enhancement over PTFE membrane for THF reached as high as 29.7% for GOIM and 82.1% for rGOIM, 163% for CNIM and 181.8 % for rGO-CNIM at 5 (w/w %) THF and 40^0C.

Separation properties of polymeric membranes typically show a tradeoff: with increase in permeability, the selectivity decreases, and vice versa [373, 374]. In our previous studies also, we have observed similar trend for VOCs removal via MD [146, 315]. With increasing THF concentration in feed, the partial vapor pressure of the component increased leading to higher mass transfer gradient and flux. On the other hand, high concentrations of organic molecules reduce the hydrophobicity of the membrane that may help wet the membrane surface and cause the permeation of water molecules across the membrane and reduce the separation factor. However, for nanocarbon immobilized membranes, the increased hydrophobicity and preferential affinity towards THF increased the overall permeation rate without significantly sacrificing the selectivity. A comparable performance was noticed by Gostoli and Sarti [38] in separating ethanol from a dilute ethanol–water mixture. Separation factor for ethanol changed significantly with variation in feed composition, and they determined that the MD process is selective for ethanol at low ethanol composition but tends to be water selective for a higher ethanol content in the feed mixture.

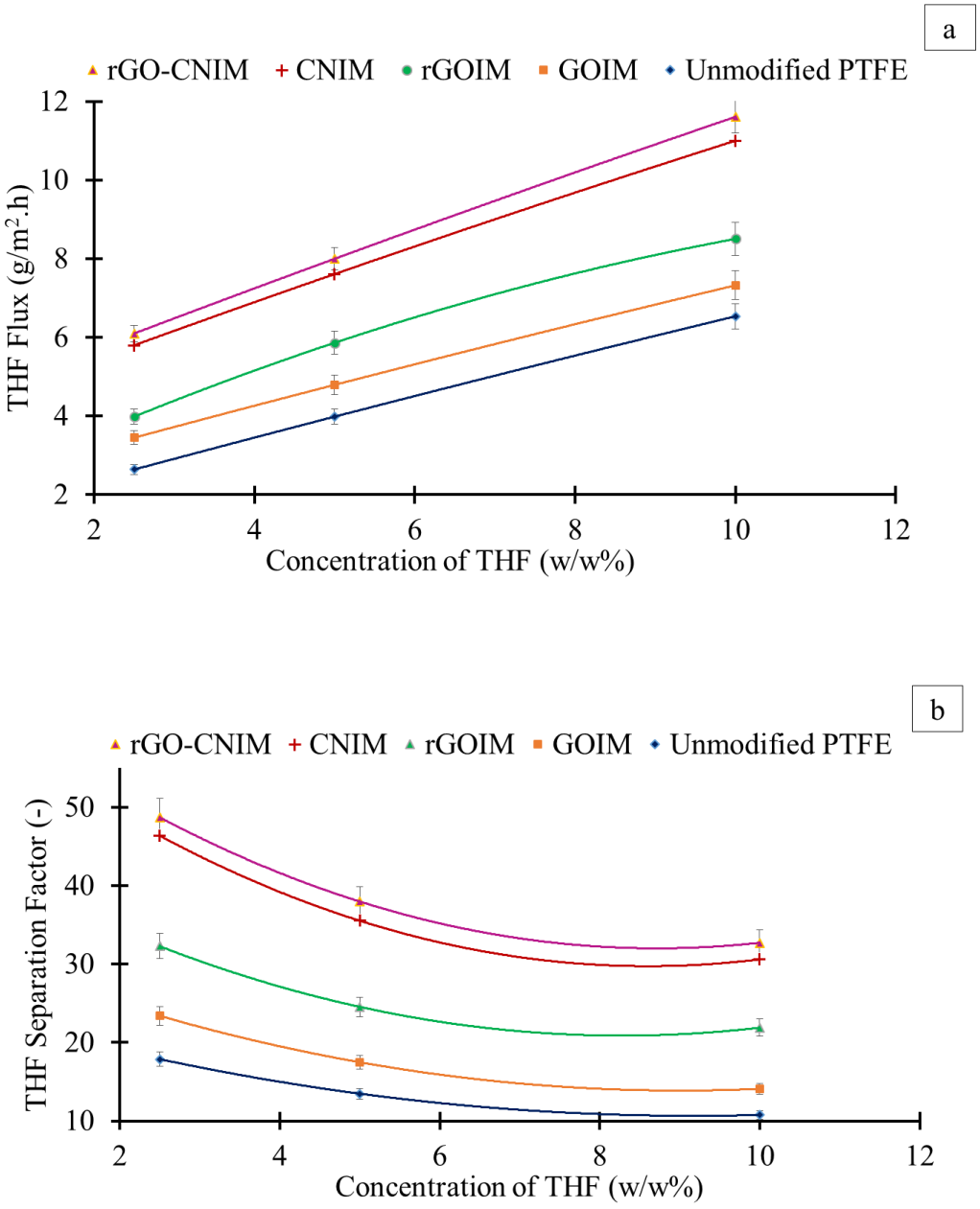

Figure 6.5 Effect of feed concentration on **a)** THF flux, and b**)** THF separation factor.

The effects of THF flux and separation factor on the unmodified PTFE, GOIM, rGOIM, CNIM and rGO-CNIM as a function of feed temperatures are demonstrated in Figure 6.6 and b. A feed concentration 5 (w/w %) THF at a feed flowrate of 112 mL/min

was maintained. The permeate fluxes for all membranes increased with increase in feed temperature. The vapor pressure has an exponential relationship with temperature and the rapid increase in THF vapor pressure (148.45 mm Hg to 439.574 mm Hg) from 40 to 60°C was reflected in the corresponding increase in THF flux. At 50 ^{0}C, the THF flux reached up to 7.2 g/m^2.h, 8.1 g/m^2.h, 9.2 g/m^2.h and 9.5 g/m^2.h for GOIM, rGOIM, CNIM and rGO-CNIM respectively with 5 (w/w%) THF in feed which were significantly higher than previously reported data for pervaporation [375, 376]. In general, higher fluxes at all temperatures for rGO-CNIM and CNIM were observed followed by rGOIM and GOIM, with a more pronounced enhancement at reduced temperature. At 50^{o}C the improvement in THF flux reached up to 26.7, 42.3, 60.8 and 66.7% for GOIM, rGOIM, CNIM and rGO-CNIM respectively, over pristine PTFE membrane. Hence, experiments can be done at a relatively lower temperature with an effort to make the process sustainable and less energy consuming. From Figure 6.6 b, it can be interpreted that at all the operating temperatures; the combination of r-GO and CNTs played a vital role in separating THF from aqueous medium compared to the commercial PTFE membrane and the other two fabricated membranes. It is interesting to note that, in general the flux reported here are significantly (nearly an order of magnitude) higher than what has been reported for other techniques such as pervaporation and extractive distillation [365, 377].

The separation factor enhancement of GOIM, rGOIM, CNIM and rGO-CNIM compared to PTFE membrane reached as high as 46.9, 123, 263 and 279.2% at 50^{o}C, respectively. A reduction in THF separation factor with increase in feed temperatures was observed for all membranes due to negative viscosity effects [220]. Increase in feed temperatures also exponentially increased the water vapor pressure that resulted in higher

amount of water diffusing through the membrane. Consequently, the partition coefficient of THF decreased with temperature, which in turn reduced the overall THF selectivity.

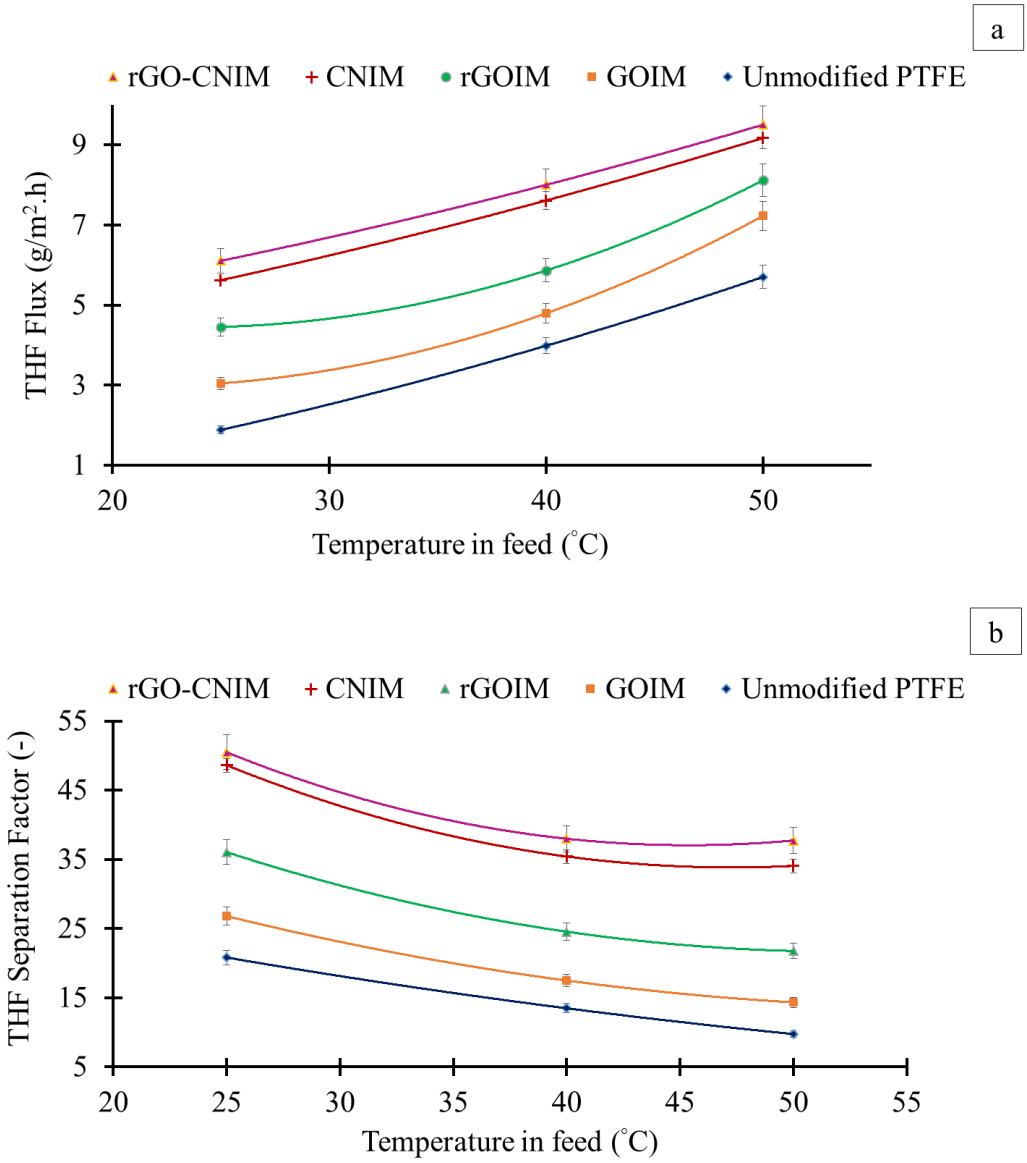

Figure 6.6 Effect of feed temperature on **a)** THF Flux, and **b)** THF Separation factor.

Figure 6.7 a and b demonstrates the effect of varying feed flowrate on THF flux and separation factor. The feed flow rate was varied from 42 to 185 mL/min. The feed temperature and concentration were kept constant at 40 °C and 5 (w/w %). The permeate

flux and separation factor for rGO-CNIM increased as high as 9.5 g/m^2 h and 34.9, respectively at the highest feed flow rate. Higher enhancement in flux for rGO-CNIM and CNIM than the unmodified PTFE was observed, and enhancement reached as high as 82.7% and 76.9%. Increasing the feed flow rate reduces the variance between the feed side concentration and the concentration on the membrane surface (known as concentration polarization). Concentration of THF was reduced at the feed–membrane interface at lower feed flowrates, resulting in lower flux. Increased THF flux can be attributed to the increased turbulence at higher flowrates which increased the THF concentration and the vapor pressure on the liquid-membrane interface. THF removal efficiency was higher due to improved heat and mass transfer from the liquid feed to the membrane surface at higher flowrates. It is evident from the figure that the rGO-CNIM and CNIM demonstrated higher separation factor at all feed flow rates over the commercial membrane and GOIM. The partitioning of the THF on the CNTs and r-GO in the rGO-CNIM also decreased with increasing feed flowrate. Residence time is short at higher flowrates and comparatively smaller amount of THF is available for partitioning on the rGO-CNIM and CNIM, resulting in a reduction in separation factor.

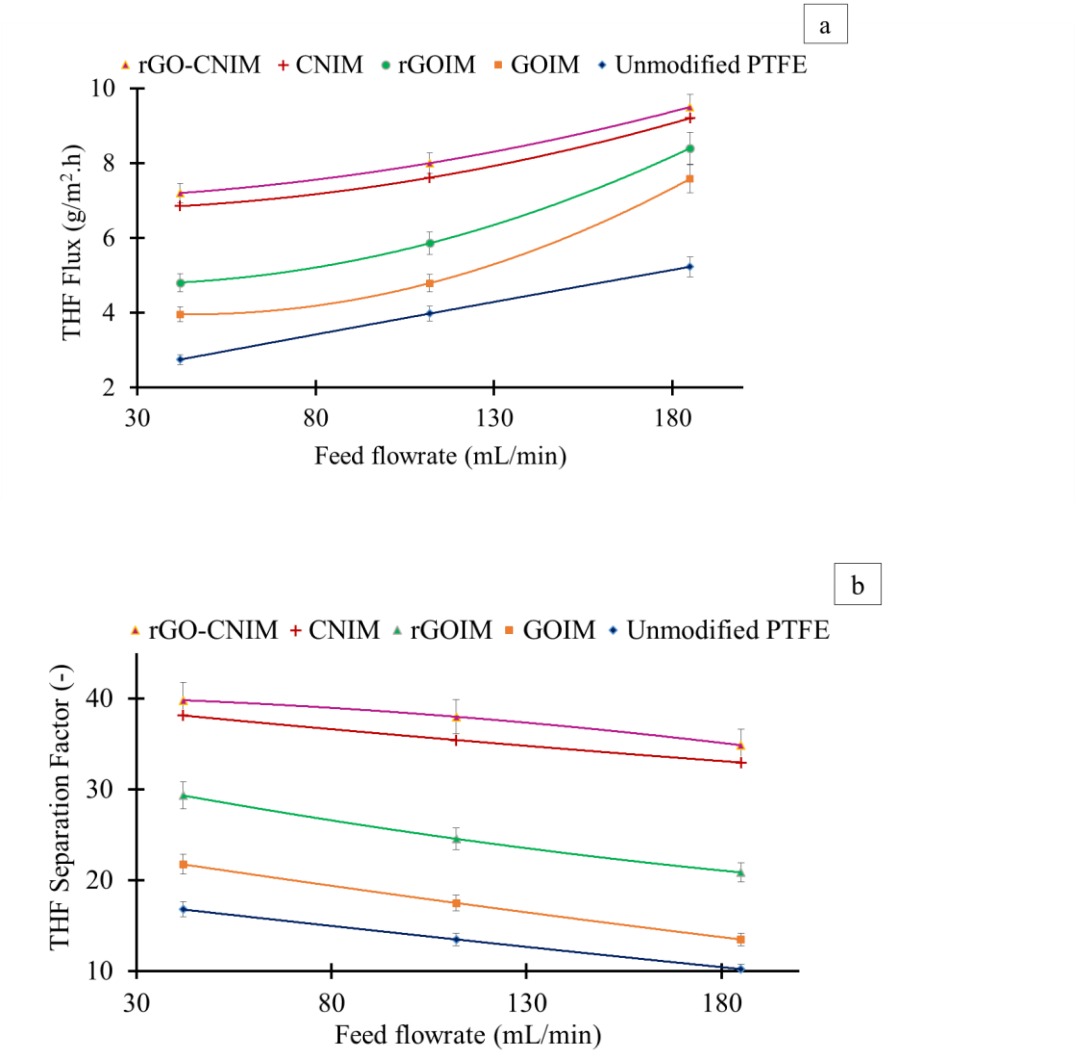

Figure 6. 7 Effect of feed flowrate on **a)** THF Flux, and **b)** Separation factor.

Apparent activation energy (E_{app}) for THF transport through porous hydrophobic membranes in SGMD mode was calculated from Eq. (6.3). The concentration of THF was kept constant at 5 (w/w %). The E_{app} values for PTFE, GOIM, rGOIM, CNIM & rGO-CNIM are shown in Table 6.1.

Table 6.1. Activation Energy of Unmodified PTFE and Fabricated Membranes

Membranes	Apparent activation energy (kJ/mol)
PTFE	31.47
GOIM	23.78
rGOIM	16.26
CNIM	13.74
rGO-CNIM	12.39

As evident from the table, that the presence of r-GO and CNTs significantly reduced the apparent activation energy for THF. Among four membranes used, rGO-CNIM showed the lowest E_{app} value followed by CNIM, rGOIM, GOIM and PTFE membranes.

6.3.3 Mass Transfer Coefficient

The mass transfer coefficient (k) can be calculated from the following equation:

$$k = \frac{J_i}{(P_f - P_p)} \tag{6.4}$$

Where, J_{wi} denotes the flux of species 'i'. P_{fi} and P_{pi} represents the feed side and permeate side partial vapor pressure, respectively. The vapor pressure of THF at a particular temperature was obtained from other sources [222]. Entirely dried sweep air was used on the permeate side of the membrane. Thus, the permeate side vapor pressure was estimated to be nearly equal to zero and hence neglected in calculating the mass transfer coefficient values.

The 'k' values of THF (5 w/w %)-water mixture at different working temperatures and a fixed feed flowrate of 112 mL/min are presented in Table 6.2. Higher mass transfer coefficient was observed for all modified membranes over pristine PTFE membrane.

Among the modified membranes, rGO-CNIM demonstrated the highest 'k', followed by CNIM, rGOIM, GOIM. The enhancement of mass transfer coefficient over PTFE reached as high as 20.3% for GO, 47.1 % for rGOIM, 90.9% for CNIM and 100.7 % for rGO-CNIM at 40 ^{0}C. The higher 'k' values can be attributed to the faster sorption/desorption characteristics of CNTs [378]. A slightly reduced or almost constant 'k' values were obtained at higher operating temperature for all membranes. Higher operating temperatures results in an increased temperature polarization phenomenon that eventually decreases the membrane mass transfer coefficient [324].

Table 6.2. Mass TransferCcoefficient of THF at Different Temperature and 5 (w/w %) THF in Feed at 112 mL/min

Temperature (^{0}C)	**Mass Transfer Coefficient (* 10^{-3} L/m^2.h.mm-Hg)**				
	PTFE	**GOIM**	**rGOIM**	**CNIM**	**rGO-CNIM**
23	12.68	20.50	29.99	37.86	41.11
40	13.21	15.89	19.43	25.22	26.51
50	12.97	16.43	18.46	20.86	21.61

6.3.4 Membrane Stability

Membrane stability in presence of strong organic solvents like THF is an important factor which needed to be considered. SGMD experiments were performed for 8 h a day for two months with 10 (w/w %) THF concentration at the highest temperature of 50^{o}C. The THF flux was estimated from time to time. No considerable decline in flux and membrane surface wetting were observed during extended usage. The recycled feed solution was carefully inspected. The change in pH of the recirculated feed was investigated and

compared to each other to watch the study the feed solution breakthrough. During long term experiments, the pH showed minor variation within ± 0.2 implying that no feed breakthrough occurred. It can be said that there was no substantial r-GO or CNT loss from the surface of the membranes with extensive use. Similar membrane stability checks have been performed before where CNIM was used at very high temperatures in aqueous solutions for prolonged periods and then inspected for nanomaterial loss [206].

6.4 Proposed Mechanism

The proposed mechanism for THF flux enhancement by rGO-CNIM is shown in Figure 6.8. Mechanistically speaking, the driving force in MD for a particular component is the difference in vapor pressure across the membrane. The higher vapor pressure of THF (301.7 mm Hg at 40 0C) compared to water (55.2 mm Hg at the same temperature) helped in preferentially generating of more THF vapor at the solvent-membrane interphase, which eventually permeated through the membrane. Among the nanomaterials immobilized membranes, GOIM exhibited lowest solvent removal performance, followed by rGOIM, CNIM and rGO-CNIM. This may be due to the presence of polar functional groups on GO surface that interact with the water molecules and eventually reduced the organic species transport through the membrane. Apart from vapor liquid equilibrium, the reduction in polar moiety on rGOIM increased the hydrophobicity, hence the organic solvent affinity which improved the solvent separation performance over GOIM. The CNTs are known to have high solvent sorption capacity and activated diffusion on its frictionless smooth surface that provides an edge over the other membranes.

The high porosity and surface area of r-GO along with its tunable hydrophobicity and nanocapillary effect has shown superior adsorption capacity for organic solvents [379]. Hydrophilicity is more at the ends of the GO and rGO nanochannels while the inner structure is more hydrophobic. The rGO membrane showed higher permeance for THF than water, respectively, which is attributed to their lower polarity (0.27) compared to water (1), resulting in less interaction with the hydrophilic portion of the nanochannels. Earlier research has also validated the high partition coefficient and fast adsorption-desorption on CNT of organic species for rapid mass transport [137, 138, 210, 326, 327, 380, 381]. Placing well-dispersed CNTs along with 2D graphene sheets provides effective sorption sites for THF vapor. The rGO had a laminate structure with nano-scale interlayer spacings, and the solvent selectively permeated via nanocapillary actions [382, 383]. It is possible that the rGO layers also acted as selective sieves for THF [174]. Alcohol molecules pass at a significantly slower rate than water through the nanochannels in rGO. However, when they form a mixture with water, the water and alcohol molecules are held together strongly via van der Waals or hydrogen bonds which pull the alcohol molecules through the nanogaps owing to their higher affinity between water and the functional groups in rGO [384].The combination of the transport mechanisms of CNTs and rGO led to the highest flux among the membranes studied here.

6.5 Concluding Remarks

In the present work, membrane distillation was used for separation of THF from water using GO, r-GO, CNTs and a hybrid r-GO-CNT system. All the nanomaterials incorporated membranes showed better performance in terms of flux and THF separation factor than

pristine PTFE membrane, and would be very useful for removal of low concentration of solvents from water. The rGO-CNIM containing r-GO and CNT exhibited highest THF flux and separation factor. The THF flux obtained here was approximately 8 times higher than existing technologies like pervaporation and extractive distillation, the only other membrane-based approaches reported for THF recovery.

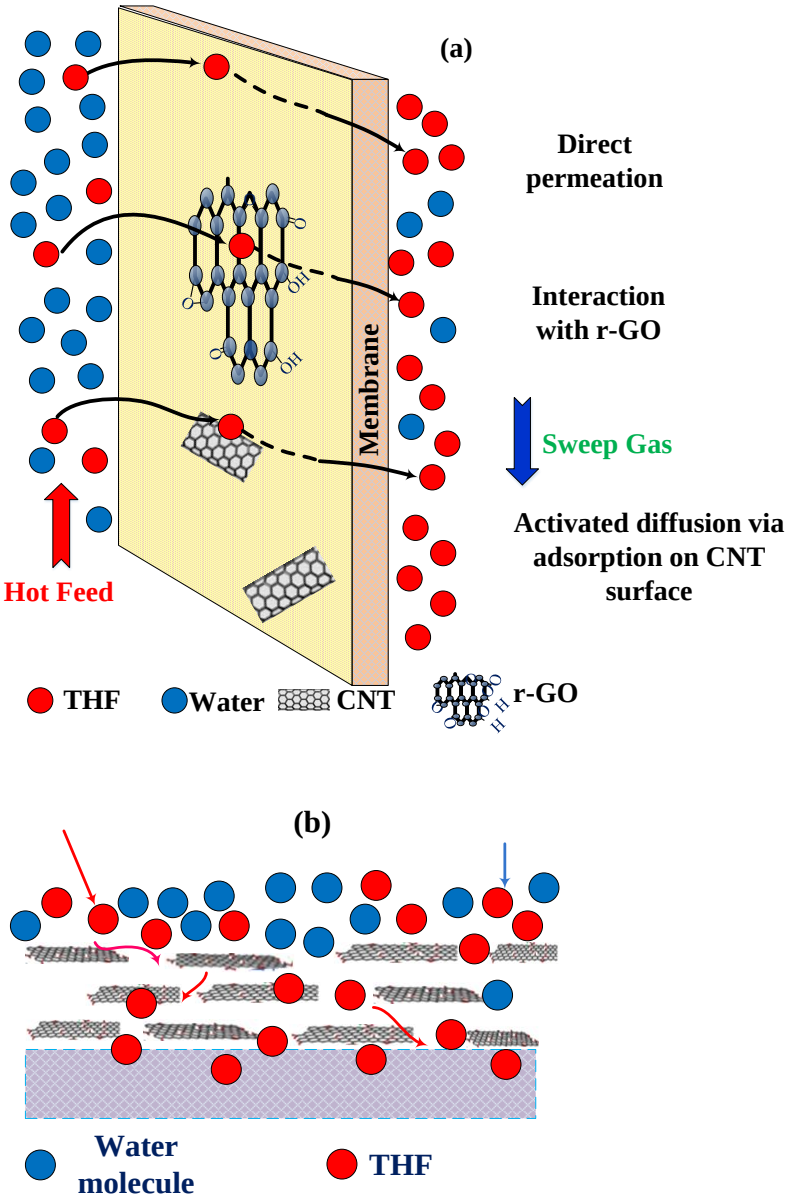

Figure 6.8 a) Schematic of the proposed mechanism for rGO-CNIM, **b)** Nanocapillary action through rGO layers.

CHAPTER 7

CONCLUSIONS AND FUTURE PERSPECTIVES

7.1 Conclusions

This thesis presents novel nanomaterial-based membranes for organic solvent separation from aqueous medium for applications in the biofuel industry. Sweep gas membrane distillation was conducted to recover organic solvents with CNTs and reduced GO that showed great potential for biofuel production by using fermentation byproducts.

Carbon nanotube immobilized membrane (CNIM) for separation of alcohol from water via sweep gas membrane distillation (SGMD) was investigated. The alcohol flux, separation factor and mass transfer coefficient obtained with CNIM are considerably higher than the unmodified membrane at different feed concentration, flow rate and temperatures. The presence of carbon nanotubes (CNTs) is believed to significantly alter the liquid–membrane interactions to promote alcohol transport in solvent-water mixture by inhibiting water penetration into the membrane pores. Performance enhancement in CNIM can be mainly attributed to the preferential sorption on the CNTs followed by rapid desorption from its surface.

Microwave-induced membrane distillation (MIMD) as a process modification technique was investigated for the improved organic solvent separation from aqueous media via sweep gas membrane distillation. Microwave heated solvent-water mixtures were separated on polytetrafluoroethylene (PTFE) and a carbon nanotube immobilized (CNIM) membranes. The combination of CNIM and microwave heating is most effective where the solvent flux obtained is as high as 11.3 $L/m^2.h$ and separation factor was 13.68,

which are 46% and 102% higher than MD carried out by conventional heating. The mass transfer coefficient in CNIM-MIMD is also 81% higher than conventional MD. The presence of carbon nanotubes (CNTs) is believed to significantly alter the liquid–membrane interactions to promote alcohol transport in solvent-water mixture by inhibiting water penetration into the membrane pores. The improvement in performance of MIMD was due to non-thermal effects such as localized superheating, and destruction of the hydrogen bond in solvent−water clusters. Moreover, MIMD required less energy to operate than conventional MD under similar conditions. Factors such as lower energy consumption, higher flux, and separation factor in MIMD coupled with strong sorption onto the CNT surface represents a major advancement in solvent separation by MD.

Acetone, butanol, and ethanol (ABE) mixture separation from dilute aqueous fermentation products is an important process for the biofuel industry. We presented a novel approach for ABE recovery using microwave induced membrane distillation (MD). Carbon nanotube (CNTs) and octadecyl amide (ODA) functionalized CNTs were immobilized on membrane surfaces and were used in sweep gas MD separation of ABE. The ABE flux, separation factor and mass transfer coefficient obtained with CNT and CNT-ODA immobilized membranes were remarkably higher than the commercial pristine membrane at various experimental conditions. The ABE flux enhancement reached as high as 105, 100 and 375% for CNIM and 63, 62 and 175% for CNIM-ODA, respectively. ABE flux obtained was nearly ten times higher than that reported previously for pervaporation. The mass transfer coefficient also increased significantly along with a lower activation energy for the modified membranes. Mechanistically speaking, the immobilization of the carbon nanotubes on the active membrane layer led to preferential sorption of ABE leading

to enhanced separation. This phenomenon has been validated by the reduction of contact angles for the aqueous ABE mixtures on the CNT and CNT-ODA immobilized membranes indicating enhanced interaction of the ABE on the membrane surface.

Next, we presented the application of nanocarbon immobilized membranes for the separation and recovery of tetrahydrofuran (THF) from water via membrane distillation. Several nanocarbons, namely carbon nanotubes (CNTs), graphene oxide (GO), reduced graphene oxide (rGO) and rGO-CNT hybrid were immobilized on PTFE membranes. Membrane distillation was carried out in sweep gas mode (SGMD) to study the separation efficiency at relatively low temperatures (25^0C to 50^0C). All the nanocarbon immobilized membranes exhibited significantly superior performance compared to an unmodified PTFE membrane. Among the nanocarbons, rGO-CNT performed the best in terms of flux and separation factor followed by the CNTs. The rGO-CNT represented an enhancement of 101% in flux, 181.78% in selectivity and 225% in mass transfer coefficient over the plain PTFE membrane for water containing 5% THF by weight and at 40^0C. The improved membrane performances of the rGO-CNT membrane was due to the preferential sorption of THF on rGO-CNTs (as evident from the contact angle measurements), nanocapillary effect through graphene sheets along with the activated diffusion of THF via frictionless CNT surface.

7.2 Future Perspectives

Although membrane distillation is a very efficient technique for organic solvent separation, trace amount of water is left behind after the separation which necessitates the coupling of this process with another membrane-based technique to recover pure form of alcohol that

is needed by pharmaceutical or biofuel industries. In pervaporation, liquid mixtures are separated by selective interaction of compounds with a dense membrane. The components are selectively transported through the membrane and then vaporized due to lower partial pressure in the permeate side, achieved using a vacuum pump or an inert gas stream. The separation is accomplished by relative permeation of solution through the membrane, which depends on both thermodynamic (adsorption) and kinetic (diffusion) aspects. MD is like pervaporation process. The main difference between the two processes is the role of the membrane. The hydrophobic microporous membrane acts only as a support to the liquid–vapor interface and does not chemically distinguish solution components. The process selectivity depends on the vapor–liquid equilibrium phase separation.

We are currently working on a hybrid system combining MD and pervaporation for ethanol separation and ABE separation from water, considering experimental data and most significantly data reported in the literature for PV, carefully selected in terms of temperature and ethanol concentration. Experiments of MD and pervaporation were performed under same operational conditions, put together in series. Our model calculations show that with 10 (v/v %) of ethanol in feed, a concentration of 73 (v/v %) for ethanol was achieved with MD. The permeate collected was then used as the feed composition for PV experiments. The PV experiments concentrated the ethanol solution up-to 96.4 % with a recovery of 90% and removing the excess water.

REFERENCES

[1] T. Barker, I. Bashmakov, L. Bernstein, J. Bogner, P. Bosch, R. Dave, B. Metz, G. Nabuurs, Contribution of Working Group III to the Fourth Assessment Report of the IPCC: Technical Summary, Climate Change 2007: Mitigation contribution of Working Group III to the Fourth Assessment Report of the Intergovernmental Panel on Climate Change, Intergovernmental Panel on Climate Change, Cambridge University Press2009, pp. 27-93.

[2] L. Bowman, E. Geiger, Optimization of fermentation conditions for alcohol production, Biotechnology and bioengineering, 26 (1984) 1492-1497.

[3] S.-i. Nakao, F. Saitoh, T. Asakura, K. Toda, S. Kimura, Continuous ethanol extraction by pervaporation from a membrane bioreactor, Journal of membrane science, 30 (1987) 273-287.

[4] M. Duke, R. Campbell, X. Cheng, A. Leo, J. Diniz da Costa, Characterization and pervaporation study on ethanol separation membranes, Drying Technology, 27 (2009) 538-541.

[5] F. Xiangli, Y. Chen, W. Jin, N. Xu, Polydimethylsiloxane (PDMS)/ceramic composite membrane with high flux for pervaporation of ethanol− water mixtures, Industrial & engineering chemistry research, 46 (2007) 2224-2230.

[6] P. Hickey, F. Juricic, C.S. Slater, The effect of process parameters on the pervaporation of alcohols through organophilic membranes, Separation science and technology, 27 (1992) 843-861.

[7] H. Choi, T. Hino, M. Shibata, Y. Negishi, H. Ohya, The characteristics of a PAA-PSf composite membrane for separation of water-ethanol mixtures through pervaporation, Journal of membrane science, 72 (1992) 259-266.

[8] H. Brüschke, Removal of ethanol from aqueous streams by pervaporation, Desalination, 77 (1990) 323-330.

[9] I. Frennesson, G. Trägårdh, B. Hahn-Hagerdal, Pervaporation and ethanol upgrading—A literature review, Chemical engineering communications, 45 (1986) 277-289.

[10] S. Noamani, M. Sadrzadeh, A.R. Tehrani-Bagha, Prospects of nanocomposite membranes for water treatment by membrane distillation, Nanocomposite Membranes for Water and Gas Separation, Elsevier2020, pp. 299-320.

[11] M.M.A. Shirazi, A. Kargari, M.J.A. Shirazi, Direct contact membrane distillation for seawater desalination, Desalination and Water Treatment, 49 (2012) 368-375.

[12] L.M. Camacho, L. Dumée, J. Zhang, J.-d. Li, M. Duke, J. Gomez, S. Gray, Advances in membrane distillation for water desalination and purification applications, Water, 5 (2013) 94-196.

[13] V. Calabrò, E. Drioli, F. Matera, Membrane distillation in the textile wastewater treatment, Desalination, 83 (1991) 209-224.

[14] Q. Ge, P. Wang, C. Wan, T.-S. Chung, Polyelectrolyte-promoted forward osmosis–membrane distillation (FO–MD) hybrid process for dye wastewater treatment, Environmental science & technology, 46 (2012) 6236-6243.

[15] S. Zhang, P. Wang, X. Fu, T.-S. Chung, Sustainable water recovery from oily wastewater via forward osmosis-membrane distillation (FO-MD), water research, 52 (2014) 112-121.

[16] L. Eykens, K. De Sitter, C. Dotremont, L. Pinoy, B. Van der Bruggen, Membrane synthesis for membrane distillation: A review, Separation and Purification Technology, 182 (2017) 36-51.

[17] N. Dow, S. Gray, J. Zhang, E. Ostarcevic, A. Liubinas, P. Atherton, G. Roeszler, A. Gibbs, M. Duke, Pilot trial of membrane distillation driven by low grade waste heat: Membrane fouling and energy assessment, Desalination, 391 (2016) 30-42.

[18] M.R. Qtaishat, F. Banat, Desalination by solar powered membrane distillation systems, Desalination, 308 (2013) 186-197.

[19] M.A. Shannon, P.W. Bohn, M. Elimelech, J.G. Georgiadis, B.J. Marinas, A.M. Mayes, Science and technology for water purification in the coming decades, Nanoscience and technology: a collection of reviews from nature Journals, World Scientific2010, pp. 337-346.

[20] J. Kong, K. Li, Oil removal from oil-in-water emulsions using PVDF membranes, Separation and purification technology, 16 (1999) 83-93.

[21] S.R.H. Abadi, M.R. Sebzari, M. Hemati, F. Rekabdar, T. Mohammadi, Ceramic membrane performance in microfiltration of oily wastewater, Desalination, 265 (2011) 222-228.

[22] V. Singh, M. Purkait, C. Das, Cross-flow microfiltration of industrial oily wastewater: experimental and theoretical consideration, Separation Science and Technology, 46 (2011) 1213-1223.

[23] M. Panar, H.H. Hoehn, R. Hebert, The nature of asymmetry in reverse osmosis membranes, Macromolecules, 6 (1973) 777-780.

[24] S. Aoyama, W.J. Kolff, Treatment of renal failure with the disposable artificial kidney: results in fifty-two patients, The American journal of medicine, 23 (1957) 565-578.

[25] M.M. Pendergast, E.M. Hoek, A review of water treatment membrane nanotechnologies, Energy & Environmental Science, 4 (2011) 1946-1971.

[26] Y. He, Z.-W. Jiang, Technology review: treating oilfield wastewater, Filtration & Separation, 45 (2008) 14-16.

[27] T. Bilstad, E. Espedal, Membrane separation of produced water, Water Science and Technology, 34 (1996) 239-246.

[28] M. Cheryan, N. Rajagopalan, Membrane processing of oily streams. Wastewater treatment and waste reduction, Journal of membrane science, 151 (1998) 13-28.

[29] E. Cornelissen, D. Harmsen, K. De Korte, C. Ruiken, J.-J. Qin, H. Oo, L. Wessels, Membrane fouling and process performance of forward osmosis membranes on activated sludge, Journal of membrane science, 319 (2008) 158-168.

[30] B. Mi, M. Elimelech, Organic fouling of forward osmosis membranes: fouling reversibility and cleaning without chemical reagents, Journal of membrane science, 348 (2010) 337-345.

[31] B.R. Bodell, Distillation of saline water using silicone rubber membrane, Google Patents, 1968.

[32] K. Esato, B. Eiseman, Experimental evaluation of Gore-Tex membrane oxygenator, The Journal of thoracic and cardiovascular surgery, 69 (1975) 690-697.

[33] D. Gore, Gore-Tex membrane distillation, Proc. 10th Ann. Con. Water, DOI (1982) 25-29.

[34] K.W. Lawson, D.R. Lloyd, Membrane distillation, Journal of membrane Science, 124 (1997) 1-25.

[35] J. Phattaranawik, R. Jiraratananon, A.G. Fane, Heat transport and membrane distillation coefficients in direct contact membrane distillation, Journal of membrane science, 212 (2003) 177-193.

[36] M. Busch, R. Chu, U. Kolbe, Q. Meng, S. Li, Ultrafiltration pretreatment to reverse osmosis for seawater desalination—three years field experience in the Wangtan Datang power plant, Desalination and water treatment, 10 (2009) 1-20.

[37] J.-P. Mericq, S. Laborie, C. Cabassud, Vacuum membrane distillation for an integrated seawater desalination process, Desalination and water treatment, 9 (2009) 287-296.

[38] C. Gostoli, G. Sarti, Separation of liquid mixtures by membrane distillation, Journal of Membrane Science, 41 (1989) 211-224.

[39] M.d.C. García-Payo, M.A. Izquierdo-Gil, C. Fernández-Pineda, Wetting study of hydrophobic membranes via liquid entry pressure measurements with aqueous alcohol solutions, Journal of colloid and interface science, 230 (2000) 420-431.

[40] A. Franken, J. Nolten, M. Mulder, D. Bargeman, C. Smolders, Wetting criteria for the applicability of membrane distillation, Journal of Membrane Science, 33 (1987) 315-328.

[41] M. Tomaszewska, Preparation and properties of flat-sheet membranes from poly (vinylidene fluoride) for membrane distillation, Desalination, 104 (1996) 1-11.

[42] E. Curcio, E. Drioli, Membrane distillation and related operations—a review, Separation and Purification Reviews, 34 (2005) 35-86.

[43] S. Khemakhem, R.B. Amar, Grafting of fluoroalkylsilanes on microfiltration Tunisian clay membrane, Ceramics International, 37 (2011) 3323-3328.

[44] S. Cerneaux, I. Strużyńska, W.M. Kujawski, M. Persin, A. Larbot, Comparison of various membrane distillation methods for desalination using hydrophobic ceramic membranes, Journal of membrane science, 337 (2009) 55-60.

[45] J. Zhang, N. Dow, M. Duke, E. Ostarcevic, S. Gray, Identification of material and physical features of membrane distillation membranes for high performance desalination, Journal of Membrane Science, 349 (2010) 295-303.

[46] A.M. Alklaibi, N. Lior, Membrane-distillation desalination: status and potential, Desalination, 171 (2005) 111-131.

[47] F.A. Banat, J. Simandl, Theoretical and experimental study in membrane distillation, Desalination, 95 (1994) 39-52.

[48] M. Khayet, K. Khulbe, T. Matsuura, Characterization of membranes for membrane distillation by atomic force microscopy and estimation of their water vapor transfer coefficients in vacuum membrane distillation process, Journal of membrane science, 238 (2004) 199-211.

[49] F. Laganà, G. Barbieri, E. Drioli, Direct contact membrane distillation: modelling and concentration experiments, Journal of Membrane Science, 166 (2000) 1-11.

[50] M. Khayet, T. Matsuura, Preparation and characterization of polyvinylidene fluoride membranes for membrane distillation, Industrial & engineering chemistry Research, 40 (2001) 5710-5718.

[51] S. Srisurichan, R. Jiraratananon, A. Fane, Mass transfer mechanisms and transport resistances in direct contact membrane distillation process, Journal of membrane science, 277 (2006) 186-194.

[52] M. El-Bourawi, Z. Ding, R. Ma, M. Khayet, A framework for better understanding membrane distillation separation process, Journal of membrane science, 285 (2006) 4-29.

[53] A. Imdakm, T. Matsuura, Simulation of heat and mass transfer in direct contact membrane distillation (MD): The effect of membrane physical properties, Journal of Membrane Science, 262 (2005) 117-128.

[54] M. Khayet, A. Velázquez, J.I. Mengual, Modelling mass transport through a porous partition: effect of pore size distribution, Journal of non-equilibrium thermodynamics, 29 (2004) 279-299.

[55] L. Martínez, F. Florido-Díaz, A. Hernandez, P. Prádanos, Estimation of vapor transfer coefficient of hydrophobic porous membranes for applications in membrane distillation, Separation and purification technology, 33 (2003) 45-55.

[56] M. Khayet, T. Matsuura, Membrane distillation: principles and applications, Elsevier2011.

[57] Y. Fujii, S. Kigoshi, H. Iwatani, M. Aoyama, Selectivity and characteristics of direct contact membrane distillation type experiment. I. Permeability and selectivity through dried hydrophobic fine porous membranes, Journal of membrane science, 72 (1992) 53-72.

[58] M. Gryta, Concentration of saline wastewater from the production of heparin, Desalination, 129 (2000) 35-44.

[59] M. Kennedy, J. Kamanyi, S.S. Rodríguez, N. Lee, J. Schippers, G. Amy, Water treatment by microfiltration and ultrafiltration, Advanced Membrane Technology and Applications, DOI (2008) 131-170.

[60] N.N. Li, A.G. Fane, W.W. Ho, T. Matsuura, Advanced membrane technology and applications, John Wiley & Sons2011.

[61] E. Staude, Marcel Mulder: Basic Principles of Membrane Technology, Kluwer Academic Publishers, Dordrecht, Boston, London, 1991, ISBN 0-7923-0978-2, 363 Seiten, Preis: DM 200,—, Berichte der Bunsengesellschaft für physikalische Chemie, 96 (1992) 741-742.

[62] T. Matsuura, Synthetic membranes and membrane separation processes, CRC press1993.

[63] I. Pinnau, B.D. Freeman, Membrane formation and modification, American Chemical Society2000.

[64] C. Feng, B. Shi, G. Li, Y. Wu, Preliminary research on microporous membrane from F2. 4 for membrane distillation, Separation and purification technology, 39 (2004) 221-228.

[65] C. Feng, B. Shi, G. Li, Y. Wu, Preparation and properties of microporous membrane from poly (vinylidene fluoride-co-tetrafluoroethylene)(F2. 4) for membrane distillation, Journal of membrane science, 237 (2004) 15-24.

[66] M. García-Payo, M. Essalhi, M. Khayet, Preparation and characterization of PVDF–HFP copolymer hollow fiber membranes for membrane distillation, Desalination, 245 (2009) 469-473.

[67] M. García-Payo, M. Essalhi, M. Khayet, Effects of PVDF-HFP concentration on membrane distillation performance and structural morphology of hollow fiber membranes, Journal of Membrane Science, 347 (2010) 209-219.

[68] M. Khayet, J. Mengual, T. Matsuura, Porous hydrophobic/hydrophilic composite membranes: application in desalination using direct contact membrane distillation, Journal of Membrane Science, 252 (2005) 101-113.

[69] Z. Jin, S.H. Zhang, X.G. Jian, Hydrophobic modification of poly (phthalazinone ether sulfone ketone) hollow fiber membrane for vacuum membrane distillation, Journal of Membrane Science, 310 (2008) 20-27.

[70] K.Y. Wang, S.W. Foo, T.-S. Chung, Mixed matrix PVDF hollow fiber membranes with nanoscale pores for desalination through direct contact membrane distillation, Industrial & Engineering Chemistry Research, 48 (2009) 4474-4483.

[71] B. Li, K.K. Sirkar, Novel membrane and device for direct contact membrane distillation-based desalination process, Industrial & Engineering Chemistry Research, 43 (2004) 5300-5309.

[72] C. Feng, K. Khulbe, T. Matsuura, R. Gopal, S. Kaur, S. Ramakrishna, M. Khayet, Production of drinking water from saline water by air-gap membrane distillation using polyvinylidene fluoride nanofiber membrane, Journal of Membrane Science, 311 (2008) 1-6.

[73] L.F. Dumée, K. Sears, J. Schütz, N. Finn, C. Huynh, S. Hawkins, M. Duke, S. Gray, Characterization and evaluation of carbon nanotube Bucky-Paper membranes for direct contact membrane distillation, Journal of Membrane Science, 351 (2010) 36-43.

[74] P. Ajayan, T. Ebbesen, T. Ichihashi, S. Iijima, K. Tanigaki, H. Hiura, Opening carbon nanotubes with oxygen and implications for filling, Nature, 362 (1993) 522.

[75] M.S. Dresselhaus, M. Endo, Relation of carbon nanotubes to other carbon materials, Carbon nanotubes, Springer2001, pp. 11-28.

[76] D.T. Mitchell, S.B. Lee, L. Trofin, N. Li, T.K. Nevanen, H. Söderlund, C.R. Martin, Smart nanotubes for bioseparations and biocatalysis, Journal of the American Chemical Society, 124 (2002) 11864-11865.

[77] B. Khare, P. Wilhite, B. Tran, E. Teixeira, K. Fresquez, D.N. Mvondo, C. Bauschlicher, M. Meyyappan, Functionalization of carbon nanotubes via nitrogen glow discharge, The Journal of Physical Chemistry B, 109 (2005) 23466-23472.

[78] E.T. Thostenson, Z. Ren, T.-W. Chou, Advances in the science and technology of carbon nanotubes and their composites: a review, Composites science and technology, 61 (2001) 1899-1912.

[79] K. Dai, L. Shi, D. Zhang, J. Fang, NaCl adsorption in multi-walled carbon nanotube/active carbon combination electrode, Chemical Engineering Science, 61 (2006) 428-433.

[80] H. Li, L. Zou, Ion-exchange membrane capacitive deionization: A new strategy for brackish water desalination, Desalination, 275 (2011) 62-66.

[81] A.T. Nasrabadi, M. Foroutan, Ion-separation and water-purification using single-walled carbon nanotube electrodes, Desalination, 277 (2011) 236-243.

[82] L. Joseph, J. Heo, Y.-G. Park, J.R. Flora, Y. Yoon, Adsorption of bisphenol A and 17α-ethinyl estradiol on single walled carbon nanotubes from seawater and brackish water, Desalination, 281 (2011) 68-74.

[83] D. Zhang, L. Shi, J. Fang, K. Dai, J. Liu, Influence of carbonization of hot-pressed carbon nanotube electrodes on removal of NaCl from saltwater solution, Materials chemistry and physics, 96 (2006) 140-144.

[84] D. Zhang, L. Shi, J. Fang, K. Dai, Influence of diameter of carbon nanotubes mounted in flow-through capacitors on removal of NaCl from salt water, Journal of materials science, 42 (2007) 2471-2475.

[85] J. Li, C. Papadopoulos, J. Xu, M. Moskovits, Highly-ordered carbon nanotube arrays for electronics applications, Applied physics letters, 75 (1999) 367-369.

[86] K. Hata, D.N. Futaba, K. Mizuno, T. Namai, M. Yumura, S. Iijima, Water-assisted highly efficient synthesis of impurity-free single-walled carbon nanotubes, Science, 306 (2004) 1362-1364.

[87] S. Talapatra, S. Kar, S. Pal, R. Vajtai, L. Ci, P. Victor, M. Shaijumon, S. Kaur, O. Nalamasu, P. Ajayan, Direct growth of aligned carbon nanotubes on bulk metals, Nature nanotechnology, 1 (2006) 112.

[88] S.A. Miller, V.Y. Young, C.R. Martin, Electroosmotic flow in template-prepared carbon nanotube membranes, Journal of the American Chemical Society, 123 (2001) 12335-12342.

[89] B.J. Hinds, N. Chopra, T. Rantell, R. Andrews, V. Gavalas, L.G. Bachas, Aligned multiwalled carbon nanotube membranes, Science, 303 (2004) 62-65.

[90] J.K. Holt, A. Noy, T. Huser, D. Eaglesham, O. Bakajin, Fabrication of a carbon nanotube-embedded silicon nitride membrane for studies of nanometer-scale mass transport, Nano letters, 4 (2004) 2245-2250.

[91] J.K. Holt, H.G. Park, Y. Wang, M. Stadermann, A.B. Artyukhin, C.P. Grigoropoulos, A. Noy, O. Bakajin, Fast mass transport through sub-2-nanometer carbon nanotubes, Science, 312 (2006) 1034-1037.

[92] Z. Mao, S.B. Sinnott, Separation of organic molecular mixtures in carbon nanotubes and bundles: molecular dynamics simulations, The journal of physical chemistry B, 105 (2001) 6916-6924.

[93] M. Elimelech, W.A. Phillip, The future of seawater desalination: energy, technology, and the environment, science, 333 (2011) 712-717.

[94] B. Corry, Designing carbon nanotube membranes for efficient water desalination, The Journal of Physical Chemistry B, 112 (2008) 1427-1434.

[95] R. Das, M.E. Ali, S.B.A. Hamid, S. Ramakrishna, Z.Z. Chowdhury, Carbon nanotube membranes for water purification: a bright future in water desalination, Desalination, 336 (2014) 97-109.

[96] M. Endo, H. Muramatsu, T. Hayashi, Y. Kim, M. Terrones, M. Dresselhaus, Nanotechnology:'Buckypaper'from coaxial nanotubes, Nature, 433 (2005) 476.

[97] X. Zhang, T. Sreekumar, T. Liu, S. Kumar, Properties and structure of nitric acid oxidized single wall carbon nanotube films, The Journal of Physical Chemistry B, 108 (2004) 16435-16440.

[98] G. Xu, Q. Zhang, W. Zhou, J. Huang, F. Wei, The feasibility of producing MWCNT paper and strong MWCNT film from VACNT array, Applied Physics A, 92 (2008) 531-539.

[99] S. Bandow, A. Rao, K. Williams, A. Thess, R. Smalley, P. Eklund, Purification of single-wall carbon nanotubes by microfiltration, The Journal of Physical Chemistry B, 101 (1997) 8839-8842.

[100] R.H. Baughman, C. Cui, A.A. Zakhidov, Z. Iqbal, J.N. Barisci, G.M. Spinks, G.G. Wallace, A. Mazzoldi, D. De Rossi, A.G. Rinzler, Carbon nanotube actuators, Science, 284 (1999) 1340-1344.

[101] Y.A. Kim, H. Muramatsu, T. Hayashi, M. Endo, M. Terrones, M.S. Dresselhaus, Fabrication of high-purity, double-walled carbon nanotube buckypaper, Chemical Vapor Deposition, 12 (2006) 327-330.

[102] J.G. Park, S. Li, R. Liang, X. Fan, C. Zhang, B. Wang, The high current-carrying capacity of various carbon nanotube-based buckypapers, Nanotechnology, 19 (2008) 185710.

[103] T.-J. Park, S. Banerjee, T. Hemraj-Benny, S.S. Wong, Purification strategies and purity visualization techniques for single-walled carbon nanotubes, Journal of Materials Chemistry, 16 (2006) 141-154.

[104] D. Basmadjian, Mass transfer: principles and applications, CRC press Boca Raton, Florida2004.

[105] H. Muramatsu, T. Hayashi, Y. Kim, D. Shimamoto, Y. Kim, K. Tantrakarn, M. Endo, M. Terrones, M. Dresselhaus, Pore structure and oxidation stability of double-walled carbon nanotube-derived bucky paper, Chemical Physics Letters, 414 (2005) 444-448.

[106] C.P. Huynh, S.C. Hawkins, Understanding the synthesis of directly spinnable carbon nanotube forests, Carbon, 48 (2010) 1105-1115.

[107] L. Dumée, K. Sears, J.r. Schü tz, N. Finn, M. Duke, S. Gray, Carbon nanotube based composite membranes for water desalination by membrane distillation, Desalination and Water treatment, 17 (2010) 72-79.

[108] C. Cabassud, D. Wirth, Membrane distillation for water desalination: how to chose an appropriate membrane?, Desalination, 157 (2003) 307-314.

[109] K.W. Lawson, M.S. Hall, D.R. Lloyd, Compaction of microporous membranes used in membrane distillation. I. Effect on gas permeability, Journal of membrane science, 101 (1995) 99-108.

[110] W.L. Kevin, R.L. Douglas, Membrane distillation, Journal of Membrane Science, 124 (1997) 1-25.

[111] L. Dumée, V. Germain, K. Sears, J. Schütz, N. Finn, M. Duke, S. Cerneaux, D. Cornu, S. Gray, Enhanced durability and hydrophobicity of carbon nanotube bucky paper membranes in membrane distillation, Journal of membrane science, 376 (2011) 241-246.

[112] P. Goh, A. Ismail, B. Ng, Carbon nanotubes for desalination: Performance evaluation and current hurdles, Desalination, 308 (2013) 2-14.

[113] H.A. Shawky, S.-R. Chae, S. Lin, M.R. Wiesner, Synthesis and characterization of a carbon nanotube/polymer nanocomposite membrane for water treatment, Desalination, 272 (2011) 46-50.

[114] S. Sanip, A. Ismail, P. Goh, T. Soga, M. Tanemura, H. Yasuhiko, Gas separation properties of functionalized carbon nanotubes mixed matrix membranes, Separation and Purification Technology, 78 (2011) 208-213.

[115] T.L. Silva, S. Morales-Torres, J.L. Figueiredo, A.M. Silva, Multi-walled carbon nanotube/PVDF blended membranes with sponge-and finger-like pores for direct contact membrane distillation, Desalination, 357 (2015) 233-245.

[116] A. Morihama, J. Mierzwa, Clay nanoparticles effects on performance and morphology of poly (vinylidene fluoride) membranes, Brazilian journal of chemical engineering, 31 (2014) 79-93.

[117] Z.-M. Huang, Y.-Z. Zhang, M. Kotaki, S. Ramakrishna, A review on polymer nanofibers by electrospinning and their applications in nanocomposites, Composites science and technology, 63 (2003) 2223-2253.

[118] Y.C. Woo, L.D. Tijing, M.J. Park, M. Yao, J.-S. Choi, S. Lee, S.-H. Kim, K.-J. An, H.K. Shon, Electrospun dual-layer nonwoven membrane for desalination by air gap membrane distillation, Desalination, 403 (2017) 187-198.

[119] L.D. Tijing, J.-S. Choi, S. Lee, S.-H. Kim, H.K. Shon, Recent progress of membrane distillation using electrospun nanofibrous membrane, Journal of Membrane Science, 453 (2014) 435-462.

[120] A.K. An, J. Guo, E.-J. Lee, S. Jeong, Y. Zhao, Z. Wang, T. Leiknes, PDMS/PVDF hybrid electrospun membrane with superhydrophobic property and drop impact dynamics for dyeing wastewater treatment using membrane distillation, Journal of Membrane Science, 525 (2017) 57-67.

[121] B.S. Lalia, E. Guillen-Burrieza, H.A. Arafat, R. Hashaikeh, Fabrication and characterization of polyvinylidenefluoride-co-hexafluoropropylene (PVDF-HFP) electrospun membranes for direct contact membrane distillation, Journal of membrane science, 428 (2013) 104-115.

[122] H. Ke, E. Feldman, P. Guzman, J. Cole, Q. Wei, B. Chu, A. Alkhudhiri, R. Alrasheed, B.S. Hsiao, Electrospun polystyrene nanofibrous membranes for direct contact membrane distillation, Journal of membrane science, 515 (2016) 86-97.

[123] M. Essalhi, M. Khayet, Self-sustained webs of polyvinylidene fluoride electrospun nanofibers at different electrospinning times: 1. Desalination by direct contact membrane distillation, Journal of membrane science, 433 (2013) 167-179.

[124] M.A. Hammami, J.G. Croissant, L. Francis, S.K. Alsaiari, D.H. Anjum, N. Ghaffour, N.M. Khashab, Engineering hydrophobic organosilica nanoparticle-doped nanofibers for enhanced and fouling resistant membrane distillation, ACS applied materials & interfaces, 9 (2017) 1737-1745.

[125] E. Shaulsky, S. Nejati, C. Boo, F. Perreault, C.O. Osuji, M. Elimelech, Post-fabrication modification of electrospun nanofiber mats with polymer coating for membrane distillation applications, Journal of Membrane Science, 530 (2017) 158-165.

[126] Y. Liao, C.-H. Loh, R. Wang, A.G. Fane, Electrospun superhydrophobic membranes with unique structures for membrane distillation, ACS applied materials & interfaces, 6 (2014) 16035-16048.

[127] F.E. Ahmed, B.S. Lalia, R. Hashaikeh, A review on electrospinning for membrane fabrication: challenges and applications, Desalination, 356 (2015) 15-30.

[128] X. Li, L. Deng, X. Yu, M. Wang, X. Wang, C. García-Payo, M. Khayet, A novel profiled core–shell nanofibrous membrane for wastewater treatment by direct contact membrane distillation, Journal of Materials Chemistry A, 4 (2016) 14453-14463.

[129] J.H. Kim, S.H. Park, M.J. Lee, S.M. Lee, W.H. Lee, K.H. Lee, N.R. Kang, H.J. Jo, J.F. Kim, E. Drioli, Thermally rearranged polymer membranes for desalination, Energy & Environmental Science, 9 (2016) 878-884.

[130] J. Lee, C. Boo, W.-H. Ryu, A.D. Taylor, M. Elimelech, Development of omniphobic desalination membranes using a charged electrospun nanofiber scaffold, ACS applied materials & interfaces, 8 (2016) 11154-11161.

[131] C. Boo, J. Lee, M. Elimelech, Engineering surface energy and nanostructure of microporous films for expanded membrane distillation applications, Environmental science & technology, 50 (2016) 8112-8119.

[132] L.D. Tijing, Y.C. Woo, W.-G. Shim, T. He, J.-S. Choi, S.-H. Kim, H.K. Shon, Superhydrophobic nanofiber membrane containing carbon nanotubes for high-performance direct contact membrane distillation, Journal of Membrane Science, 502 (2016) 158-170.

[133] J.-G. Lee, Y.-D. Kim, W.-S. Kim, L. Francis, G. Amy, N. Ghaffour, Performance modeling of direct contact membrane distillation (DCMD) seawater desalination process using a commercial composite membrane, Journal of membrane science, 478 (2015) 85-95.

[134] J.-G. Lee, E.-J. Lee, S. Jeong, J. Guo, A.K. An, H. Guo, J. Kim, T. Leiknes, N. Ghaffour, Theoretical modeling and experimental validation of transport and separation properties of carbon nanotube electrospun membrane distillation, Journal of Membrane Science, 526 (2017) 395-408.

[135] C.Y. Khripin, J.A. Fagan, M. Zheng, Spontaneous partition of carbon nanotubes in polymer-modified aqueous phases, Journal of the American Chemical Society, 135 (2013) 6822-6825.

[136] O. Sae-Khow, S. Mitra, Simultaneous extraction and concentration in carbon nanotube immobilized hollow fiber membranes, Analytical chemistry, 82 (2010) 5561-5567.

[137] O. Sae-Khow, S. Mitra, Carbon nanotube immobilized composite hollow fiber membranes for pervaporative removal of volatile organics from water, The Journal of Physical Chemistry C, 114 (2010) 16351-16356.

[138] K. Gethard, O. Sae-Khow, S. Mitra, Water desalination using carbon-nanotube-enhanced membrane distillation, ACS applied materials & interfaces, 3 (2010) 110-114.

[139] K. Gethard, O. Sae-Khow, S. Mitra, Carbon nanotube enhanced membrane distillation for simultaneous generation of pure water and concentrating pharmaceutical waste, Separation and purification technology, 90 (2012) 239-245.

[140] M. Bhadra, S. Roy, S. Mitra, Flux enhancement in direct contact membrane distillation by implementing carbon nanotube immobilized PTFE membrane, Separation and Purification Technology, 161 (2016) 136-143.

[141] S. Roy, S.A. Ntim, S. Mitra, K.K. Sirkar, Facile fabrication of superior nanofiltration membranes from interfacially polymerized CNT-polymer composites, Journal of membrane science, 375 (2011) 81-87.

[142] M. Bhadra, S. Roy, S. Mitra, Enhanced desalination using carboxylated carbon nanotube immobilized membranes, Separation and Purification Technology, 120 (2013) 373-377.

[143] M. Bhadra, S. Roy, S. Mitra, A bilayered structure comprised of functionalized carbon nanotubes for desalination by membrane distillation, ACS applied materials & interfaces, 8 (2016) 19507-19513.

[144] S. Ragunath, S. Roy, S. Mitra, Carbon nanotube immobilized membrane with controlled nanotube incorporation via phase inversion polymerization for membrane distillation based desalination, Separation and Purification Technology, 194 (2018) 249-255.

[145] W. Intrchom, S. Roy, S. Mitra, Functionalized carbon nanotube immobilized membrane for low temperature ammonia removal via membrane distillation, Separation and Purification Technology, 235 (2020) 116188.

[146] O. Gupta, S. Roy, S. Mitra, Enhanced membrane distillation of organic solvents from their aqueous mixtures using a carbon nanotube immobilized membrane, Journal of membrane science, 568 (2018) 134-140.

[147] M.S. Humoud, S. Roy, S. Mitra, Scaling Reduction in Carbon Nanotube-Immobilized Membrane during Membrane Distillation, Water, 11 (2019) 2588.

[148] S.P. Koenig, L. Wang, J. Pellegrino, J.S. Bunch, Selective molecular sieving through porous graphene, Nature nanotechnology, 7 (2012) 728-732.

[149] S.C. O'Hern, M.S. Boutilier, J.-C. Idrobo, Y. Song, J. Kong, T. Laoui, M. Atieh, R. Karnik, Selective ionic transport through tunable subnanometer pores in single-layer graphene membranes, Nano letters, 14 (2014) 1234-1241.

[150] A.K. Geim, K.S. Novoselov, The rise of graphene, Nanoscience and technology: a collection of reviews from nature journals, World Scientific2010, pp. 11-19.

[151] V. Berry, Impermeability of graphene and its applications, Carbon, 62 (2013) 1-10.

[152] S. Hu, M. Lozada-Hidalgo, F. Wang, A. Mishchenko, F. Schedin, R. Nair, E. Hill, D. Boukhvalov, M. Katsnelson, R. Dryfe, Proton transport through one-atom-thick crystals, Nature, 516 (2014) 227-230.

[153] F. Guo, G. Silverberg, S. Bowers, S.-P. Kim, D. Datta, V. Shenoy, R.H. Hurt, Graphene-based environmental barriers, Environmental science & technology, 46 (2012) 7717-7724.

[154] D. Prasai, J.C. Tuberquia, R.R. Harl, G.K. Jennings, K.I. Bolotin, Graphene: corrosion-inhibiting coating, ACS nano, 6 (2012) 1102-1108.

[155] R. Nair, H. Wu, P. Jayaram, I. Grigorieva, A. Geim, Unimpeded permeation of water through helium-leak–tight graphene-based membranes, Science, 335 (2012) 442-444.

[156] Y. Han, Z. Xu, C. Gao, Ultrathin graphene nanofiltration membrane for water purification, Advanced functional materials, 23 (2013) 3693-3700.

[157] W.-S. Hung, Q.-F. An, M. De Guzman, H.-Y. Lin, S.-H. Huang, W.-R. Liu, C.-C. Hu, K.-R. Lee, J.-Y. Lai, Pressure-assisted self-assembly technique for fabricating composite membranes consisting of highly ordered selective laminate layers of amphiphilic graphene oxide, Carbon, 68 (2014) 670-677.

[158] K. Huang, G. Liu, Y. Lou, Z. Dong, J. Shen, W. Jin, A graphene oxide membrane with highly selective molecular separation of aqueous organic solution, Angewandte Chemie, 126 (2014) 7049-7052.

[159] H.W. Kim, H.W. Yoon, S.-M. Yoon, B.M. Yoo, B.K. Ahn, Y.H. Cho, H.J. Shin, H. Yang, U. Paik, S. Kwon, Selective gas transport through few-layered graphene and graphene oxide membranes, Science, 342 (2013) 91-95.

[160] J. Shen, G. Liu, K. Huang, W. Jin, K.R. Lee, N. Xu, Membranes with fast and selective gas-transport channels of laminar graphene oxide for efficient CO2 capture, Angewandte Chemie, 127 (2015) 588-592.

[161] K. Cao, Z. Jiang, J. Zhao, C. Zhao, C. Gao, F. Pan, B. Wang, X. Cao, J. Yang, Enhanced water permeation through sodium alginate membranes by incorporating graphene oxides, Journal of membrane science, 469 (2014) 272-283.

[162] H. Huang, Z. Song, N. Wei, L. Shi, Y. Mao, Y. Ying, L. Sun, Z. Xu, X. Peng, Ultrafast viscous water flow through nanostrand-channelled graphene oxide membranes, Nature communications, 4 (2013) 1-9.

[163] M. Hu, B. Mi, Enabling graphene oxide nanosheets as water separation membranes, Environmental science & technology, 47 (2013) 3715-3723.

[164] S.P. Surwade, S.N. Smirnov, I.V. Vlassiouk, R.R. Unocic, G.M. Veith, S. Dai, S.M. Mahurin, Water desalination using nanoporous single-layer graphene, Nature nanotechnology, 10 (2015) 459-464.

[165] M. Hu, B. Mi, Layer-by-layer assembly of graphene oxide membranes via electrostatic interaction, Journal of Membrane Science, 469 (2014) 80-87.

[166] W.-S. Hung, C.-H. Tsou, M. De Guzman, Q.-F. An, Y.-L. Liu, Y.-M. Zhang, C.-C. Hu, K.-R. Lee, J.-Y. Lai, Cross-linking with diamine monomers to prepare composite graphene oxide-framework membranes with varying d-spacing, Chemistry of Materials, 26 (2014) 2983-2990.

[167] S. Pei, H.-M. Cheng, The reduction of graphene oxide, Carbon, 50 (2012) 3210-3228.

[168] A.K. Geim, Graphene: status and prospects, science, 324 (2009) 1530-1534.

[169] Z. Wang, H. Yu, J. Xia, F. Zhang, F. Li, Y. Xia, Y. Li, Novel GO-blended PVDF ultrafiltration membranes, Desalination, 299 (2012) 50-54.

[170] A. Shanmugharaj, J. Yoon, W. Yang, S.H. Ryu, Synthesis, characterization, and surface wettability properties of amine functionalized graphene oxide films with varying amine chain lengths, Journal of colloid and interface science, 401 (2013) 148-154.

[171] P.G. Ren, H. Wang, H.D. Huang, D.X. Yan, Z.M. Li, Characterization and performance of dodecyl amine functionalized graphene oxide and dodecyl amine functionalized graphene/high-density polyethylene nanocomposites: A comparative study, Journal of Applied Polymer Science, 131 (2014).

[172] K.-J. Lu, J. Zuo, T.-S. Chung, Novel PVDF membranes comprising n-butylamine functionalized graphene oxide for direct contact membrane distillation, Journal of Membrane Science, 539 (2017) 34-42.

[173] C. Athanasekou, A. Sapalidis, I. Katris, E. Savopoulou, K. Beltsios, T. Tsoufis, A. Kaltzoglou, P. Falaras, G. Bounos, M. Antoniou, Mixed Matrix PVDF/Graphene and Composite-Skin PVDF/Graphene Oxide Membranes Applied in Membrane Distillation, Polymer Engineering & Science, 59 (2019) E262-E278.

[174] D. Cohen-Tanugi, J.C. Grossman, Water desalination across nanoporous graphene, Nano letters, 12 (2012) 3602-3608.

[175] D.R. Dreyer, A.D. Todd, C.W. Bielawski, Harnessing the chemistry of graphene oxide, Chemical Society Reviews, 43 (2014) 5288-5301.

[176] H. Yang, F. Li, C. Shan, D. Han, Q. Zhang, L. Niu, A. Ivaska, Covalent functionalization of chemically converted graphene sheets via silane and its reinforcement, Journal of Materials Chemistry, 19 (2009) 4632-4638.

[177] Z. Xu, J. Zhang, M. Shan, Y. Li, B. Li, J. Niu, B. Zhou, X. Qian, Organosilane-functionalized graphene oxide for enhanced antifouling and mechanical properties of polyvinylidene fluoride ultrafiltration membranes, Journal of Membrane Science, 458 (2014) 1-13.

[178] S. Leaper, A. Abdel-Karim, B. Faki, J.M. Luque-Alled, M. Alberto, A. Vijayaraghavan, S.M. Holmes, G. Szekely, M.I. Badawy, N. Shokri, Flux-enhanced PVDF mixed matrix membranes incorporating APTS-functionalized graphene oxide for membrane distillation, Journal of Membrane Science, 554 (2018) 309-323.

[179] B. Van der Bruggen, Integrated membrane separation processes for recycling of valuable wastewater streams: nanofiltration, membrane distillation, and membrane crystallizers revisited, Industrial & Engineering Chemistry Research, 52 (2013) 10335-10341.

[180] K. Karakulski, M. Gryta, A. Morawski, Membrane processes used for potable water quality improvement, Desalination, 145 (2002) 315-319.

[181] S. Yarlagadda, L.M. Camacho, V.G. Gude, Z. Wei, S. Deng, Membrane distillation for desalination and other separations, Recent Patents on Chemical Engineering, 2 (2009) 128-158.

[182] L. Bazinet, S. Brianceau, P. Dubé, Y. Desjardins, Evolution of cranberry juice physico-chemical parameters during phenolic antioxidant enrichment by electrodialysis with filtration membrane, Separation and Purification Technology, 87 (2012) 31-39.

[183] D.S. Couto, M. Dornier, D. Pallet, M. Reynes, D. Dijoux, S.P. Freitas, L.M. Cabral, Evaluation of nanofi ltration membranes for the retention of anthocyanins of açai (Euterpe oleracea Mart.) juice, Desalination and Water Treatment, 27 (2011) 108-113.

[184] F. dos Santos Gomes, P. Albuquerque da Costa, M.B. Domingues de Campos, S. Couri, L.M.C. Cabral, Concentration of watermelon juice by reverse osmosis process, Desalination and Water Treatment, 27 (2011) 120-122.

[185] D.M. Warsinger, S. Chakraborty, E.W. Tow, M.H. Plumlee, C. Bellona, S. Loutatidou, L. Karimi, A.M. Mikelonis, A. Achilli, A. Ghassemi, A review of polymeric membranes and processes for potable water reuse, Progress in Polymer Science, DOI (2018).

[186] I. Janajreh, D. Suwwan, R. Hashaikeh, Theoretical and experimental study of direct contact membrane distillation, Desalination and Water Treatment, 57 (2016) 15660-15675.

[187] M. Tomaszewska, M. Gryta, Studies on membrane scaling during water desalination by direct contact membrane distillation, DESALINATION AND WATER TREATMENT, 64 (2017) 272-278.

[188] Y.C. Woo, L.D. Tijing, W.-G. Shim, J.-S. Choi, S.-H. Kim, T. He, E. Drioli, H.K. Shon, Water desalination using graphene-enhanced electrospun nanofiber membrane via air gap membrane distillation, Journal of Membrane Science, 520 (2016) 99-110.

[189] X.-L. Hou, Y.-L. Wu, T. Yang, X.-D. Du, Multi-walled carbon nanotubes–dispersive solid-phase extraction combined with liquid chromatography–tandem mass spectrometry for the analysis of 18 sulfonamides in pork, Journal of Chromatography B, 929 (2013) 107-115.

[190] V.G. Gude, Energy storage for desalination processes powered by renewable energy and waste heat sources, Applied Energy, 137 (2015) 877-898.

[191] D.S. Kenney, R. Wilkinson, The water-energy nexus in the American West, Edward Elgar Publishing2011.

[192] M. García-Payo, C. Rivier, I. Marison, U. Von Stockar, Separation of binary mixtures by thermostatic sweeping gas membrane distillation: II. Experimental results with aqueous formic acid solutions, Journal of Membrane Science, 198 (2002) 197-210.

[193] L. Basini, G. D'Angelo, M. Gobbi, G. Sarti, C. Gostoli, A desalination process through sweeping gas membrane distillation, Desalination, 64 (1987) 245-257.

[194] M. Khayet, P. Godino, J.I. Mengual, Theory and experiments on sweeping gas membrane distillation, Journal of Membrane Science, 165 (2000) 261-272.

[195] M. Khayet, Membranes and theoretical modeling of membrane distillation: a review, Advances in colloid and interface science, 164 (2011) 56-88.

[196] S.R. Krajewski, W. Kujawski, M. Bukowska, C. Picard, A. Larbot, Application of fluoroalkylsilanes (FAS) grafted ceramic membranes in membrane distillation process of NaCl solutions, Journal of membrane science, 281 (2006) 253-259.

[197] M. Khayet, T. Matsuura, J. Mengual, Porous hydrophobic/hydrophilic composite membranes: Estimation of the hydrophobic-layer thickness, Journal of membrane science, 266 (2005) 68-79.

[198] M. Qtaishat, M. Khayet, T. Matsuura, Novel porous composite hydrophobic/hydrophilic polysulfone membranes for desalination by direct contact membrane distillation, Journal of Membrane science, 341 (2009) 139-148.

[199] S. Bonyadi, T.S. Chung, Flux enhancement in membrane distillation by fabrication of dual layer hydrophilic–hydrophobic hollow fiber membranes, Journal of membrane science, 306 (2007) 134-146.

[200] S. Ragunath, S. Roy, S. Mitra, Selective hydrophilization of the permeate surface to enhance flux in membrane distillation, Separation and Purification Technology, 170 (2016) 427-433.

[201] F. Edwie, T.-S. Chung, Development of hollow fiber membranes for water and salt recovery from highly concentrated brine via direct contact membrane distillation and crystallization, Journal of membrane science, 421 (2012) 111-123.

[202] J. Prince, D. Rana, G. Singh, T. Matsuura, T.J. Kai, T. Shanmugasundaram, Effect of hydrophobic surface modifying macromolecules on differently produced PVDF membranes for direct contact membrane distillation, Chemical Engineering Journal, 242 (2014) 387-396.

[203] Y.T. Ong, A.L. Ahmad, S.H.S. Zein, K. Sudesh, S.H. Tan, Poly (3-hydroxybutyrate)-functionalised multi-walled carbon nanotubes/chitosan green nanocomposite membranes and their application in pervaporation, Separation and Purification Technology, 76 (2011) 419-427.

[204] Y.-x. Jia, H.-l. Li, M. Wang, L.-y. Wu, Y.-d. Hu, Carbon nanotube: possible candidate for forward osmosis, Separation and Purification Technology, 75 (2010) 55-60.

[205] V. Vatanpour, S.S. Madaeni, R. Moradian, S. Zinadini, B. Astinchap, Fabrication and characterization of novel antifouling nanofiltration membrane prepared from oxidized multiwalled carbon nanotube/polyethersulfone nanocomposite, Journal of Membrane Science, 375 (2011) 284-294.

[206] S. Roy, M. Bhadra, S. Mitra, Enhanced desalination via functionalized carbon nanotube immobilized membrane in direct contact membrane distillation, Separation and Purification Technology, 136 (2014) 58-65.

[207] A. Peigney, C. Laurent, E. Flahaut, R. Bacsa, A. Rousset, Specific surface area of carbon nanotubes and bundles of carbon nanotubes, Carbon, 39 (2001) 507-514.

[208] D.A. Britz, A.N. Khlobystov, Noncovalent interactions of molecules with single walled carbon nanotubes, Chemical Society Reviews, 35 (2006) 637-659.

[209] Q. Yang, L. Li, H. Cheng, M. Wang, J. Bai, Inner-tubular physicochemical processes of carbon nanotubes, Chinese Science Bulletin, 48 (2003) 2395-2403.

[210] W. Intrchom, S. Mitra, Analytical sample preparation, preconcentration and chromatographic separation on carbon nanotubes, Current opinion in chemical engineering, 16 (2017) 102-114.

[211] C.M. Hussain, C. Saridara, S. Mitra, Modifying the sorption properties of multi-walled carbon nanotubes via covalent functionalization, Analyst, 134 (2009) 1928-1933.

[212] Q. Li, Y. Ding, D. Yuan, Electrosorption-enhanced solid-phase microextraction of trace anions using a platinum plate coated with single-walled carbon nanotubes, Talanta, 85 (2011) 1148-1153.

[213] S. Kalla, S. Upadhyaya, K. Singh, R.K. Dohare, M. Agarwal, A case study on separation of IPA-water mixture by extractive distillation using aspen plus, International Journal of Advanced Technology and Engineering Exploration, 3 (2016) 187.

[214] B. Smitha, D. Suhanya, S. Sridhar, M. Ramakrishna, Separation of organic–organic mixtures by pervaporation—a review, Journal of membrane science, 241 (2004) 1-21.

[215] S. Roy, N.R. Singha, Polymeric nanocomposite membranes for next generation pervaporation process: strategies, challenges and future prospects, Membranes, 7 (2017) 53.

[216] M. Khayet, M. Godino, J. Mengual, Theoretical and experimental studies on desalination using the sweeping gas membrane distillation method, Desalination, 157 (2003) 297-305.

[217] L. Li, K.K. Sirkar, Studies in vacuum membrane distillation with flat membranes, Journal of Membrane Science, 523 (2017) 225-234.

[218] D. Wang, K. Li, W. Teo, Preparation and characterization of polyvinylidene fluoride (PVDF) hollow fiber membranes, Journal of membrane science, 163 (1999) 211-220.

[219] C.M. Hussain, C. Saridara, S. Mitra, Carbon nanotubes as sorbents for the gas phase preconcentration of semivolatile organics in a microtrap, Analyst, 133 (2008) 1076-1082.

[220] C.H. Lee, W.H. Hong, Effect of operating variables on the flux and selectivity in sweep gas membrane distillation for dilute aqueous isopropanol, Journal of Membrane Science, 188 (2001) 79-86.

[221] C.M. Hussain, C. Saridara, S. Mitra, Altering the polarity of self-assembled carbon nanotubes stationary phase via covalent functionalization, RSC Advances, 1 (2011) 685-689.

[222] G.S. Parks, B. Barton, Vapor pressure data for isopropyl alcohol and tertiary butyl alcohol, Journal of the American Chemical Society, 50 (1928) 24-26.

[223] Y. Yun, R. Ma, W. Zhang, A. Fane, J. Li, Direct contact membrane distillation mechanism for high concentration NaCl solutions, Desalination, 188 (2006) 251-262.

[224] M. Bhadra, S. Roy, S. Mitra, Nanodiamond immobilized membranes for enhanced desalination via membrane distillation, Desalination, 341 (2014) 115-119.

[225] S. Roy, C.M. Hussain, S. Mitra, Carbon nanotube-immobilized super-absorbent membrane for harvesting water from the atmosphere, Environmental Science: Water Research & Technology, 1 (2015) 753-760.

[226] S. Ragunath, S. Mitra, Carbon nanotube immobilized composite hollow fiber membranes for extraction of volatile organics from air, The Journal of Physical Chemistry C, 119 (2015) 13231-13237.

[227] C. Saridara, S. Ragunath, Y. Pu, S. Mitra, Methane preconcentration in a microtrap using multiwalled carbon nanotubes as sorbents, Analytica chimica acta, 677 (2010) 50-54.

[228] W. Chen, S. Chen, T. Liang, Q. Zhang, Z. Fan, H. Yin, K.-W. Huang, X. Zhang, Z. Lai, P. Sheng, High-flux water desalination with interfacial salt sieving effect in nanoporous carbon composite membranes, Nature nanotechnology, 13 (2018) 345.

[229] S. Al-Obaidani, E. Curcio, F. Macedonio, G. Di Profio, H. Al-Hinai, E. Drioli, Potential of membrane distillation in seawater desalination: thermal efficiency, sensitivity study and cost estimation, Journal of Membrane Science, 323 (2008) 85-98.

[230] L. Song, Z. Ma, X. Liao, P.B. Kosaraju, J.R. Irish, K.K. Sirkar, Pilot plant studies of novel membranes and devices for direct contact membrane distillation-based desalination, Journal of Membrane Science, 323 (2008) 257-270.

[231] S.S. Madaeni, E. Salehi, Membrane-Adsorption Integrated Systems/Processes, John Wiley & Sons: Oxford, UK2015.

[232] G. Zakrzewska-Trznadel, M. Harasimowicz, A.G. Chmielewski, Concentration of radioactive components in liquid low-level radioactive waste by membrane distillation, Journal of Membrane Science, 163 (1999) 257-264.

[233] A. Alkhudhiri, N. Darwish, N. Hilal, Membrane distillation: a comprehensive review, Desalination, 287 (2012) 2-18.

[234] P. Onsekizoglu, Membrane distillation: principle, advances, limitations and future prospects in food industry, Distillation-Advances from Modeling to Applications, InTech2012.

[235] S. Roy, S. Ragunath, S. Mitra, Effect of module configuration on the overall mass recovery in membrane distillation, DESALINATION AND WATER TREATMENT, 95 (2017) 74-79.

[236] D. Wirth, C. Cabassud, Water desalination using membrane distillation: comparison between inside/out and outside/in permeation, Desalination, 147 (2002) 139-145.

[237] L. Martínez-Díez, M.I. Vazquez-Gonzalez, Temperature and concentration polarization in membrane distillation of aqueous salt solutions, Journal of membrane science, 156 (1999) 265-273.

[238] M. Tomaszewska, M. Gryta, A. Morawski, The influence of salt in solutions on hydrochloric acid recovery by membrane distillation, Separation and Purification Technology, 14 (1998) 183-188.

[239] R. Bagger-Jørgensen, A.S. Meyer, C. Varming, G. Jonsson, Recovery of volatile aroma compounds from black currant juice by vacuum membrane distillation, Journal of Food Engineering, 64 (2004) 23-31.

[240] V. Soni, J. Abildskov, G. Jonsson, R. Gani, Modeling and analysis of vacuum membrane distillation for the recovery of volatile aroma compounds from black currant juice, Journal of Membrane Science, 320 (2008) 442-455.

[241] R. Bagger-Jørgensen, A.S. Meyer, M. Pinelo, C. Varming, G. Jonsson, Recovery of volatile fruit juice aroma compounds by membrane technology: Sweeping gas versus vacuum membrane distillation, Innovative Food Science & Emerging Technologies, 12 (2011) 388-397.

[242] K.J. Chua, S.K. Chou, W. Yang, Advances in heat pump systems: A review, Applied energy, 87 (2010) 3611-3624.

[243] M. Grätzel, Conversion of sunlight to electric power by nanocrystalline dye-sensitized solar cells, Journal of Photochemistry and Photobiology A: Chemistry, 164 (2004) 3-14.

[244] X. Gou, H. Xiao, S. Yang, Modeling, experimental study and optimization on low-temperature waste heat thermoelectric generator system, Applied energy, 87 (2010) 3131-3136.

[245] S. Roy, S. Ragunath, Emerging Membrane Technologies for Water and Energy Sustainability: Future Prospects, Constrains and Challenges, Energies, 11 (2018) 1-32.

[246] I. Gil, A. Uyazán, J. Aguilar, G. Rodríguez, L. Caicedo, Separation of ethanol and water by extractive distillation with salt and solvent as entrainer: process simulation, Brazilian Journal of Chemical Engineering, 25 (2008) 207-215.

[247] D. Barba, V. Brandani, G. di Giacomo, Hyperazeotropic ethanol salted-out by extractive distillation. Theoretical evaluation and experimental check, Chemical Engineering Science, 40 (1985) 2287-2292.

[248] I.D. Gil, J.M. Gómez, G. Rodríguez, Control of an extractive distillation process to dehydrate ethanol using glycerol as entrainer, Computers & Chemical Engineering, 39 (2012) 129-142.

[249] J. Fu, Simulation of salt-containing extractive distillation for the system of ethanol/water/ethanediol/KAc. 2. Simulation of salt-containing extractive distillation, Industrial & engineering chemistry research, 43 (2004) 1279-1283.

[250] F.M. Lee, R.H. Pahl, Solvent screening study and conceptual extractive distillation process to produce anhydrous ethanol from fermentation broth, Industrial & Engineering Chemistry Process Design and Development, 24 (1985) 168-172.

[251] R. Pinto, M. Wolf-Maciel, L. Lintomen, Saline extractive distillation process for ethanol purification, Computers & Chemical Engineering, 24 (2000) 1689-1694.

[252] S. Roy, N. Singha, Polymeric nanocomposite membranes for next generation pervaporation process: Strategies, challenges and future prospects, Membranes, 7 (2017) 53.

[253] M. Izquierdo-Gil, G. Jonsson, Factors affecting flux and ethanol separation performance in vacuum membrane distillation (VMD), Journal of Membrane Science, 214 (2003) 113-130.

[254] F.A. Banat, F.A. Al-Rub, M. Shannag, Modeling of dilute ethanol–water mixture separation by membrane distillation, Separation and Purification Technology, 16 (1999) 119-131.

[255] F.A. Banat, J. Simandl, Membrane distillation for dilute ethanol: separation from aqueous streams, Journal of Membrane Science, 163 (1999) 333-348.

[256] S. Bandini, C. Gostoli, G. Sarti, Separation efficiency in vacuum membrane distillation, Journal of Membrane Science, 73 (1992) 217-229.

[257] G. Lewandowicz, W. Białas, B. Marczewski, D. Szymanowska, Application of membrane distillation for ethanol recovery during fuel ethanol production, Journal of membrane science, 375 (2011) 212-219.

[258] R.L. Calibo, M. Matsumura, H. Kataoka, Continuous ethanol fermentation of concentrated sugar solutions coupled with membrane distillation using a PTFE module, Journal of Fermentation and Bioengineering, 67 (1989) 40-45.

[259] H. Udriot, S. Ampuero, I. Marison, U. Von Stockar, Extractive fermentation of ethanol using membrane distillation, Biotechnology letters, 11 (1989) 509-514.

[260] R.J. Giguere, T.L. Bray, S.M. Duncan, G. Majetich, Application of commercial microwave ovens to organic synthesis, Tetrahedron letters, 27 (1986) 4945-4948.

[261] A. De la Hoz, A. Diaz-Ortiz, A. Moreno, Microwaves in organic synthesis. Thermal and non-thermal microwave effects, Chemical Society Reviews, 34 (2005) 164-178.

[262] C.O. Kappe, Controlled microwave heating in modern organic synthesis, Angewandte Chemie International Edition, 43 (2004) 6250-6284.

[263] A.J. Norton, S. Jordan, P. Yeomans, Brief, high-temperature heat denaturation (pressure cooking): A simple and effective method of antigen retrieval for routinely processed tissues, The Journal of pathology, 173 (1994) 371-379.

[264] D. Adam, Microwave chemistry: Out of the kitchen, Nature Publishing Group, 2003.

[265] B. Kaufmann, P. Christen, Recent extraction techniques for natural products: microwave-assisted extraction and pressurised solvent extraction, Phytochemical analysis, 13 (2002) 105-113.

[266] D. Stuerga, Microwave-material interactions and dielectric properties, key ingredients for mastery of chemical microwave processes, Microwaves in organic synthesis, 2 (2006) 1-59.

[267] E. Grant, B.J. Halstead, Dielectric parameters relevant to microwave dielectric heating, Chemical society reviews, 27 (1998) 213-224.

[268] D. Michael P áMingos, Tilden Lecture. Applications of microwave dielectric heating effects to synthetic problems in chemistry, Chemical Society Reviews, 20 (1991) 1-47.

[269] J.R. Lill, Microwave assisted proteomics, Royal Society of Chemistry2009.

[270] R.N. Gedye, W. Rank, K.C. Westaway, The rapid synthesis of organic compounds in microwave ovens. II, Canadian journal of chemistry, 69 (1991) 706-711.

[271] Y. Wang, Z. Iqbal, S. Mitra, Microwave-induced rapid chemical functionalization of single-walled carbon nanotubes, Carbon, 43 (2005) 1015-1020.

[272] J. Hong, N. Ta, S.-g. Yang, Y.-z. Liu, C. Sun, Microwave-assisted direct photolysis of bromophenol blue using electrodeless discharge lamps, Desalination, 214 (2007) 62-69.

[273] Y.-S. Bae, S.-C. Jung, A study of the photocatalytic destruction of propylene using microwave discharge electrodeless lamp, Journal of Industrial and Engineering Chemistry, 16 (2010) 947-951.

[274] L. Wang, X. Miao, G. Pan, Microwave-Induced Interfacial Nanobubbles, Langmuir, 32 (2016) 11147-11154.

[275] N. Ishida, T. Inoue, M. Miyahara, K. Higashitani, Nano bubbles on a hydrophobic surface in water observed by tapping-mode atomic force microscopy, Langmuir, 16 (2000) 6377-6380.

[276] E.S. Kryachko, Ab initio studies of the conformations of water hexamer: modelling the penta-coordinated hydrogen-bonded pattern in liquid water, Chemical physics letters, 314 (1999) 353-363.

[277] M.L. Rao, S.R. Sedlmayr, R. Roy, J. Kanzius, Polarized microwave and RF radiation effects on the structure and stability of liquid water, Current Science, 98 (2010) 1500-1504.

[278] M. Mohamadi, T. Shamspur, A. Mostafavi, Comparison of microwave-assisted distillation and conventional hydrodistillation in the essential oil extraction of flowers Rosa damascena Mill, Journal of essential oil research, 25 (2013) 55-61.

[279] C. Zhao, X. He, C. Li, L. Yang, Y. Fu, K. Wang, Y. Zhang, Y. Ni, A Microwave-Assisted Simultaneous Distillation and Extraction Method for the Separation of Polysaccharides and Essential Oil from the Leaves of Taxus chinensis Var. mairei, Applied Sciences, 6 (2016) 19.

[280] Z. Ji, J. Wang, D. Hou, Z. Yin, Z. Luan, Effect of microwave irradiation on vacuum membrane distillation, Journal of membrane science, 429 (2013) 473-479.

[281] S. Roy, M.S. Humoud, W. Intrchom, S. Mitra, Microwave-induced desalination via direct contact membrane distillation, ACS Sustainable Chemistry & Engineering, 6 (2017) 626-632.

[282] M. Komorowska-Durka, R. van Houten, G.D. Stefanidis, Application of microwave heating to pervaporation: A case study for separation of ethanol–water mixtures, Chemical Engineering and Processing: Process Intensification, 81 (2014) 35-40.

[283] M.M.A. Shirazi, A. Kargari, M. Tabatabaei, Sweeping gas membrane distillation (SGMD) as an alternative for integration of bioethanol processing: study on a commercial membrane and operating parameters, Chemical Engineering Communications, 202 (2015) 457-466.

[284] L. Guixia, M. Meizhong, G. Tao, Z. Zhenghe, Exploring the Effects of an External Electric Field on the Characteristics of the Cyclic Water Trimer, Chinese Journal of Chemical Physics, 18 (2005) 952.

[285] N.J. English, J. MacElroy, Molecular dynamics simulations of microwave heating of water, The Journal of chemical physics, 118 (2003) 1589-1592.

[286] N.J. English, J. MacElroy, Hydrogen bonding and molecular mobility in liquid water in external electromagnetic fields, The Journal of chemical physics, 119 (2003) 11806-11813.

[287] R. Brand, P. Lunkenheimer, U. Schneider, A. Loidl, Excess wing in the dielectric loss of glass-forming ethanol: a relaxation process, Physical Review B, 62 (2000) 8878.

[288] W. Routray, V. Orsat, Dielectric properties of concentration-dependent ethanol+ acids solutions at different temperatures, Journal of Chemical & Engineering Data, 58 (2013) 1650-1661.

[289] N. Qureshi, T.C. Ezeji, Butanol,'a superior biofuel'production from agricultural residues (renewable biomass): recent progress in technology, Biofuels, Bioproducts and Biorefining: Innovation for a sustainable economy, 2 (2008) 319-330.

[290] K. Ramanathan, C.K. Koch, S.H. Oh, Kinetic modeling of hydrocarbon adsorbers for gasoline and ethanol fuels, Chemical engineering journal, 207 (2012) 175-194.

[291] S. Rabelo, H. Carrere, R. Maciel Filho, A. Costa, Production of bioethanol, methane and heat from sugarcane bagasse in a biorefinery concept, Bioresource technology, 102 (2011) 7887-7895.

[292] S.M. Gwaltney-Brant, Miscellaneous indoor toxicants, Small Animal Toxicology, Elsevier2013, pp. 291-308.

[293] S. Ray, S. Ray, Dehydration of acetic acid, alcohols, and acetone by pervaporation using acrylonitrile-maleic anhydride copolymer membrane, Separation science and technology, 40 (2005) 1583-1596.

[294] P.P. Peralta-Yahya, J.D. Keasling, Advanced biofuel production in microbes, Biotechnology journal, 5 (2010) 147-162.

[295] M.K. Jain, D. Beacom, R. Datta, Mutant strain of C. acetobutylicum and process for making butanol, Google Patents, 1993.

[296] S.B. Bankar, S.A. Survase, H. Ojamo, T. Granström, Biobutanol: the outlook of an academic and industrialist, Rsc Advances, 3 (2013) 24734-24757.

[297] J. Gapes, The economics of acetone-butanol fermentation: theoretical and market considerations, Journal of Molecular Microbiology and Biotechnology, 2 (2000) 27-32.

[298] B. Ennis, N. Qureshi, I. Maddox, In-line toxic product removal during solvent production by continuous fermentation using immobilized Clostridium acetobutylicum, Enzyme and Microbial Technology, 9 (1987) 672-675.

[299] T. Ezeji, N. Qureshi, H. Blaschek, Acetone butanol ethanol (ABE) production from concentrated substrate: reduction in substrate inhibition by fed-batch technique and product inhibition by gas stripping, Applied microbiology and biotechnology, 63 (2004) 653-658.

[300] N. Qureshi, I.S. Maddox, Continuous production of acetone-butanol-ethanol using immobilized cells of Clostridium acetobutylicum and integration with product removal by liquid-liquid extraction, Journal of fermentation and bioengineering, 80 (1995) 185-189.

[301] N.G. Grobben, G. Eggink, F.P. Cuperus, H.J. Huizing, Production of acetone, butanol and ethanol (ABE) from potato wastes: fermentation with integrated membrane extraction, Applied Microbiology and Biotechnology, 39 (1993) 494-498.

[302] N. Qureshi, H.P. Blaschek, Production of acetone butanol ethanol (ABE) by a hyper-producing mutant strain of Clostridium beijerinckii BA101 and recovery by pervaporation, Biotechnology progress, 15 (1999) 594-602.

[303] A. Kujawska, J.K. Kujawski, M. Bryjak, M. Cichosz, W. Kujawski, Removal of volatile organic compounds from aqueous solutions applying thermally driven membrane processes. 2. Air gap membrane distillation, Journal of Membrane Science, 499 (2016) 245-256.

[304] A. Garcia III, E.L. Iannotti, J.L. Fischer, Butanol fermentation liquor production and separation by reverse osmosis, Biotechnology and bioengineering, 28 (1986) 785-791.

[305] S. Roy, S. Ragunath, Emerging membrane technologies for water and energy sustainability: Future prospects, constraints and challenges, Energies, 11 (2018) 2997.

[306] F. Banat, M. Al-Shannag, Recovery of dilute acetone–butanol–ethanol (ABE) solvents from aqueous solutions via membrane distillation, Bioprocess Engineering, 23 (2000) 643-649.

[307] F. Banat, F. Al-Rub, M. Shannag, Simultaneous removal of acetone and ethanol from aqueous solutions by membrane distillation: prediction using the Fick's and the exact and approximate Stefan-Maxwell relations, Heat and mass transfer, 35 (1999) 423-431.

[308] A. Kujawska, J. Kujawski, M. Bryjak, W. Kujawski, Removal of volatile organic compounds from aqueous solutions applying thermally driven membrane

processes. 1. Thermopervaporation, Chemical Engineering and Processing: Process Intensification, 94 (2015) 62-71.

[309] M. Kumar, M. Ulbricht, Novel antifouling positively charged hybrid ultrafiltration membranes for protein separation based on blends of carboxylated carbon nanotubes and aminated poly (arylene ether sulfone), Journal of membrane science, 448 (2013) 62-73.

[310] Z. Shi, W. Zhang, F. Zhang, X. Liu, D. Wang, J. Jin, L. Jiang, Ultrafast separation of emulsified oil/water mixtures by ultrathin free-standing single-walled carbon nanotube network films, Advanced materials, 25 (2013) 2422-2427.

[311] J. Gu, P. Xiao, J. Chen, J. Zhang, Y. Huang, T. Chen, Janus polymer/carbon nanotube hybrid membranes for oil/water separation, ACS applied materials & interfaces, 6 (2014) 16204-16209.

[312] L.N. Nthunya, L. Gutierrez, S. Derese, E.N. Nxumalo, A.R. Verliefde, B.B. Mamba, S.D. Mhlanga, A review of nanoparticle-enhanced membrane distillation membranes: membrane synthesis and applications in water treatment, Journal of Chemical Technology & Biotechnology, DOI (2019).

[313] D. Yang, C. Cheng, M. Bao, L. Chen, Y. Bao, C. Xue, The pervaporative membrane with vertically aligned carbon nanotube nanochannel for enhancing butanol recovery, Journal of membrane science, 577 (2019) 51-59.

[314] M.S. Humoud, W. Intrchom, S. Roy, S. Mitra, Reduction of scaling in microwave induced membrane distillation on a carbon nanotube immobilized membrane, Environmental Science: Water Research & Technology, 5 (2019) 1012-1021.

[315] O. Gupta, S. Roy, S. Mitra, Microwave Induced Membrane Distillation for Enhanced Ethanol–Water Separation on a Carbon Nanotube Immobilized Membrane, Industrial & Engineering Chemistry Research, 58 (2019) 18313-18319.

[316] R.A. Abramovitch, Applications of microwave energy in organic chemistry. A review, Organic preparations and procedures international, 23 (1991) 683-711.

[317] J. Reuß, D. Bathen, H. Schmidt-Traub, Desorption by microwaves: mechanisms of multicomponent mixtures, Chemical engineering & technology, 25 (2002) 381-384.

[318] S. Roy, R.S. Petrova, S. Mitra, Effect of carbon nanotube (CNT) functionalization in epoxy-CNT composites, Nanotechnology reviews, 7 (2018) 475-485.

[319] S.O. Olatunji, L.M. Camacho, Heat and Mass Transfer in Modeling Membrane Distillation Configurations: A Review, Frontiers in Energy Research, 6 (2018) 130.

[320] J. Kujawa, S. Cerneaux, S. Koter, W. Kujawski, Highly efficient hydrophobic titania ceramic membranes for water desalination, ACS Applied Materials & Interfaces, 6 (2014) 14223-14230.

[321] F. Liu, L. Liu, X. Feng, Separation of acetone–butanol–ethanol (ABE) from dilute aqueous solutions by pervaporation, Separation and Purification Technology, 42 (2005) 273-282.

[322] S. Van Wyk, A. Van Der Ham, S. Kersten, Pervaporative separation and intensification of downstream recovery of acetone-butanol-ethanol (ABE), Chemical Engineering and Processing-Process Intensification, 130 (2018) 148-159.

[323] H. Zhou, Y. Su, X. Chen, Y. Wan, Separation of acetone, butanol and ethanol (ABE) from dilute aqueous solutions by silicalite-1/PDMS hybrid pervaporation membranes, Separation and Purification Technology, 79 (2011) 375-384.

[324] J. Phattaranawik, R. Jiraratananon, Direct contact membrane distillation: effect of mass transfer on heat transfer, Journal of Membrane Science, 188 (2001) 137-143.

[325] S. Agnihotri, M.J. Rood, M. Rostam-Abadi, Adsorption equilibrium of organic vapors on single-walled carbon nanotubes, Carbon, 43 (2005) 2379-2388.

[326] C.M. Hussain, C. Saridara, S. Mitra, Self-assembly of carbon nanotubes via ethanol chemical vapor deposition for the synthesis of gas chromatography columns, Analytical chemistry, 82 (2010) 5184-5188.

[327] H. Verweij, M.C. Schillo, J. Li, Fast mass transport through carbon nanotube membranes, small, 3 (2007) 1996-2004.

[328] M.J. Raymond, C.S. Slater, M.J. Savelski, LCA approach to the analysis of solvent waste issues in the pharmaceutical industry, Green chemistry, 12 (2010) 1826-1834.

[329] N. Ramzan, S. Degenkolbe, W. Witt, Evaluating and improving environmental performance of HC's recovery system: A case study of distillation unit, Chemical Engineering Journal, 140 (2008) 201-213.

[330] Z. Lei, C. Li, B. Chen, Extractive distillation: a review, Separation & Purification Reviews, 32 (2003) 121-213.

[331] H.J. Kim, S.S. Nah, B.R. Min, A new technique for preparation of PDMS pervaporation membrane for VOC removal, Advances in Environmental Research, 6 (2002) 255-264.

[332] D. Roizard, V. Teplyakov, E. Favre, L. Fefilatiev, N. Lagunstsov, V. Khotimsky, VOC's removal from water with a hybrid system coupling a PTMSP membrane module with a stripper, Desalination, 162 (2004) 41-46.

[333] P. Marchetti, A. Butté, A. Livingston, Reactive peptide nanofiltration, Sustainable Nanotechnology and the Environment: Advances and Achievements, ACS Publications2013, pp. 121-150.

[334] I.B. Valtcheva, S.C. Kumbharkar, J.F. Kim, Y. Bhole, A.G. Livingston, Beyond polyimide: crosslinked polybenzimidazole membranes for organic solvent nanofiltration (OSN) in harsh environments, Journal of membrane science, 457 (2014) 62-72.

[335] P. Vandezande, L.E. Gevers, I.F. Vankelecom, Solvent resistant nanofiltration: separating on a molecular level, Chemical Society Reviews, 37 (2008) 365-405.

[336] M. Gryta, K. Karakulski, A. Morawski, Purification of oily wastewater by hybrid UF/MD, Water research, 35 (2001) 3665-3669.

[337] A. Criscuoli, E. Drioli, Energetic and exergetic analysis of an integrated membrane desalination system, Desalination, 124 (1999) 243-249.

[338] H. Kurokawa, T. Sawa, Heat recovery characteristics of membrane distillation, Heat Transfer-Japanese Research: Co-sponsored by the Society of Chemical Engineers of Japan and the Heat Transfer Division of ASME, 25 (1996) 135-150.

[339] J.B. Gálvez, L. García-Rodríguez, I. Martín-Mateos, Seawater desalination by an innovative solar-powered membrane distillation system: the MEDESOL project, Desalination, 246 (2009) 567-576.

[340] O. Gupta, S. Roy, S. Mitra, Microwave Induced Membrane Distillation for Enhanced Ethanol–Water Separation on a Carbon Nanotube Immobilized Membrane, Industrial & Engineering Chemistry Research, DOI (2019).

[341] C.H. Cho, K.Y. Oh, S.K. Kim, J.G. Yeo, P. Sharma, Pervaporative seawater desalination using NaA zeolite membrane: mechanisms of high water flux and high salt rejection, Journal of Membrane Science, 371 (2011) 226-238.

[342] J. Prince, G. Singh, D. Rana, T. Matsuura, V. Anbharasi, T. Shanmugasundaram, Preparation and characterization of highly hydrophobic poly (vinylidene fluoride)–Clay nanocomposite nanofiber membranes (PVDF–clay NNMs) for desalination using direct contact membrane distillation, Journal of Membrane Science, 397 (2012) 80-86.

[343] S. Khemakhem, R.B. Amar, Modification of Tunisian clay membrane surface by silane grafting: Application for desalination with Air Gap Membrane Distillation process, Colloids and Surfaces A: Physicochemical and Engineering Aspects, 387 (2011) 79-85.

[344] H. Fang, J. Gao, H. Wang, C. Chen, Hydrophobic porous alumina hollow fiber for water desalination via membrane distillation process, Journal of membrane science, 403 (2012) 41-46.

[345] M.S. Humoud, W. Intrchom, S. Roy, S. Mitra, Reduction of Scaling in Microwave Induced Membrane Distillation on Carbon Nanotube Immobilized Membrane, Environmental Science: Water Research & Technology, DOI (2019).

[346] K.A. Mahmoud, B. Mansoor, A. Mansour, M. Khraisheh, Functional graphene nanosheets: The next generation membranes for water desalination, Desalination, 356 (2015) 208-225.

[347] P. Goh, A. Ismail, Graphene-based nanomaterial: The state-of-the-art material for cutting edge desalination technology, Desalination, 356 (2015) 115-128.

[348] D. Cohen-Tanugi, J.C. Grossman, Mechanical strength of nanoporous graphene as a desalination membrane, Nano letters, 14 (2014) 6171-6178.

[349] K. Yang, L.-j. Huang, Y.-x. Wang, Y.-c. Du, Z.-j. Zhang, Y. Wang, M.J. Kipper, L.A. Belfiore, J.-g. Tang, Graphene Oxide Nanofiltration Membranes Containing Silver Nanoparticles: Tuning Separation Efficiency via Nanoparticle Size, Nanomaterials, 10 (2020) 454.

[350] M.-m. Cheng, L.-j. Huang, Y.-x. Wang, Y.-c. Zhao, J.-g. Tang, Y. Wang, Y. Zhang, M. Hedayati, M.J. Kipper, S.R. Wickramasinghe, Synthesis of graphene oxide/polyacrylamide composite membranes for organic dyes/water separation in water purification, Journal of Materials Science, 54 (2019) 252-264.

[351] Y. Zhang, L.-j. Huang, Y.-x. Wang, J.-g. Tang, Y. Wang, M.-m. Cheng, Y.-c. Du, K. Yang, M.J. Kipper, M. Hedayati, The preparation and study of ethylene glycol-modified graphene oxide membranes for water purification, Polymers, 11 (2019) 188.

[352] K. Huang, G. Liu, Y. Lou, Z. Dong, J. Shen, W. Jin, A graphene oxide membrane with highly selective molecular separation of aqueous organic solution, Angewandte chemie international edition, 53 (2014) 6929-6932.

[353] B. Mi, Graphene oxide membranes for ionic and molecular sieving, Science, 343 (2014) 740-742.

[354] P. Dreyfuss, Poly (tetrahydrofuran), CRC Press1982.

[355] R.J. Reid, B.H. Werner, Solutions of vinylidene chloride terpolymers in tetrahydrofuran and uses thereof, Google Patents, 1957.

[356] S.E. Hunter, C.E. Ehrenberger, P.E. Savage, Kinetics and mechanism of tetrahydrofuran synthesis via 1, 4-butanediol dehydration in high-temperature water, The Journal of organic chemistry, 71 (2006) 6229-6239.

[357] S. Vaidya, V. Bhandari, R. Chaudhari, Reaction kinetics studies on catalytic dehydration of 1, 4-butanediol using cation exchange resin, Applied Catalysis A: General, 242 (2003) 321-328.

[358] P.S. Rao, S. Sridhar, M.Y. Wey, A. Krishnaiah, Pervaporation performance and Transport phenomenon of PVA blend membranes for the separation of THF/water azeotropic mixtures, Polymer Bulletin, 59 (2007) 289-298.

[359] Y.-J. Han, W.-C. Su, J.-Y. Lai, Y.-L. Liu, Hydrophilically surface-modified and crosslinked polybenzimidazole membranes for pervaporation dehydration on tetrahydrofuran aqueous solutions, Journal of Membrane Science, 475 (2015) 496-503.

[360] S. Kuila, S. Ray, Sorption and permeation studies of tetrahydrofuran–water mixtures using full interpenetrating network membranes, Separation and purification technology, 89 (2012) 39-50.

[361] S. Ray, S. Ray, Dehydration of tetrahydrofuran (THF) by pervaporation using crosslinked copolymer membranes, Chemical Engineering and Processing: Process Intensification, 47 (2008) 1620-1630.

[362] S. Ray, S. Ray, Permeation studies of tetrahydrofuran–water mixtures by pervaporation experiments, Separation and purification technology, 50 (2006) 156-160.

[363] P.D. Chapman, T. Oliveira, A.G. Livingston, K. Li, Membranes for the dehydration of solvents by pervaporation, Journal of Membrane Science, 318 (2008) 5-37.

[364] S. Claes, P. Vandezande, S. Mullens, P. Adriaensens, R. Peeters, F.H. Maurer, M.K. Van Bael, Crosslinked poly [1-(trimethylsilyl)-1-propyne] membranes: Characterization and pervaporation of aqueous tetrahydrofuran mixtures, Journal of membrane science, 389 (2012) 459-469.

[365] S. Ray, N. Singha, S. Ray, Removal of tetrahydrofuran (THF) from water by pervaporation using homo and blend polymeric membranes, Chemical Engineering Journal, 149 (2009) 153-161.

[366] X. Mei, J. Ouyang, Ultrasonication-assisted ultrafast reduction of graphene oxide by zinc powder at room temperature, Carbon, 49 (2011) 5389-5397.

[367] S. Azizighannad, S. Mitra, Stepwise reduction of graphene oxide (GO) and its effects on chemical and colloidal properties, Scientific reports, 8 (2018) 1-8.

[368] S. Azizighannad, S. Mitra, Stepwise Reduction of Graphene Oxide (GO) and Its Effects on Chemical and Colloidal Properties, Scientific reports, 8 (2018) 10083.

[369] S.-J. Qiao, X.-N. Xu, Y. Qiu, H.-C. Xiao, Y.-F. Zhu, Simultaneous reduction and functionalization of graphene oxide by 4-Hydrazinobenzenesulfonic acid for polymer nanocomposites, Nanomaterials, 6 (2016) 29.

[370] R.B. Saffarini, B. Mansoor, R. Thomas, H.A. Arafat, Effect of temperature-dependent microstructure evolution on pore wetting in PTFE membranes under

membrane distillation conditions, Journal of membrane science, 429 (2013) 282-294.

[371] A. Rozicka, J. Niemistö, R.L. Keiski, W. Kujawski, Apparent and intrinsic properties of commercial PDMS based membranes in pervaporative removal of acetone, butanol and ethanol from binary aqueous mixtures, Journal of membrane science, 453 (2014) 108-118.

[372] X. Feng, R.Y. Huang, Estimation of activation energy for permeation in pervaporation processes, Journal of Membrane Science, 118 (1996) 127-131.

[373] H.B. Park, J. Kamcev, L.M. Robeson, M. Elimelech, B.D. Freeman, Maximizing the right stuff: The trade-off between membrane permeability and selectivity, Science, 356 (2017) eaab0530.

[374] B.D. Freeman, Basis of permeability/selectivity tradeoff relations in polymeric gas separation membranes, Macromolecules, 32 (1999) 375-380.

[375] P. Das, S.K. Ray, Pervaporative recovery of tetrahydrofuran from water with plasticized and filled polyvinylchloride membranes, Journal of industrial and engineering chemistry, 34 (2016) 321-336.

[376] S. Li, V.A. Tuan, R.D. Noble, J.L. Falconer, Pervaporation of water/THF mixtures using zeolite membranes, Industrial & engineering chemistry research, 40 (2001) 4577-4585.

[377] J. Mencarini Jr, R. Coppola, C.S. Slater, Separation of tetrahydrofuran from aqueous mixtures by pervaporation, Separation science and technology, 29 (1994) 465-481.

[378] J.-J. Shang, Q.-S. Yang, X.-H. Yan, X.-Q. He, K.-M. Liew, Ionic adsorption and desorption of CNT nanoropes, Nanomaterials, 6 (2016) 177.

[379] H. Ren, X. Shi, J. Zhu, Y. Zhang, Y. Bi, L. Zhang, Facile synthesis of N-doped graphene aerogel and its application for organic solvent adsorption, Journal of Materials Science, 51 (2016) 6419-6427.

[380] F. Su, C. Lu, Adsorption kinetics, thermodynamics and desorption of natural dissolved organic matter by multiwalled carbon nanotubes, Journal of Environmental Science and Health, Part A, 42 (2007) 1543-1552.

[381] B. Pan, B. Xing, Adsorption mechanisms of organic chemicals on carbon nanotubes, Environmental science & technology, 42 (2008) 9005-9013.

[382] K. Raidongia, J. Huang, Nanofluidic ion transport through reconstructed layered materials, Journal of the American Chemical Society, 134 (2012) 16528-16531.

[383] Y. Zhu, S. Murali, W. Cai, X. Li, J.W. Suk, J.R. Potts, R.S. Ruoff, Graphene and graphene oxide: synthesis, properties, and applications, Advanced materials, 22 (2010) 3906-3924.

[384] R. Liu, G. Arabale, J. Kim, K. Sun, Y. Lee, C. Ryu, C. Lee, Graphene oxide membrane for liquid phase organic molecular separation, Carbon, 77 (2014) 933-938.